UNIVERSIDADE FEDERAL DE MINAS GERAIS

PROGRAMA DE PÓS-GRADUAÇÃO EM

ENGENHARIA MECÂNICA

AIRCRAFT DYNAMIC ANALYSIS METHODS USING FLIGHT TESTS

JOEL LAGUÁRDIA CAMPOS REIS

Belo Horizonte, 16 de Dezembro de 2016

Joel Laguárdia Campos Reis

AIRCRAFT DYNAMIC ANALYSIS METHODS USING FLIGHT TESTS

Dissertação apresentada ao Programa de Pós-Graduação em Engenharia Mecânica da Universidade Federal de Minas Gerais, como requisite parcial à obtenção do título de Metre em Engenharia Mecânica.

Área de concentração: Projetos Mecânicos

Orientador: Prof. Dimas Abreu Dutra

(Universidade Federal de Minas Gerais)

Co-orientador: Prof. Ricardo Luiz Utsch de F. Pinto

(Universidade Federal de Minas Gerais)

Belo Horizonte

Escola de Engenharia da UFMG

2016

AGRADECIMENTOS

A Deus pela beleza, complexidade e simplicidade da sua criação. A meus pais e irmão que são peças fundamentais para que eu pudesse chegar aqui. A minha noiva Izabela, por ser sempre meu braço direito que me ajuda a levantar nos dias difíceis e que sorri comigo nas conquistas. Ao meu orientador Prof. Dimas Dutra por toda sua dedicação e paciência que teve comigo nesses últimos anos, e também por sempre me motivar a fazer coisas novas. Ao meu co-orientador Prof. Ricardo Utsch, por suas importantes opiniões e por sempre se mostrar disponível para abrir novas questões sobre os assuntos estudados. Ao meu amigo Luciano Frágola, por compartilhar seu conhecimento e tempo comigo nas discussões sobre quais os melhores caminhos para trilhar e por me ensinar a observar com mais calma o porquê das coisas. Ao caro Otávio Kovacs, que me ensinou muito sobre ensaios em voo e que se tornou um exemplo para mim de longanimidade e amizade. Aos meus amigos do CEA, em especial aqueles que participaram de forma mais direta nesse trabalho, Marcos Torres, Lucas Pereira, Danilo Azevedo e Julliardy Matoso. Ao Prof. Ravindra pela disponibilização dos dados para as análises realizadas. Esse trabalho é fruto da participação de cada um de vocês.

Deixo aqui meus sinceros agradecimentos.

“*Grandes são as obras do Senhor;nelas meditam todos os que as apreciam.”*
(Salmos 111.2)

TABLE OF CONTENTS

LIST OF FIGURES

LIST OF TABLES

LIST OF SYMBOLS

α	Angle of attack
$[\boldsymbol{A}]_{Long}$, $[\boldsymbol{A}]_{LatDir}$	Plant matrices
β	Sideslip angle
$[\boldsymbol{B}]_{Long}$, $[\boldsymbol{B}]_{LatDir}$	Control matrices
C	Observation matrix of the linearized system
δ_E, δ_A, δ_R, i_H	Elevator, aileron, rudder and stabilator deflections
ε	Residuals
f	State space function
F	Process noise distribution matrix
$\vec{F}_A$, $\vec{F}_T$	Aerodynamic and propulsive force vectors
$\vec{g}$	Gravity vector
g	Output functions
G	Additive measurements noise distribution matrix
I_{ii}, I_{ij}	Inertial moments and products of inertia
J	Cost function
$\boldsymbol{K}$	Kalman gain matrix
L, M, N	Components of the moment vector
m	Aircraft mass
$\vec{M}_A$, $\vec{M}_T$	Aerodynamic and propulsive moments vector
P, Q, R	Angular rates components
$\boldsymbol{P}$	Covariance matrix of the state-prediction error
$\boldsymbol{R}$	Covariance matrix of the measurement noise
$\boldsymbol{\theta}$	Parameters vector
T	Period
U, V, W	Linear velocity components
$\vec{V}_p$	Aircraft airspeed
$\vec{\omega}$	Angular speed vector
ω_n	Natural frequency
ζ	Damping coefficient
τ	Time constant

Φ, Θ, Ψ	Euler angle components
$y(t)$	Outputs
v	Measurement noise
$z(t)$	Measurements
X', Y', Z'	Earth coordinates frame
X, Y, Z	Body based coordinates frame
X_s, Y_s, Z_s	Wind coordinates frame
ACS	Advanced Composite Solution
ATTAS	Advanced Technologies Testing Aircraft System
CEA	Center for Aeronautical Studies
DLR	German Aerospace Center
EEM	Equation Error Method
FEM	Filter Error Method
MS	Maximum Slope
NLS	Nonlinear Least Squares
OEM	Output Error Method
TR	Time Ratio
TPR	Transient Peak Ratio

RESUMO

A resposta dinâmica de uma aeronave é um importante aspecto a ser analisado durante o seu desenvolvimento. Quando um aeronave é perturbada de seu estado estacionário devido a rajadas ou comandos, a forma como ela retorna para o equilíbrio é crucial para a opinião do piloto sobre as qualidades de voo. As características da resposta da aeronave podem ser quantificadas por parâmetros como a frequência natural, coeficiente de amortecimento e pelas constantes de tempo para cada um dos modos dinâmicos conhecidos: Fugóide, Curto-Período, Dutch Roll, Espiral e Rolamento puro. Esses modos estão relacionados às propriedades aerodinâmicas, inerciais e propulsivas da aeronave, as quais são inicialmente obtidas de formulações semi-empíricas e refinadas por dados de ensaios em túnel de vento. No entanto, para a validação desses parâmetros e para uma análise experimental, ensaios em voo devem ser realizados, nos quais o real comportamento da aeronave pode ser observado.

Neste trabalho apresentamos técnicas comumente utilizadas para a execução de ensaios em voo, i.e., procedimentos para excitar a aeronave em cada um dos modos dinâmicos em voo. Inicialmente, uma metodologia clássica é utilizada para a redução dos dados. Tal metodologia é baseada em análises gráficas, onde modelos dinâmicos simplificados da aeronave são utilizados para estimar suas características. Tais técnicas dependem de dados com alta qualidade e com baixo nível de ruído, e da interpretação pessoal do engenheiro de ensaios, o que pode gerar resultados imprecisos. Portanto, outros diferentes métodos são utilizados para análise, o quais são baseados em técnicas de identificação de sistemas onde diferentes modelos da mecânica de voo podem ser utilizados durante a análise.

Para comparar os diferentes métodos, duas aeronaves distintas (VFW-Fokker 614 e ACS-100 Sora) são avaliadas. As manobras são executas mais de uma vez sobre as mesmas condições de voo para se obter diferentes conjuntos de dados, para estimação e validação. Apesar das muitas fontes de erro, as metodologias clássicas mostraram uma boa proximidade quando comparadas com os outros métodos aplicados. Os parâmetros obtidos utilizando as técnicas de identificação de sistema têm maior confiabilidade devido às propriedades estatísticas dos métodos. De fato, os resultados obtidos por estes métodos mostram uma maior consistência com os dados medidos, onde se observa um menor grau de dispersão quando comparados os resultados para as diferentes técnicas de identificação do sistema. Assim, os métodos de identificação do sistema são mais adequados para a avaliação da dinâmica de voo.
Palavras-chave: ensaios em voo; identificação de sistemas; mecânica de voo; dinâmica de aeronave

ABSTRACT

The dynamic response of an aircraft is an important aspect to be analyzed during its development program. When the airplane is disturbed from its steady state due to a wind gust or commands, the way by which it returns to the equilibrium is crucial for the pilot's opinion of the aircraft's handling qualities. The characteristics of the aircraft response can be quantified by parameters such as the natural frequency, damping coefficient and time constant values of each of the well-known dynamic modes: Phugoid, Short-Period, Dutch Roll, Spiral and Roll subsidence. These modes are related to aerodynamic, inertial and propulsive properties of the aircraft, which are initially obtained from semi-empirical formulations and refined from wind tunnel tests data. However, for the validation of these parameters and for experimental analysis, flight test must be performed, in which the actual aircraft behavior can be observed.

In this work we present techniques commonly used for flight tests execution, i.e., procedures to excite each of the aircraft's dynamical modes in flight. Initially, a classical methodology is used for data reduction. Such methodology is based on graphical analysis, where simplified dynamic models for the aircraft are used to estimate its characteristics. Such techniques depend on high data quality with low noise level and on the personal interpretation of the flight test engineer, which can generate inaccurate results. Therefore, other different methods are used for analysis, which are based on system identification techniques where different models of the flight mechanics can be used during analysis.

To compare the different methods presented, two distinct aircrafts (VFW-Fokker 614 and ACS-100 Sora) are evaluated. The maneuvers are executed more than once over the same flight conditions to obtain different datasets, for the estimation and validation.

Despite the many error sources, the classical methodologies has shown a great proximity when compared with the other applied methods. The parameters obtained using the system identification techniques have a higher reliability due to the statistical properties of the methods. Indeed, the results obtained by these methods show a greater consistency with the measured data, where a lower degree of dispersion is observed when comparing the results for the different system identification techniques. Thus, the system identification methods are more suitable for the evaluation of the flight dynamics.

Key words: flight tests; system identification; flight mechanics; aircraft dynamics

1 INTRODUCTION

Flight testing is one of the most important steps during the development of a new aircraft. Several procedures are adopted to evaluate the aircraft's performance, stability, controls, structures, aerodynamics, and other properties, in flight. Thus, the obtained data is used to compare with the pre-estimated calculations, allowing to feed back the original design for the accomplishment of the aeronautical regulations and to achieve the pre-specified project goals.

Among these tests, we have the dynamic stability type, which are responsible to observe and analyze the aircraft behavior after a perturbation by the wind or by the pilot's input from its steady state condition. The form of such response is closely related to the handling qualities and crew workload, thus, it will be a determinant factor in the pilot's opinion about the quality of flight. For a satisfactory result of such type of flight tests, it is required a group with the knowledge about: stability and control principles; instrumentation, for data acquisition in flight; standard inputs for the controls, for an adequate excitation of the aircraft; and at least, an understanding about the interpretation of the obtained data in flight. In addition, it is important to have a good communication with the pilot to have an insight of its opinion about the flight and to show him better forms to execute a required maneuver (WARD and STRGANAC, 1998).

General aircraft have five well-known typical dynamic modes, they are: Phugoid, Short-Period, Dutch Roll, Roll Subsidence and Spiral (PAMADI, 2004). The Phugoid and the Short-Period are modes of the longitudinal aircrafts motion, where the first is mainly characterized by oscillation in the aircraft airspeed with a long period in its response. On the other hand, the Short-Period is represented by oscillations in the aircraft's angle of attack; it has a higher frequency and is related with typical maneuvers used during the aircraft operation. The Dutch Roll is the only oscillatory mode of the lateral-directional motion of an aircraft and is represented mainly by variation in the sideslip angle along the time. The Roll subsidence is a first order mode, and is very important in the determination of the maneuverability characteristics of an aircraft. The Spiral, also a first order response, is a mode that can be observed by the bank angle behavior along the time. It is common for this mode to be unstable or neutral, which does not strongly affect the flight quality, since it has a very slow response and can be easily corrected by the pilot. The dynamic modes of an aircraft can be obtained from the calculation of the eigenvalues of the linearized plant matrix (obtained from the aircraft's equations of motion, for the longitudinal and for the lateral-directional), which parameters are

directly related to the aerodynamic, inertial and propulsive properties of the aircraft (NAPOLITANO, 2012).

The determination of the characteristics of these modes may be related to the flight quality of the aircraft, which can be verified with the data obtained in the tests. For this purpose, maneuvers must be used in flight to excite each mode in order to observe its characteristics, i.e., its natural frequency, damping and time constants (SCHMIDT, 1998). To excite slower modes such as Phugoid and Spiral, pulse maneuvers can be applied using the elevator and the rudder (or aileron), respectively. For Roll subsidence it is common to use a maneuver denoted bank-to-bank, in which the pilot varies the bank angle of the aircraft from side to side by approximately 30°. For Dutch Roll and Short-Period, it is common to use a maneuver called doublet, which has good efficiency in avoiding that other modes are also excited together. For the Short-Period, usually the highest frequency mode of an aircraft, a maneuver called "3-2-1-1" is presented, which has a higher quality for a satisfactory excitation of the mode. Each maneuver must be carefully applied by the pilot for a correct excitation of the modes, in order to allow them to be observed in the collected data (JATEGAONKAR, 2015).

During the tests the aircraft is instrumented in order to record the various states of motion such as linear velocity, angular rate, attitude, wind angles related to the body frame, deflection of the control surfaces, and others. The measurements are used in a data reduction process to evaluate the aircraft behavior.

For data reduction, classic techniques are used (WARD e STRGANAC, 1998), among which we have: the Transient Peak Ratio (TPR), the Modified Peak Ratio (MTPR), the Maximum Slope Method (MS) and Time Ratio method (TR). The scope of application of each of these methods depends on the characteristics of the mode analyzed. In general, TPR and MTPR are used for responses with a lower degree of damping than those that are analyzed by MS or TR. These methods assume simplifications in aircraft movement where modes are observed in the behavior of only one variable over time, where some measurements are made on the data to obtain parameters for the interpretation of the graphic (KIMBERLIN, 2003). These methods, despite the simplicity of use, depend on data with good quality and low noise level, since such factors interfere in the determination of the points and curves to be measured. Furthermore, during the measurements only a few points of the response are used for analysis. In addition, their results suffer greatly interference from the engineer's personal interpretation. Nevertheless, graphical methods are commonly used to carry out analyzes of the flight quality of the aircraft (FUJINO, MAHIKO, *et al.*, 2004; NICOLOSI, MARCO e VECCHIA, 2001).

Another way to determine the characteristics of dynamic modes is to use system identification methods (JATEGAONKAR, 2015; KLEIN e MORELLI, 2006; RAOL, GIRIJA e SINGH, 2004; JATEGAONKAR, FISCHENBERG e GRUENHAGEN, 2004). In this work, we use identification methods in the time domain, with them the parameters of the plant matrix are estimated and the properties of the modes are obtained by calculating the eigenvalues for each motion, i.e., longitudinal and lateral-directional. The first method applied is the Equation Error Method (EEM), which assumes that there is no noise in the measurements, but only in the process. This technique is based on the principle of least squares and has the advantage of not needing an initial guess of the parameters for the estimation process, its solution is obtained in a single step. However, such method is sensitive to the noise level in the measurements, which in practice cannot be extinguished. Another estimation method is the Output Error Method (OEM), which assumes that there is only noise in the measurements. This technique is based on the principle of maximum likelihood, which gives it good statistical properties. In this technique, the parameters are estimated iteratively, where it is assumed that the system is deterministic, that is, the parameters of the model do not suffer interferences of external effects not included in the process. Therefore, for a suitable estimation, the tests should be performed in a mild atmosphere. Finally, we have the Filter Error Method (FEM), which assumes that the system has noise both in the measurements and in the process, i.e., the system is stochastic. This method, is also based on the principle of maximum likelihood, where parameter estimation is based on an iterative process. However, during the estimation, corrections are made using a Kalman Filter to adjust the errors due to process noise. Thus, the FEM can be used to analyze data collected in a turbulent atmosphere, which is common occurrence due to the limit in the schedule of an aircraft's flight test campaign.

These methods make better use of the data acquired in the tests because they take into account all the variables of the motion, using all the data points collected during the maneuver and even the system inputs, that is, the deflections in the commands. Another advantage is that the inputs are used in the identification process, so they can be performed in a more general way and it is not necessary to return the commands to the equilibrium position, simplifying the execution of the test for the pilot. In addition, they have good statistical qualities, which give greater reliability to the estimated parameters. These methods can be used for different models of the aircraft motion, which makes them even more flexible. In the most simplified models, a smaller amount of data is used in the identification process; however, it converges with greater ease, since a smaller number of parameters is being estimated. Moreover, if the assumed simplifications are reasonable, one can obtain parameters with satisfactory reliability.

Finally, the author proposes the use of the Nonlinear Least Squares Method for data reduction (STRUTZ, 2011). This method, like the EEM, is based on the principle of least squares. However, here, it is assumed that there is a non-linear dependence between the parameters and the independent variable. To estimate the characteristics of each mode, one assumes that its response is in the form of a damped sinusoid or first-order response, depending on the mode. Then, the parameters are estimate iteratively, by the measurements of the variable that represents the mode under analysis, as well as in the graphical methods. An advantage of this method is that its algorithm is readily available in programming languages, such as C++, Python, Matlab, etc. In addition, its analysis uses all points of the natural response of the variable, whereas in graphical methods only some data is used for estimation. The initial parameters can be obtained from the analysis of the graphical methods or from data available from similar aircrafts.

The graphical methods were develop based on exponential fitting assumption that were used for aircraft dynamic analysis in old times, when the acquisition system available did not have the capability to obtain digital data. In the end of the tests, a series of curves representing the behavior of each variable measured were available, and the engineer had to interpret the data based on such curves. Nowadays, there is the viability of more modern computers and instruments that are capable to deal with the acquisition and evaluation of digital data. The motivation of this work is to compare the results obtained for each of the different methods, since the graphical methods are still used nowadays for analysis. Thus, we aim to perform a comparative study of various methods for aircrafts dynamic analysis using flight test data using each of the different excitation maneuvers of the modes (as shown in FIG. 1.1), in order to observe the advantages and disadvantages of each type of analysis. This work allows the flight test engineer a better judgment in choosing the most appropriate method to analyze the dynamic behavior of an aircraft during a flight test campaign.

For this purpose, data from two different aircraft are used: the VFW-Fokker 614 (JORDAN, 2000) and the ACS-100 Sora (ACS AVIATION, 2006). The data of each aircraft have different characteristics, i.e., noise level, frequency, etc., since they were obtained using different data acquisition systems. These aircraft were designed for different types of operation; in addition, they are widely different from aerodynamic, inertial and propulsive viewpoint. This scenario allows a better analysis of the test methods shown, since they are used in situation with clear differences, allowing the observation of the most reliable procedures to be used in a dynamic flight test campaign, in a more general perspective.

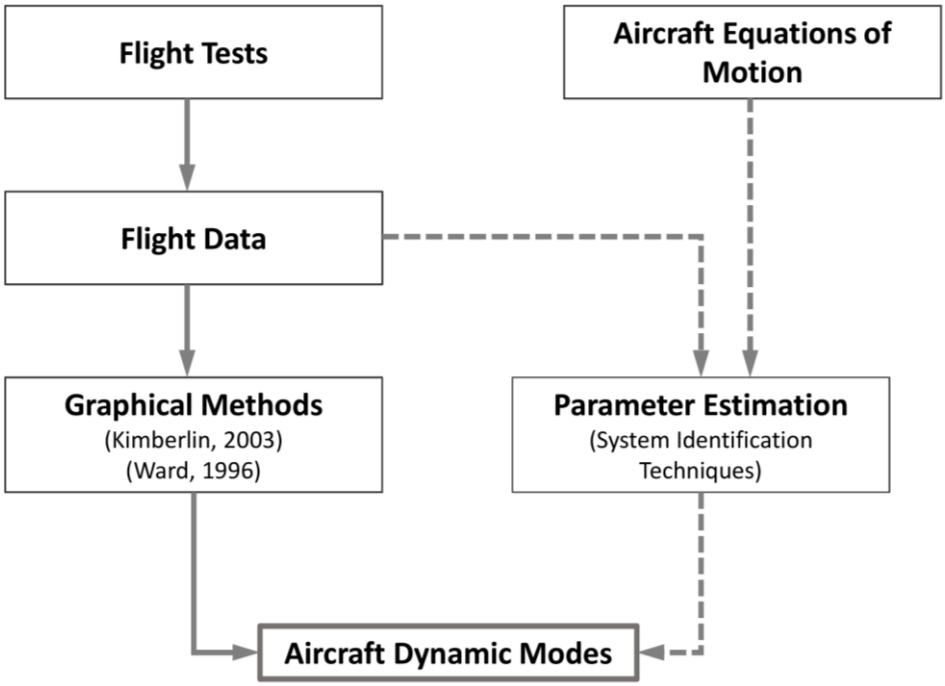

FIGURE 1.1 - Methods for aircraft dynamic analysis using flight tests

For the development of this work, in Chapter 2 we obtain the dynamic models of the aircraft, which are derived from fundamental physical principles. The coordinate systems adopted in the modeling are shown, as well as the forces and moments that act on the aircraft and the simplifications assumed for a condition of small perturbations. From symmetry considerations, sets of equations are obtained for longitudinal and lateral-directional motions, separately. Each of the dynamic modes is presented, as well as its main characteristics. Finally, approximation models are presented for two important modes: the Short-Period and the Dutch-Roll.

In Chapter 3, the main detail for the accomplishment of the flight tests are shown, as well as the necessary instrumentation, test procedures and maneuvers indicated for the excitation of each mode.

Chapter 4 presents each of the different techniques for data reduction. Their characteristics and the theories on which they are based.

Finally, in Chapter 5 and 6 are presented the results and conclusions obtained in the analysis of the two aircrafts. The greatest challenges in the application of each method are presented, as well as their advantages and disadvantages. Also, future work to be performed from the results presented here is pointed out.

2 AIRCRAFT FLIGHT DYNAMICS

The flight dynamics involves subjects like performance, stability and control of flight vehicles. It is concerned with how the forces and moments acting on the aircraft influence its speed and attitude in time. It started after the first flights in the early 20th century, with the development of the aircraft equations of motion by LANCHESTER (1908) and BRYAN (1911). The theoretical work developed by Bryan, introduced almost 90 years ago, led to the development of the aircraft equations of motions in the same form as they are known today, and they are used in the study of dynamic stability, control and response of airplane. His formulation was based on two principal assumptions: i) the instantaneous aerodynamic forces and moments depend only on instantaneous values of the motion variables and ii) the aerodynamic forces and moments vary linearly with motion variables.

The equations of motion of the aircraft are derived for six-degreed-of-freedom analysis (three translational, three rotational). These equations are, in general, coupled and nonlinear, which make its analytical solution a hard task. Because of it, the following assumptions are adopted (NAPOLITANO, 2012):

- The aircraft is assumed as a continuous system;
- The Earth curvature is neglected, that is, the Earth is assumed as a flat surface;
- The airplane is assumed as a rigid body, and the elastic deformations and their effects on motion are neglected;
- The aircraft mass distribution is assumed constant along the time, which implies that the moments and products of inertia can also be assumed constant in time;
- The aircrafts motion following disturbances is one of small amplitude in all the disturbed variables, which permits the linearization of the aircrafts equations of motion;
- The aircraft is symmetric about its vertical plane, which allows decoupling the motion into two sets, one for the longitudinal motion and another for the lateral-directional motion.

2.1 Reference frames

To describe the aircraft motion we introduce several coordinate systems to specify the position, velocity, accelerations, forces and moments on the vehicle. It is important to recall that Newton’s second law is expressed with respect to an inertial frame. Here, the aircraft is assumed as a system that moves in the lower regions of the Earth atmosphere, therefore, an

Earth-based reference axes system is selected. This selection implies that the effects of the rotational velocity of the Earth can be neglected, since the Earth is assumed as a flat surface (PAMADI, 2004). Then, the following reference frames are introduced:

- Navigational or Earth frame (X_e, Y_e, Z_e or X', Y', Z'): the origin of this frame is located on the surface of the Earth such that the Z_e axis is pointing towards the center of the spherical Earth. The X_e axis points to the local north, and the Y_e is directed to the local east, forming a right-hand system (FIG. 2.1).

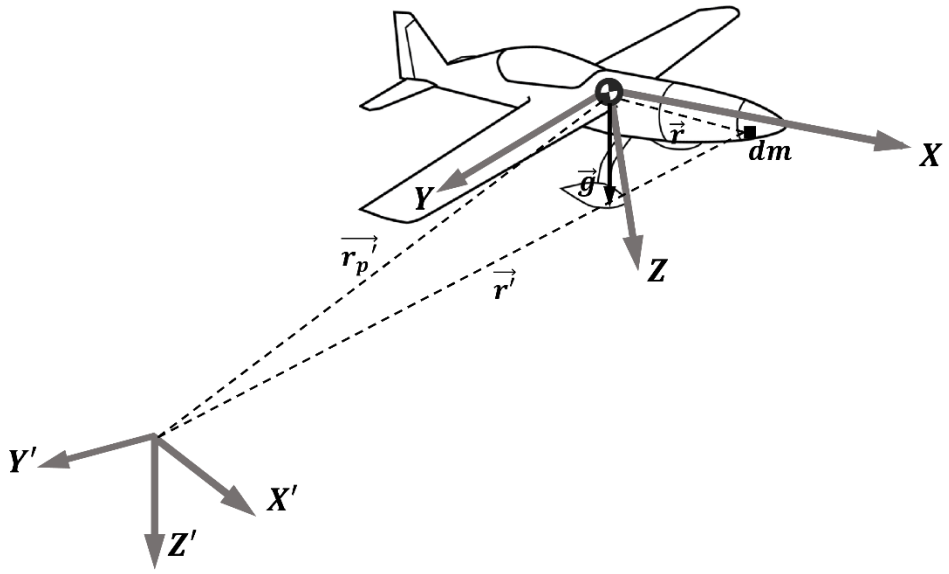

FIGURE 2.1 - Earth and Body frame references

- Aircraft body frame (X_b, Y_b, Z_b or X, Y, Z): the aircraft body frame is located at the center of gravity of the aircraft (FIG. 2.1). The X_b axis usually lies along the longitudinal centerline of the aircraft and points in the direction of the motion. Since, generally, the aircraft has a plane of symmetry; the X_bZ_b plane coincides with this plane.
- Wind or Stability frame (X_s, Y_s, Z_s): The axes used to calculate the forces and moments acting on the aircraft, where the axis X_s has the property to be aligned with direction of steady-state airspeed. The Y_s and Z_s will compose a right hand system with the right wing with positive Y_s. The angle between the airspeed vector V_P and the X_bY_b plane is the angle of attack α. Other important angle is the sideslip angle β, which measures the deviation of the airspeed V_P with the respect to the longitudinal aircraft's plane (FIG. 2.2). The sideslip angle is positive when the lateral component of the airspeed component is in the opposite direction of Y_b, this is, "cutting" the right wing (FIG. 2.2).

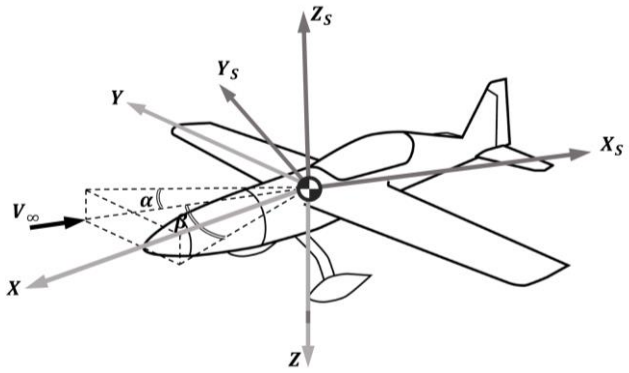

FIGURE 2.2 - Wind Frame

2.2 Variation of the Linear Momentum Equations

Newton's second law states that variation of the linear momentum $\vec{p}$ is a result from the external forces $\vec{F}$ acting over a body (NAPOLITANO, 2012), when observed from an inertial reference:

$$\vec{F} = \dot{\vec{p}} = \frac{d}{dt}(m\,\vec{v}) \tag{2.1}$$

Here, the Earth frame is assumed as inertial. Moreover, it is assumed that the aircraft mass is concentrated at its center of gravity (CG), and it is constant in time ($dm/dt = 0$), which is a reasonable assumption for a short period of flight where there is a relatively low fuel consumption rate. Besides, we have that the external forces acting on the aircraft are the aerodynamic, thrust and gravity forces. Then, Eq. (2.1) can be expressed by:

$$\int_V \rho_A\,\vec{g}\,dV + \int_S (\vec{F}_A + \vec{F}_T)\,dS = \frac{d}{dt}\int_V \rho_A \frac{d\overrightarrow{r'}}{dt}\,dV \tag{2.2}$$

where S and V represent the aircraft surface area and volume, respectively. Eq. (2.2) reduces to:

$$m\vec{g} + (\vec{F}_A + \vec{F}_T) = m\frac{d\vec{V}_p}{dt} \tag{2.3}$$

where the aircraft's CG velocity relative to the Earth frame is defined by:

$$\vec{V}_p \triangleq \dot{\vec{r}}_p \tag{2.4}$$

For the motion analysis, it is more convenient to represent the equations with respect to the body frame X, Y, Z, located at the aircraft center of gravity. In agreement with Chasles'

theorem (SHAMES, 2003), which states that a rigid body displacement is composed by a translation followed by a rotation, we can express a generic vector $\vec{A}$ defined with respect to the Earth frame X_e,Y_e,Z_e, and in the body frame, the angular velocity $\vec{\omega}$ of X,Y,Z with respect to X_e,Y_e,Z_e. Thus,

$$\frac{d\vec{A}}{dt} = \frac{\partial \vec{A}}{\partial t} + \vec{\omega} \text{ x } \vec{A} \tag{2.5}$$

Using Eq. (2.6), we have that:

$$m\left(\frac{\partial \vec{V}_p}{\partial t} + \vec{\omega} \text{ x } \vec{V}_p\right) = m\vec{g} + (\vec{F}_A + \vec{F}_T) \tag{2.6}$$

We observe that cross product on the left-hand side represents a force that is always perpendicular to the velocity, than it does not change the velocity modulus, but only its direction. Further, each vector is expressed with respect to the body frame (FIG. 2.3) by:

$$\begin{aligned}
\vec{V}_p &= U\vec{\imath} + V\vec{\jmath} + W\vec{k} \\
\dot{\vec{V}}_p &= \dot{U}\vec{\imath} + \dot{V}\vec{\jmath} + \dot{W}\vec{k} \\
\vec{\omega} &= P\vec{\imath} + Q\vec{\jmath} + R\vec{k} \\
\vec{F}_A &= F_{A_x}\vec{\imath} + F_{A_y}\vec{\jmath} + F_{A_z}\vec{k} \\
\vec{F}_T &= F_{T_x}\vec{\imath} + F_{T_y}\vec{\jmath} + F_{T_z}\vec{k} \\
\vec{g} &= g_x\vec{\imath} + g_y\vec{\jmath} + g_z\vec{k}
\end{aligned} \tag{2.7}$$

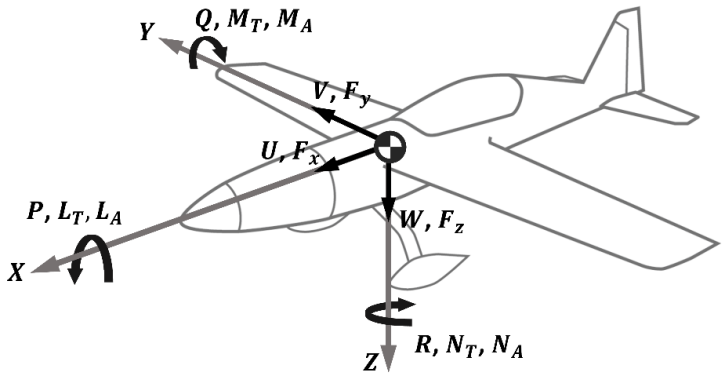

FIGURE 2.3 - Linear velocities, angular rates, moments and forces

Thus, expanding the cross product in Eq. (2.6), the variation of linear momentum equations are given by:

$$\begin{aligned} m(\dot{U} + QW - RV) &= mg_x + (F_{A_x} + F_{T_x}) \\ m(\dot{V} + UR - PW) &= mg_y + (F_{A_y} + F_{T_y}) \\ m(\dot{W} + PV - QU) &= mg_z + (F_{A_z} + F_{T_z}) \end{aligned} \tag{2.8}$$

2.3 Variation of the Angular Momentum Equations

In the same way as for Linear Momentum, we have that the angular momentum's variation around the aircraft's CG is a result from the external moments relative to the CG, when observed from an inertial reference (Earth frame) (NAPOLITANO, 2012).

$$\vec{M} = \dot{\vec{h}} \tag{2.9}$$

Based on the assumptions stated for the linear momentum equations of constant and concentrated mass and knowing that the external moments acting in the aircraft are due to aerodynamics and thrust effects, it can be demonstrated that

$$\vec{M}_A + \vec{M}_T = \frac{d}{dt}\int_V \vec{r}\,\mathrm{x}\,\rho_A \frac{d\vec{r}}{dt} dV \tag{2.10}$$

Since the aircraft is assumed as a rigid body, based on Chasles' theorem, the Eq. (2.10) is expanded to

$$\begin{aligned} \vec{M}_A + \vec{M}_T = &\int_V [\vec{\omega}(\vec{r}.\vec{r})]\rho_A dV + \int_V [-\vec{r}(\vec{r}.\vec{\omega})]\rho_A dV \\ &+ \int_V [\vec{r}\,\mathrm{x}\,\vec{\omega}(\vec{\omega}.\vec{r})]\rho_A dV \end{aligned} \tag{2.11}$$

where, each vector is expressed with respect to the body frame by

$$\begin{aligned} \vec{r} &= X\vec{\imath} + Y\vec{\jmath} + Z\vec{k} \\ \vec{\omega} &= P\vec{\imath} + Q\vec{\jmath} + R\vec{k} \\ \dot{\vec{\omega}} &= \dot{P}\vec{\imath} + \dot{Q}\vec{\jmath} + \dot{R}\vec{k} \\ \vec{M}_A &= L_A\vec{\imath} + M_A\vec{\jmath} + N_A\vec{k} \\ \vec{M}_T &= L_T\vec{\imath} + M_T\vec{\jmath} + N_T\vec{k} \end{aligned} \tag{2.12}$$

Solving the integrals of Eq. (2.11) we obtain the variation of angular momentum equations:

$$\begin{aligned} \dot{P}I_{xx} - \dot{R}I_{xz} - PQI_{xz} + RQ\left(I_{zz} - I_{yy}\right) &= L_A + L_T \\ \dot{Q}I_{yy} + PR(I_{xx} - I_{zz}) + (P^2 - R^2)I_{xz} &= M_A + M_T \\ \dot{R}I_{zz} - \dot{P}I_{xz} + PQ\left(I_{yy} - I_{xx}\right) + QRI_{xz} &= N_A + N_T \end{aligned} \tag{2.13}$$

where I_{XX}, I_{YY}, I_{ZZ} and I_{XZ} are the well-known moments and product of inertia terms. It is important to observe that the obtained equations were simplified by the assumption that the XZ plane is a plane of symmetry, thus, we have that $I_{XY} = I_{YZ} = 0$. Also, we can observe that, in the presented derivation, the aircraft is assumed as a single rigid body, not including the gyroscopic effects associated due to the propeller, turbine blades, or other rotating components of the propulsion system. Another important observation is related to the aircraft plane of symmetry XZ, which implies that Y is one of the principal axis of inertia, thus a torque applied in this axis will not cause rotation in the other axis.

2.4 Euler Angles

The obtained equations for the variation of linear and angular momentum provides the dynamics of the aircraft with respect to the body reference frame X, Y, Z. However, for a complete description of the aircraft dynamics, it is important the describe its motion relative to the Earth inertial frame X_e, Y_e, Z_e. The body orientation relative to the Earth, also known as attitude, is most commonly described by the Euler Angles, which is based on a sequence of successive rotations around the aircraft's CG, known as the Z, Y, X right-handed rotation sequence (SHAMES, 2003).

We introduce a base reference frame X_1, Y_1, Z_1 that moves with the aircraft CG and is parallel to the Earth frame X_e, Y_e, Z_e, which is also called North-East-Down (NED) frame. Then, the Euler angles transformation is done in a sequence of three rotations (FIG. 2.4) as follows:

i. The reference frame rotates about its Z_1 axis an angle Ψ (yaw angle), defining a second coordinate system (X_2, Y_2, Z_2);
ii. The second coordinate system rotates about Y_2 axis by an angle Θ (pitch angle), defining a third coordinate system (X_3, Y_3, Z_3);
iii. The third coordinate system rotates about X_3 axis by an angle Φ (roll angle), to the aircrafts body frame X, Y, Z;

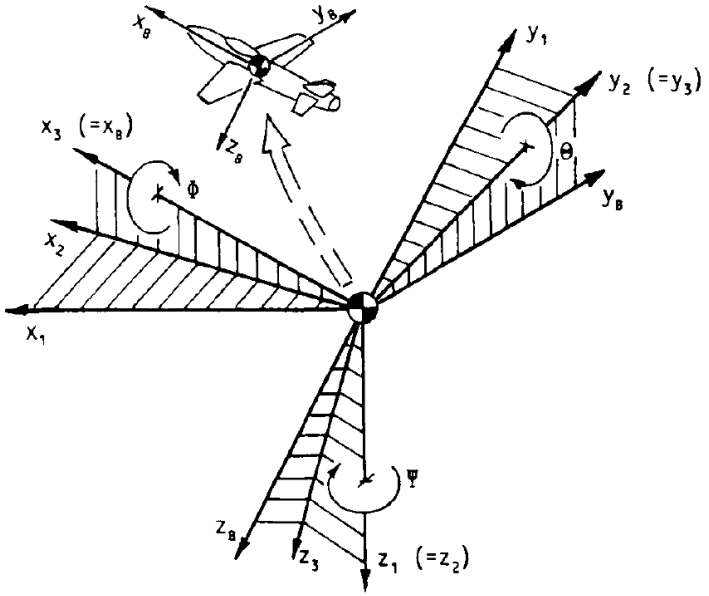

FIGURE 2.4 - Euler angle rotation sequence.
SOURCE - (SCHMIDT, 1998, p. 94)

Transformation matrices are used to represent these rotations, transforming a coordinate system to another. Then, the final transformation from the based reference frame X_1, Y_1, Z_1 is the ordered multiplication of the individual transformation matrices, given by:

$$\begin{Bmatrix} X \\ Y \\ Z \end{Bmatrix} = \boldsymbol{T_\Phi T_\Theta T_\Psi} \begin{Bmatrix} X_1 \\ Y_1 \\ Z_1 \end{Bmatrix} \tag{2.14}$$

where

$$\begin{aligned} \boldsymbol{T_\Phi} &= \begin{bmatrix} 1 & 0 & 0 \\ 0 & \cos\Phi & \sin\Phi \\ 0 & -\sin\Phi & \cos\Phi \end{bmatrix} \\ \boldsymbol{T_\Theta} &= \begin{bmatrix} \cos\Theta & 0 & \sin\Theta \\ 0 & 1 & 0 \\ -\sin\Theta & 0 & \cos\Theta \end{bmatrix} \\ \boldsymbol{T_\Psi} &= \begin{bmatrix} \cos\Psi & \sin\Psi & 0 \\ -\sin\Psi & \cos\Psi & 0 \\ 0 & 0 & 1 \end{bmatrix} \end{aligned} \tag{2.15}$$

In agreement with this process, an expression for the angular velocity vector is given by:

$$\vec{\omega} = \vec{\dot{\Psi}} + \vec{\dot{\Theta}} + \vec{\dot{\Phi}} \tag{2.16}$$

By definition, we also have that

$$\vec{\omega} = P\vec{\imath} + Q\vec{\jmath} + R\vec{k} \tag{2.17}$$

The angular velocity vector of the body related to the Earth is described by the individual contribution of each Euler angle rates component, then

$$\begin{Bmatrix} P \\ Q \\ R \end{Bmatrix} = \begin{bmatrix} \dot{\phi} \\ 0 \\ 0 \end{bmatrix} + \boldsymbol{T_{\Phi}} \left(\begin{bmatrix} 0 \\ \dot{\Theta} \\ 0 \end{bmatrix} + \boldsymbol{T_{\Theta}} \begin{bmatrix} 0 \\ 0 \\ \dot{\Psi} \end{bmatrix} \right) \tag{2.18}$$

Which can be expanded to

$$\begin{Bmatrix} P \\ Q \\ R \end{Bmatrix} = \begin{bmatrix} 1 & 0 & -\sin\Theta \\ 0 & \cos\Phi & \sin\Phi\cos\Theta \\ 0 & -\sin\Phi & \cos\Phi\cos\Theta \end{bmatrix} \begin{Bmatrix} \dot{\Phi} \\ \dot{\Theta} \\ \dot{\Psi} \end{Bmatrix} \tag{2.19}$$

Inverting the relationship shown in Eq. (2.19), we obtain the differential equations that describe the Euler angles rate given an angular velocity for the body. Then, the expression for the known Euler's Kinematic Equations is given by

$$\begin{Bmatrix} \dot{\Phi} \\ \dot{\Theta} \\ \dot{\Psi} \end{Bmatrix} = \begin{bmatrix} 1 & \sin\Phi\tan\Theta & \cos\Phi\tan\Theta \\ 0 & \cos\Phi & -\sin\Phi \\ 0 & \sin\Phi\sec\Theta & \cos\Phi\sec\Theta \end{bmatrix} \begin{Bmatrix} P \\ Q \\ R \end{Bmatrix} \tag{2.20}$$

Here we observe that Eq. (2.20) is valid subject to the constraint $\Theta \neq 90°$. For this value of pitch angle, there is ambiguity between roll and yaw, thus the matrix of Eq. (2.20) is non-invertible. For the analyses presented in this work, the aircraft pitch angle is constrained to small angles, which corresponds to common flight conditions. One alternative for the Euler angle approach is based on the use of quaternions, which can be applied for broader cases.

2.5 Forces and Moments

To complete the obtained aircraft dynamic models it is necessary to describe the forces and moments due to aerodynamics, propulsive and gravity effects. (NAPOLITANO, 2012)

2.5.1 Gravity forces

The gravity force is the product of the aircraft mass by the gravity acceleration. The gravity vector is parallel to the Z_e axis in the Earth inertial frame and can be expressed as

$$\vec{g} = g\vec{k} \tag{2.21}$$

In the body frame X, Y, Z, the gravity vector is defined by

$$\vec{g} = g_x\vec{i} + g_y\vec{j} + g_z\vec{k} \tag{2.22}$$

Then, based on the transformations shown in Section 2.4 we can relate these frames using Euler Angles, which are used to provide inputs for the Eq. (2.8).

$$\begin{aligned} g_x &= -g\sin\Theta \\ g_y &= g\cos\Theta\sin\Phi \\ g_z &= g\cos\Theta\cos\Phi \end{aligned} \tag{2.23}$$

2.5.2 Aerodynamic forces

The aerodynamic forces and moments acting in the aircraft are due to the pressure distribution over its surface, which depends of its geometry and of the relative motion between the aircraft and the wind. These aerodynamic effects can be calculated by empirical methods, computational fluid dynamics (CFD) software, wind-tunnel test or flight tests.

The small perturbation components of the forces are associated with the perturbation terms of linear and angular velocities, which is related to the relative motion between the aircraft and the wind. In addition, the deflections of the control surfaces for controlling the longitudinal and the lateral directional motion can be taken as small perturbation terms, since it does change the aircraft geometry.

Observing FIG. 2.3, we have that the angles of the wind relative to the body frame can be assumed as:

$$\begin{aligned} \tan\alpha = \frac{\sin\alpha}{\cos\alpha} \approx \frac{w}{V_{P_1}} \;\rightarrow\; \alpha \approx \frac{w}{V_{P_1}}, \quad \dot{\alpha} \approx \frac{\dot{w}}{V_{P_1}} \\ \tan\beta = \frac{\sin\beta}{\cos\beta} \approx \frac{v}{V_{P_1}} \rightarrow\; \beta \approx \frac{v}{V_{P_1}}, \quad \dot{\beta} \approx \frac{\dot{v}}{V_{P_1}} \end{aligned} \tag{2.24}$$

Therefore, assuming that the aircraft features elevator (δ_E), stabilators (i_H), ailerons (δ_A) and rudder (δ_R), we obtain the following relations to describe the small perturbation aerodynamic forces and moments:

$$\begin{aligned} f_{A_X} &= f_{A_X}(u, \alpha, \dot{\alpha}, q, \delta_E, i_H) \\ f_{A_Y} &= f_{A_Y}(\beta, \dot{\beta}, p, r, \delta_A, \delta_R) \\ f_{A_Z} &= f_{A_Z}(u, \alpha, \dot{\alpha}, q, \delta_E, i_H) \\ l_A &= l_A(\beta, \dot{\beta}, p, r, \delta_A, \delta_R) \\ m_A &= m_A(u, \alpha, \dot{\alpha}, q, \delta_E, i_H) \\ n_A &= n_A(\beta, \dot{\beta}, p, r, \delta_A, \delta_R) \end{aligned} \tag{2.25}$$

These forces and moments are expanded into first-order Taylor series with respect to its variables around the steady-state condition, then:

$$\begin{aligned} f_{A_X} = {} & \left.\frac{\partial F_{A_X}}{\partial u}\right|_{SS} u + \left.\frac{\partial F_{A_X}}{\partial \alpha}\right|_{SS} \alpha + \left.\frac{\partial F_{A_X}}{\partial \dot{\alpha}}\right|_{SS} \dot{\alpha} + \left.\frac{\partial F_{A_X}}{\partial q}\right|_{SS} q + \left.\frac{\partial F_{A_X}}{\partial \delta_E}\right|_{SS} \delta_E \\ & + \left.\frac{\partial F_{A_X}}{\partial i_H}\right|_{SS} i_H \end{aligned} \tag{2.26}$$

$$\begin{aligned} f_{A_Y} = {} & \left.\frac{\partial F_{A_Y}}{\partial \beta}\right|_{SS} \beta + \left.\frac{\partial F_{A_Y}}{\partial \dot{\beta}}\right|_{SS} \dot{\beta} + \left.\frac{\partial F_{A_Y}}{\partial p}\right|_{SS} p + \left.\frac{\partial F_{A_Y}}{\partial r}\right|_{SS} r + \left.\frac{\partial F_{A_Y}}{\partial \delta_A}\right|_{SS} \delta_A \\ & + \left.\frac{\partial F_{A_Y}}{\partial \delta_R}\right|_{SS} \delta_R \end{aligned}$$

$$\begin{aligned} f_{A_Z} = {} & \left.\frac{\partial F_{A_Z}}{\partial u}\right|_{SS} u + \left.\frac{\partial F_{A_Z}}{\partial \alpha}\right|_{SS} \alpha + \left.\frac{\partial F_{A_Z}}{\partial \dot{\alpha}}\right|_{SS} \dot{\alpha} + \left.\frac{\partial F_{A_Z}}{\partial q}\right|_{SS} q + \left.\frac{\partial F_{A_Z}}{\partial \delta_E}\right|_{SS} \delta_E \\ & + \left.\frac{\partial F_{A_Z}}{\partial i_H}\right|_{SS} i_H \end{aligned}$$

$$l_A = \left.\frac{\partial L_A}{\partial \beta}\right|_{SS} \beta + \left.\frac{\partial L_A}{\partial \dot{\beta}}\right|_{SS} \dot{\beta} + \left.\frac{\partial L_A}{\partial p}\right|_{SS} p + \left.\frac{\partial L_A}{\partial r}\right|_{SS} r + \left.\frac{\partial L_A}{\partial \delta_A}\right|_{SS} \delta_A + \left.\frac{\partial L_A}{\partial \delta_R}\right|_{SS} \delta_R$$

$$m_A = \left.\frac{\partial M_A}{\partial u}\right|_{SS} u + \left.\frac{\partial M_A}{\partial \alpha}\right|_{SS} \alpha + \left.\frac{\partial M_A}{\partial \dot{\alpha}}\right|_{SS} \dot{\alpha} + \left.\frac{\partial M_A}{\partial q}\right|_{SS} q + \left.\frac{\partial M_A}{\partial \delta_E}\right|_{SS} \delta_E + \left.\frac{\partial M_A}{\partial i_H}\right|_{SS} i_H$$

$$n_A = \left.\frac{\partial N_A}{\partial \beta}\right|_{SS} \beta + \left.\frac{\partial N_A}{\partial \dot{\beta}}\right|_{SS} \dot{\beta} + \left.\frac{\partial N_A}{\partial p}\right|_{SS} p + \left.\frac{\partial N_A}{\partial r}\right|_{SS} r + \left.\frac{\partial N_A}{\partial \delta_A}\right|_{SS} \delta_A + \left.\frac{\partial N_A}{\partial \delta_R}\right|_{SS} \delta_R$$

2.5.3 Propulsive forces

Unlike the small perturbations in the aerodynamic forces and moments, only a limited number of variables will significantly affect the propulsion characteristics. The following relations can be described:

$$\begin{array}{ccc} f_{T_X} = f_{T_X}(u,\alpha) & f_{T_Y} = f_{A_Y}(\beta) & f_{T_Z} = f_{A_Z}(u,\alpha) \\ l_T = l_A(\beta) & m_T = m_A(u,\alpha) & n_T = n_A(\beta) \end{array} \tag{2.27}$$

Assuming a nominal engine operating condition for general aircraft, we observe that the effects on thrust due to some variables are negligible, thus, the first-order Taylor series expansion around the steady-state condition are represented by:

$$\begin{array}{ccc} f_{T_X} = \left.\dfrac{\partial F_{T_X}}{\partial u}\right|_{SS} u & f_{T_Y} = 0 & f_{T_Z} = 0 \\ l_T = 0 & m_T = \left.\dfrac{\partial M_{T_X}}{\partial u}\right|_{SS} u + \left.\dfrac{\partial M_{T_X}}{\partial \alpha}\right|_{SS} \alpha & n_T = 0 \end{array} \tag{2.28}$$

2.6 Complete Model

Based on Sections 2.1 to 2.4, we have that the complete set of equations describing the aircraft motion is given by

$$\begin{aligned} &m\left(\dot{U} + QW - RV\right) = -mg\sin\Theta + \left(F_{A_x} + F_{T_x}\right) \\ &m\left(\dot{V} + UR - PW\right) = mg\,cos\Theta\sin\Phi + \left(F_{A_y} + F_{T_y}\right) \\ &m\left(\dot{W} + PV - QU\right) = mg\cos\Theta\cos\Phi + \left(F_{A_z} + F_{T_z}\right) \\ &\dot{P}I_{xx} - \dot{R}I_{xz} - PQI_{xz} + RQ\left(I_{zz} - I_{yy}\right) = L_A + L_T \\ &\dot{Q}I_{yy} + PR(I_{xx} - I_{zz}) + (P^2 - R^2)I_{xz} = M_A + M_T \\ &\dot{R}I_{zz} - \dot{P}I_{xz} + PQ\left(I_{yy} - I_{xx}\right) + QRI_{xz} = N_A + N_T \end{aligned} \tag{2.29}$$

Since general aircraft fly at a few specific flight condition, it is interesting to solve this set of equations of motion under stead-state and perturbed flight conditions, where the last is an important frame for analyzing the aircraft dynamics under maneuvers or atmospheric turbulence.

The steady-state condition for the motion variables are indicated here by the subscript "1" and the perturbations by lowercase. Thus, based on these notations, we have:

$$
\begin{array}{lll}
U = U_1 + u & V = V_1 + v & W = W_1 + w \\
P = P_1 + p & Q = Q_1 + q & R = R_1 + r \\
\Phi = \Phi_1 + \phi & \Theta = \Theta_1 + \theta & \Psi = \Psi_1 + \psi \\
F_{A_X} = F_{A_{X1}} + f_{A_X} & F_{A_Y} = F_{A_{Y1}} + f_{A_Y} & F_{A_Z} = F_{A_{Z1}} + f_{A_Z} \\
L_A = L_{A_1} + l_A & M_A = M_{A_1} + m_A & N_A = N_{A_1} + n_A \\
F_{T_X} = F_{T_{X1}} + f_{T_X} & F_{T_Y} = F_{T_{Y1}} + f_{T_Y} & F_{T_Z} = F_{T_{Z1}} + f_{T_Z} \\
L_T = L_{T_1} + l_T & M_T = M_{T_1} + m_T & N_T = N_{T_1} + n_T
\end{array}
\tag{2.30}
$$

The linear and angular accelerations with respect to the body frame are zero, then:

$$
\begin{array}{l}
\dot{U}_1 = \dot{V}_1 = \dot{W}_1 = 0 \\
\dot{P}_1 = \dot{Q}_1 = \dot{R}_1 = 0 \\
\dot{U} = \dot{u}, \quad \dot{V} = \dot{v}, \quad \dot{W} = \dot{w} \\
\dot{P} = \dot{p}, \quad \dot{Q} = \dot{q}, \quad \dot{R} = \dot{r} \\
\dot{\Phi} = \dot{\phi}, \quad \dot{\Theta} = \dot{\theta}, \quad \dot{\Psi} = \dot{\psi}
\end{array}
\tag{2.31}
$$

Given these definitions, we assume a small perturbation condition where:

- The products of linear and angular velocities are always zero
- The products of the Euler angles are negligible, $\sin(x) \approx x$, $\cos(x) \approx 1$ and $\tan(x) \approx x$.

We also assume that the perturbed conditions start from a steady-state rectilinear wing-level flight (PAMADI, 2004). Thus, the equations of motion take on the following simplified form:

$$
\begin{array}{l}
m(\dot{u} + qW_1) = -mg\ \theta \cos\Theta_1 + \left(f_{A_x} + f_{T_x}\right) \\
m(\dot{v} + U_1 r - pW_1) = mg\ \phi\ cos\Theta_1 + \left(f_{A_y} + f_{T_y}\right) \\
m(\dot{w} - U_1 q) = -mg\ \theta \sin\Theta_1 + \left(f_{A_z} + f_{T_z}\right) \\
\dot{p}I_{xx} - \dot{r}I_{xz} = (l_A + l_T) \\
\dot{q}I_{yy} = (m_A + m_T) \\
\dot{r}I_{zz} - \dot{p}I_{xz} = (n_A + n_T) \\
p = \dot{\phi} - \dot{\psi} \sin\Theta_1 \\
q = \dot{\theta} \\
r = \dot{\psi} \cos\Theta_1
\end{array}
\tag{2.32}
$$

2.7 Uncoupled Aircraft Equations of Motion

In the simplified form of the aircraft equations of motion, obtained due to the small-perturbations assumption, and taking the consideration for XZ symmetric plane, we observe that aircraft motion can be decoupled in two: longitudinal and lateral-directional. This separation allows us to evaluate each motion individually, which simplifies the system identification process and the dynamic mode analysis.

External forces and moments can be represented by aerodynamic and control coefficients. Here we use the dimensional stability and control derivatives to describe the forces and moments based on aircraft's geometry, inertial characteristics, flight speed, altitude and other flight conditions. They are represented as follows, observing that some derivatives from linearization in Eq. (2.29) are negligible (NAPOLITANO, 2012):

$$X_u = \frac{1}{m}\frac{\partial F_{A_X}}{\partial u} \quad X_{T_u} = \frac{1}{m}\frac{\partial F_{T_X}}{\partial u} \quad X_\alpha = \frac{1}{m}\frac{\partial F_{A_X}}{\partial \alpha} \quad X_{\delta_E} = \frac{1}{m}\frac{\partial F_{A_X}}{\partial \delta_E}$$

$$Y_\beta = \frac{1}{m}\frac{\partial F_{A_Y}}{\partial \beta} \quad Y_p = \frac{1}{m}\frac{\partial F_{A_Y}}{\partial p} \quad Y_r = \frac{1}{m}\frac{\partial F_{A_Y}}{\partial r} \quad Y_{\delta_A} = \frac{1}{m}\frac{\partial F_{A_Y}}{\partial \delta_A}$$

$$Y_{\delta_R} = \frac{1}{m}\frac{\partial F_{A_Y}}{\partial \delta_R} \quad Z_u = \frac{1}{m}\frac{\partial F_{A_Z}}{\partial u} \quad Z_\alpha = \frac{1}{m}\frac{\partial F_{A_Z}}{\partial \alpha} \quad Z_{\dot\alpha} = \frac{1}{m}\frac{\partial F_{A_Z}}{\partial \dot\alpha}$$

$$Z_q = \frac{1}{m}\frac{\partial F_{A_Z}}{\partial q} \quad Z_{\delta_E} = \frac{1}{m}\frac{\partial F_{A_Z}}{\partial \delta_E} \quad L_\beta = \frac{1}{I_{xx}}\frac{\partial L_A}{\partial \beta} \quad L_p = \frac{1}{I_{xx}}\frac{\partial L_A}{\partial p}$$

$$L_r = \frac{1}{I_{xx}}\frac{\partial L_A}{\partial r} \quad L_{\delta_A} = \frac{1}{I_{xx}}\frac{\partial L_A}{\partial \delta_A} \quad L_{\delta_R} = \frac{1}{I_{xx}}\frac{\partial L_A}{\partial \delta_R} \quad M_u = \frac{1}{I_{yy}}\frac{\partial M_A}{\partial u}$$

$$M_{T_u} = \frac{1}{I_{yy}}\frac{\partial M_{T_X}}{\partial u} \quad M_\alpha = \frac{1}{I_{yy}}\frac{\partial M_A}{\partial \alpha} \quad M_{\dot\alpha} = \frac{1}{I_{yy}}\frac{\partial M_A}{\partial \dot\alpha} \quad M_{T_\alpha} = \frac{1}{I_{yy}}\frac{\partial M_{T_X}}{\partial \alpha}$$

$$M_q = \frac{1}{I_{yy}}\frac{\partial M_A}{\partial q} \quad M_{\delta_E} = \frac{1}{I_{yy}}\frac{\partial M_A}{\partial \delta_E} \quad N_\beta = \frac{1}{I_{zz}}\frac{\partial N_A}{\partial \beta} \quad N_p = \frac{1}{I_{zz}}\frac{\partial N_A}{\partial p}$$

$$N_{\delta_A} = \frac{1}{I_{zz}}\frac{\partial N_A}{\partial \delta_A} \quad N_{\delta_R} = \frac{1}{I_{zz}}\frac{\partial N_A}{\partial \delta_R}$$

We assume that the body axes system coincides with the stability axes frame in the steady-state condition before the perturbation (PAMADI, 2004). Further, the aerodynamic forces and moments are expressed on the wind frame, we have that the only nonzero component of the linear velocity is along the X_S axis, then $U_{1_S} = V_{P_1}$ and $W_{1_S} = 0$. For small perturbation formulation, we have:

$$q \approx \dot{\theta}, \quad \dot{q} \approx \ddot{\theta}, \quad w \approx V_{P_1}\alpha, \quad \dot{w} \approx V_{P_1}\dot{\alpha}$$
$$v \approx V_{P_1}\beta, \quad \dot{v} \approx V_{P_1}\dot{\beta}, \quad p \approx \dot{\phi}, \quad \dot{p} \approx \ddot{\phi}, \quad r \approx \dot{\psi}, \quad \dot{r} \approx \ddot{\psi} \tag{2.33}$$

Therefore, using these dimensional coefficients and the previous considerations, the set of equations for each independent motion can be determined.

For both longitudinal and lateral-directional motions we will discuss the aircraft's free response, where we assume that the controls are held fixed (stick-fixed), in its neutral position, after the perturbation. These perturbations can be due a suddenly imposed gust or by moving the aircrafts controls.

2.7.1 Longitudinal

The longitudinal aircraft's motion is its behavior about the pitch-axis body reference frame. It is represented here by a set of four ordinary differential equations, with constant coefficients. Rearranging the equations from Eq. (2.32), which represent the longitudinal motion, and based on the previous assumptions, the aircrafts motion for elevator control is given by:

$$\begin{aligned}
\dot{u} &= \left(X_u + X_{T_u}\right)u + X_\alpha \alpha - g\cos\Theta_1\,\theta + X_{\delta_E}\delta_E \\
\dot{\alpha} &= \frac{Z_u}{\left(V_{P_1} - Z_{\dot{\alpha}}\right)}u + \frac{Z_\alpha}{\left(V_{P_1} - Z_{\dot{\alpha}}\right)}\alpha - \frac{g\sin\Theta_1}{\left(V_{P_1} - Z_{\dot{\alpha}}\right)}\theta + \frac{\left(Z_q + V_{P_1}\right)}{\left(V_{P_1} - Z_{\dot{\alpha}}\right)}q + \\
&\quad + \frac{Z_{\delta_E}}{\left(V_{P_1} - Z_{\dot{\alpha}}\right)}\delta_E \\
\dot{q} &= \left[M_{\dot{\alpha}}\left(\frac{Z_u}{\left(V_{P_1} - Z_{\dot{\alpha}}\right)}\right) + M_u\right]u + \left[M_{\dot{\alpha}}\left(\frac{Z_\alpha}{\left(V_{P_1} - Z_{\dot{\alpha}}\right)}\right) + M_\alpha\right]\alpha + \\
&\quad + \left[M_{\dot{\alpha}}\left(\frac{-g\sin\Theta_1}{\left(V_{P_1} - Z_{\dot{\alpha}}\right)}\right)\right]\theta + \left[M_{\dot{\alpha}}\left(\frac{\left(Z_q + V_{P_1}\right)}{\left(V_{P_1} - Z_{\dot{\alpha}}\right)}\right) + M_q\right]q + \\
&\quad + \left[M_{\dot{\alpha}}\left(\frac{Z_{\delta_E}}{\left(V_{P_1} - Z_{\dot{\alpha}}\right)}\right) + M_{\delta_E}\right]\delta_E \\
\dot{\theta} &= q
\end{aligned} \tag{2.34}$$

Here, we neglected the contribution associated with the propulsive dimensional coefficients in the pitch moment. Eq. (2.34) can be expressed in the state-space form as:

$$\{\dot{x}\} = [\boldsymbol{A}]_{Long}\{x\} + [\boldsymbol{B}]_{Long}\{\delta\} \tag{2.35}$$

where

$$\{x\} \triangleq \begin{Bmatrix} u \\ \alpha \\ q \\ \theta \end{Bmatrix}, \quad \{\delta\} = \{\delta_E\}$$
$$[\boldsymbol{A}]_{Long} = \begin{bmatrix} A_{11} & A_{12} & 0 & A_{14} \\ A_{21} & A_{22} & A_{23} & A_{24} \\ A_{31} & A_{32} & A_{33} & A_{34} \\ 0 & 0 & 1 & 0 \end{bmatrix}, \quad [\boldsymbol{B}]_{Long} = \begin{bmatrix} B_{11} \\ B_{21} \\ B_{31} \\ 0 \end{bmatrix} \tag{2.36}$$

The elements of matrices $[\boldsymbol{A}]$ and $[\boldsymbol{B}]$ are described by a relation between aerodynamic, propulsive and inertial coefficients, more detailed by NAPOLITANO (2012).

For a dynamically stable general aircraft, two longitudinal oscillation modes can be observed, which are represented by two pairs of complex conjugate roots of matrix $[A]_{Long}$. FIG. 2.5 shows typical values for the longitudinal complex conjugate roots for a general aircraft. The pair of the left correspond to a fast mode, also known as "short-period" and the pair of the right, known as "phugoid" is the long period (KIMBERLIN, 2003).

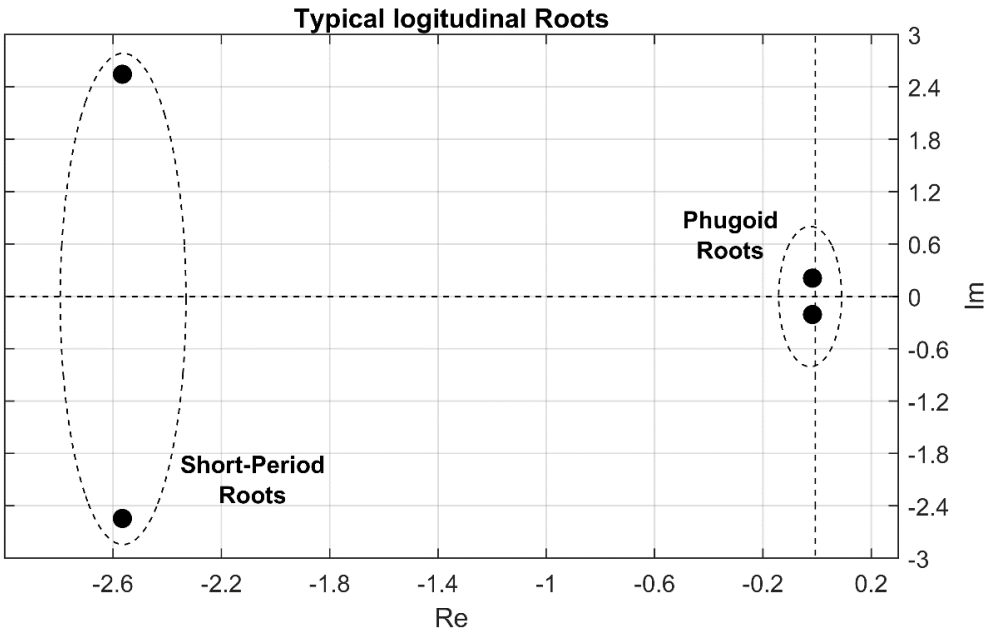

FIGURE 2.5 - Typical longitudinal roots for a general aircraft

The Phugoid mode is a lightly damped motion of low frequency. It is essentially an oscillation of the airspeed and altitude at a near constant angle of attack, alternating in climbing and diving, as shown in FIG. 2.6. It can also be interpreted as a swapping between gravitational potential energy and kinetic energy.

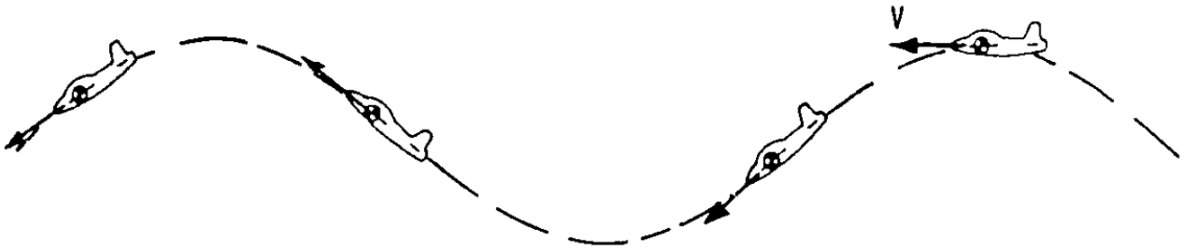

FIGURE 2.6 - Representation for the Phugoid mode
SOURCE - (SCHMIDT, 1998, p. 27)

The long period oscillations during a VFR (Visual Flight Rules) operation has such a long period that it does not make a significant difference to the pilot, which can suppress the motion based on the natural horizon with the pitch control. However, an IFR (Instrument Flight Rules) operation will require greater attention from the pilot to keep the airplane at the selected airspeed and altitude. Thus, it can be observed the importance to determine its characteristics, i.e., its natural frequency ($\omega_{n_{PH}}$) and damping coefficient (ζ_{PH}).

FIG. 2.7 shows a typical aircraft response after the “phugoid” excitation. It can be observed that the long period oscillation is predominantly represented by pitch angle and longitudinal speed oscillation in time, with a relatively low value of natural frequency and damping coefficient.

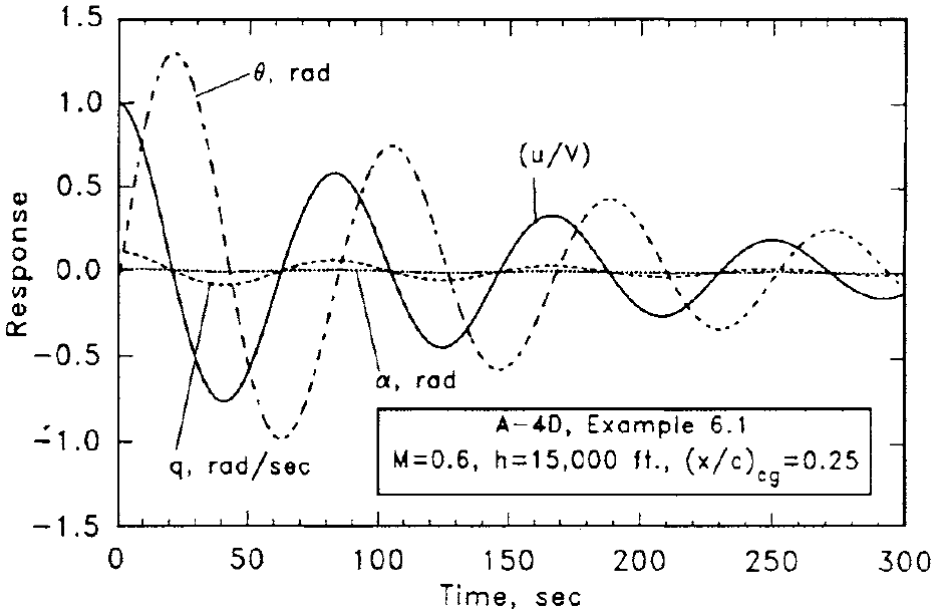

FIGURE 2.7 - Typical aircraft response during the Phugoid motion
SOURCE - (SCHMIDT, 1998, p. 171)

The Short-Period normally has a higher frequency and it is highly damped. Generally, in this mode a very small velocity perturbation (u) is observed when compared to the angle of

attack (α) or pitch-rate (q) components. In this natural response, the pitch attitude term (θ) has nearly the same magnitude as the angle of attack. Due to this, the aircraft CG will approach a straight horizontal path for this mode (SCHMIDT, 1998), as shown in FIG. 2.8.

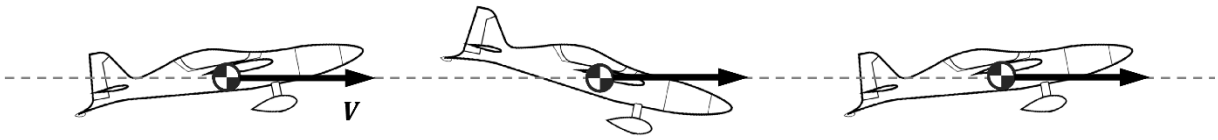

FIGURE 2.8 - Representation for the Short-Period mode

Due to the nature and frequency of the Short-Period mode, its motion is more closely related to typical maneuvering tasks which can turn the operation workload high during flight. If the aircraft presents a low natural frequency value, the pilot may think that the airplane is sluggish and, for some situations, hard to trim. If the mode presents a very high natural frequency value the airplane tends to respond too quickly, making any precise tracking task difficult (KIMBERLIN, 2003). Thus, the importance to determining its characteristics ($\omega_{n_{SP}}$ and ζ_{SP}).

FIG. 2.9 shows a typical aircraft response after the "short-period" perturbed excitation. As can be noted, the angle of attack and the pitch attitude respond nearly with the same magnitude by a small phase angle, with a very small velocity perturbation value. In addition, it can be observed that the mode is well damped with a faster decay of the oscillatory response.

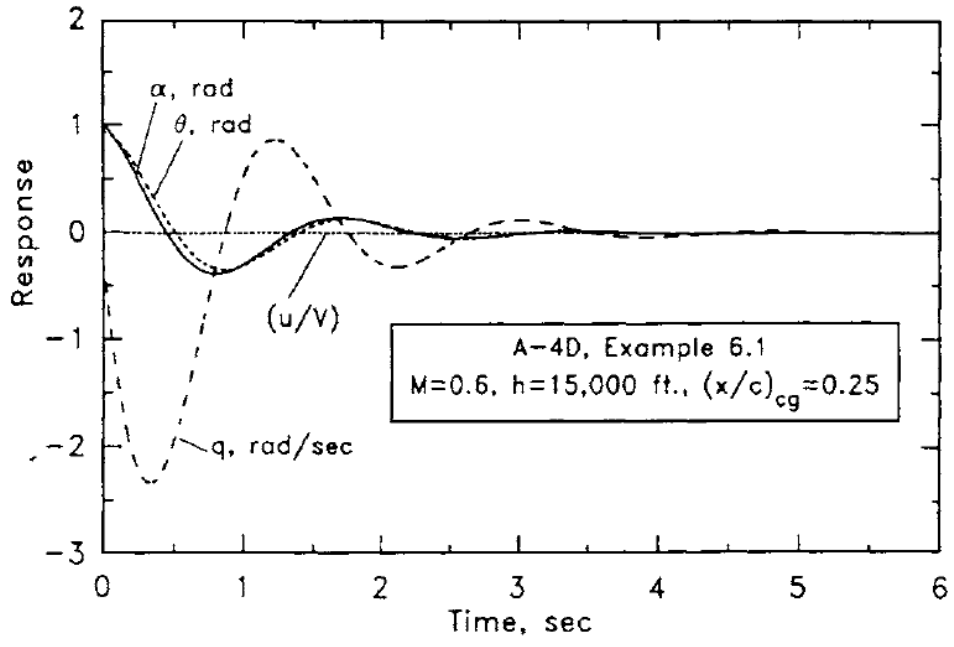

FIGURE 2.9 - Typical aircraft response during the Short-Period motion
SOURCE - (SCHMIDT, 1998, p. 169)

In summary, the preceding longitudinal parameters will depend on the specific aircraft, since each aircraft will have a specific mission and thus a particular design. However the following relationships can always be applied to them:

$$\omega_{n_{SP}} \gg \omega_{n_{PH}}, \qquad \zeta_{SP} \gg \zeta_{PH} \tag{2.37}$$

2.7.2 Lateral-Directional

The lateral-directional aircraft motion is its behavior about its roll and yaw axes. Such as for longitudinal motion, the lateral-directional motion is also represented by a set of four ordinary differential equations with constant coefficients. The equations to represent this motion can be obtained from Eq. (2.32) when $\dot{u} = \dot{w} = 0$, thus, $\dot{q} = 0$. Therefore, based on the previous assumptions, the aircraft motion for rudder and ailerons controls is given by:

$$\begin{aligned}
\dot{\beta} &= \frac{Y_\beta}{V_{P_1}}\beta + \frac{Y_p}{V_{P_1}}p + \frac{(Y_r - V_{P_1})}{V_{P_1}}r + \frac{g\cos\Theta_1}{V_{P_1}}\phi + \frac{Y_{\delta_A}}{V_{P_1}}\delta_A + \frac{Y_{\delta_R}}{V_{P_1}}\delta_R \\
\dot{p} &= \frac{(L_\beta + I_1 N_\beta)}{(1 - I_1 I_2)}\beta + \frac{(L_p + I_1 N_p)}{(1 - I_1 I_2)}p + \frac{(L_r + I_1 N_r)}{(1 - I_1 I_2)}r + \frac{(L_{\delta_A} + I_1 N_{\delta_A})}{(1 - I_1 I_2)}\delta_A + \\
&\quad + \frac{(L_{\delta_R} + I_1 N_{\delta_R})}{(1 - I_1 I_2)}\delta_R \\
\dot{r} &= \frac{(I_2 L_\beta + N_\beta)}{(1 - I_1 I_2)}\beta + \frac{(I_2 L_p + N_p)}{(1 - I_1 I_2)}p + \frac{(I_2 L_r + N_r)}{(1 - I_1 I_2)}r + \frac{(I_2 L_{\delta_A} + N_{\delta_A})}{(1 - I_1 I_2)}\delta_A + \\
&\quad + \frac{(I_2 L_{\delta_R} + N_{\delta_R})}{(1 - I_1 I_2)}\delta_R \\
\dot{\phi} &= p
\end{aligned} \tag{2.38}$$

where:

$$I_1 = \frac{I_{xy}}{I_{xx}}, \qquad I_2 = \frac{I_{xz}}{I_{zz}} \tag{2.39}$$

As in the previous case of the longitudinal equations, the Eq. (2.38) can be expressed in the state-space form as:

$$\{\dot{x}\} = [\boldsymbol{A}]_{LatDir}\{x\} + [\boldsymbol{B}]_{LatDir}\{\delta\} \tag{2.40}$$

where:

$$\{x\} \triangleq \begin{Bmatrix} \beta \\ p \\ r \\ \phi \end{Bmatrix}, \qquad \{\delta\} = \begin{Bmatrix} \delta_A \\ \delta_R \end{Bmatrix}$$

$$[\boldsymbol{A}]_{LatDir} = \begin{bmatrix} A_{11} & A_{12} & A_{13} & A_{14} \\ A_{21} & A_{22} & A_{23} & 0 \\ A_{31} & A_{32} & A_{33} & 0 \\ 0 & 1 & 0 & 0 \end{bmatrix}, \quad [\boldsymbol{B}]_{LatDir} = \begin{bmatrix} B_{11} & B_{12} \\ B_{21} & B_{22} \\ B_{31} & B_{32} \\ 0 & 0 \end{bmatrix}, \tag{2.41}$$

The elements of matrices $[\boldsymbol{A}]$ and $[\boldsymbol{B}]$ are described by a relation between aerodynamic, propulsive and inertial coefficients, more detailed in NAPOLITANO (2012).

In the lateral-directional motion, for a dynamically stable aircraft, three oscillation modes can be observed, which are represented by two real roots and a pair of complex conjugate roots of matrix $[\boldsymbol{A}]_{LatDir}$. The first real root is highly negative and represents the Roll Subsidence mode. The second real root is small, and can be negative or positive, that is when the mode is slightly divergent, and corresponds to the Spiral mode. The pair of complex roots, which represent an oscillatory motion, is associated to the Dutch Roll mode (PAMADI, 2004). FIG. 2.10 shows typical values for the lateral-directional roots.

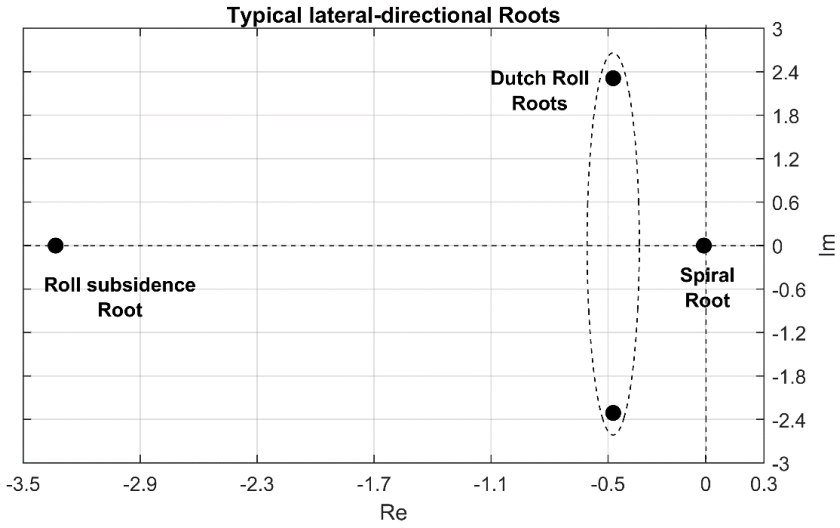

FIGURE 2.10 - Typical lateral-directional roots for a general aircraft

The Dutch Roll mode can be described as an oscillation motion coupling roll and yaw. Its behavior is very significant to the pilot's opinion of the aircraft, since this mode is related to sideslip angle variation during crosswind landings and can be excited by lateral-directional control input during flight. Thus, it is desirable to have a relatively heavy damped motion. FIG.2.11 shows a schematic of the aircraft response after during a Dutch Roll excitation.

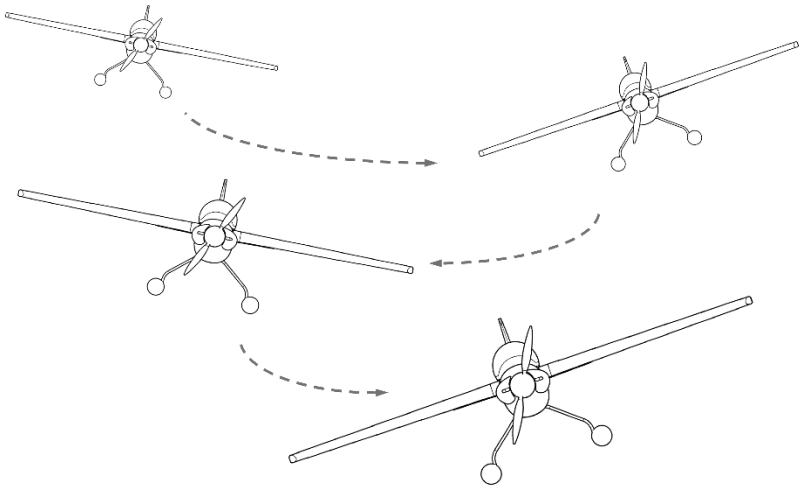

FIGURE 2.11 - Representation for the Dutch Roll mode

From the evolution of the jet aircraft with swept-back wings for high-speed flight operations, they began to observe aircrafts with lightly damped or even unstable Dutch Roll modes. From this, it was introduced a feedback control concept, known as yaw damper, which is better designed when the Dutch Roll characteristics are well known. Therefore, the importance to determine the Dutch-Roll's characteristics as much precise as possible.

The Roll Subsidence can be observed as a first order response in roll rate about the longitudinal body axis X (FIG. 2.12). It involves the ability to develop roll rates and roll angles during maneuvers in flight, since one way to make a heading change is to bank the aircraft. The ailerons are the primarily control to roll the aircraft, and it is important for the pilot to understand the roll acceleration and rate when the controls are moved or when an anti-symmetric wing span loads are induced by atmospheric turbulence. Based on the simplified model, when an aileron step is applied, the aircraft will roll until it reaches a steady-state, then it will continue to roll, but at a constant value of p.

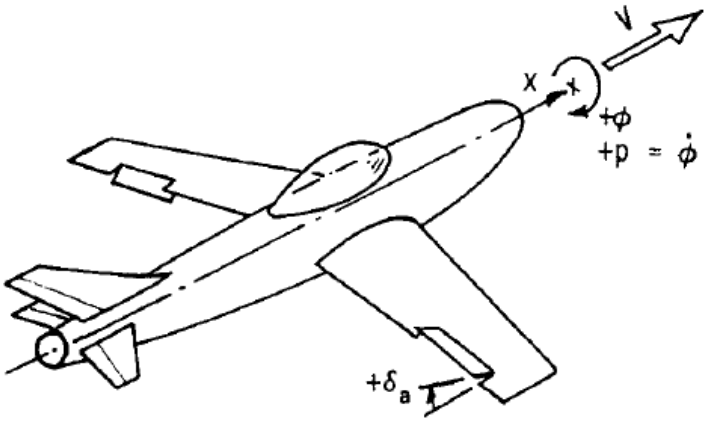

FIGURE 2.12 - Representation for the Roll subsidence mode
SOURCE - (SCHMIDT, 1998, p. 209)

The Spiral mode of motion can be described as bank angle variation after a disturbance from wings level flight. It can increase or decrease, since the Spiral can be slightly divergent. The bank angle variation in this mode is very gentle, which makes it easily controlled by the pilot. However, during IFR condition, the pilot can experience an undesirable condition, which can be refined using a feedback control system. Thus, the importance to evaluate spiral characteristics (ROSKAM, 2001). A schematic of the Spiral mode can be observed in FIG.2.13.

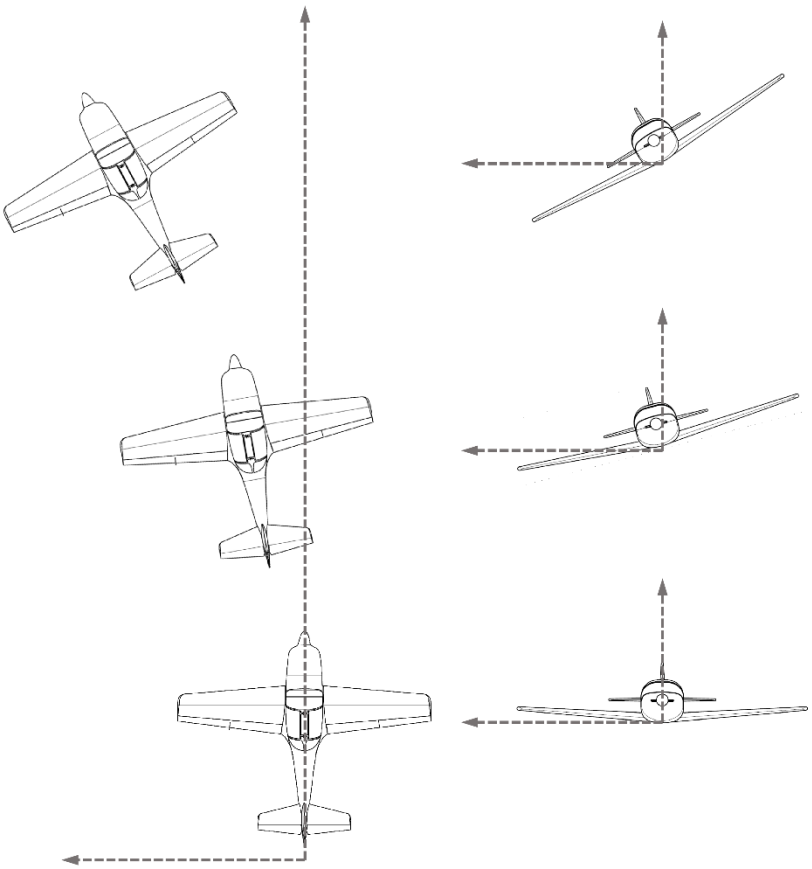

FIGURE 2.13 - Representation for the Spiral mode

In summary, we observe that the lateral-directional motion will influence in the aircraft's capacity to develop sideslip for purposes to maintaining a desired ground track during landing and takeoff flight phases. Moreover, to maintain a trim condition for straight flight while asymmetrical forces and moments are experienced due to atmospheric-turbulences or to an engine-out situation in a multi-engine aircraft (SCHMIDT, 1998).

2.8 Model Approximations

As shown, the Short-Period mode is an oscillatory motion mainly observed through the angle of attack (α) and pitch rate (p) responses. Its motion can be approximated by a 2nd order

model assuming that: i) the aircraft airspeed is maintained constant along the motion; ii) the aircraft only rotates about its CG and slightly varies in the Z direction; iii) the perturbation starts from a steady state level flight with $\theta_0 \approx 0$. Thus a simplified expression is obtained, as shown in Eq. (2.42). More details about the coefficients of matrices $[\boldsymbol{A}]$ and $[\boldsymbol{B}]$ can be obtained in PAMADI (1949) and SCHMIDT (1998).

$$\begin{Bmatrix} \dot{\alpha} \\ \dot{q} \end{Bmatrix} = \begin{bmatrix} A_{11} & A_{12} \\ A_{21} & A_{22} \end{bmatrix} \begin{Bmatrix} \alpha \\ q \end{Bmatrix} + \begin{bmatrix} B_{11} \\ B_{21} \end{bmatrix} \{\delta_E - \bar{\delta}_E\} \tag{2.42}$$

An approximation model is also obtained for the Dutch Roll mode, assuming that the rolling motion during the response is small and also the variation in the bank angle, i.e., $\phi = p \approx 0$. Thus, the Dutch-Roll is mainly observed through the sideslip angle and the yaw rate after the perturbation. The approximated mode can be expressed by Eq. (2.43). More details about the coefficients of matrices $[\boldsymbol{A}]$ and $[\boldsymbol{B}]$ can be obtained in PAMADI (2004).

$$\begin{Bmatrix} \dot{\beta} \\ \dot{r} \end{Bmatrix} = \begin{bmatrix} A_{11} & A_{12} \\ A_{21} & A_{22} \end{bmatrix} \begin{Bmatrix} \beta \\ r \end{Bmatrix} + \begin{bmatrix} B_{11} & B_{12} \\ B_{21} & B_{22} \end{bmatrix} \begin{Bmatrix} \delta_A - \bar{\delta}_A \\ \delta_R - \bar{\delta}_R \end{Bmatrix} \tag{2.43}$$

3 FLIGHT TESTING AND DATA ACQUISITION

The flight test presented here belongs to the class “flight testing for system identification”. These tests are carried out to analyze the dynamic response of the aircraft to specific control inputs, or perturbation. It can be used for the estimation of stability and control derivatives and also for flight quality determination.

For flight tests, the aircraft must be instrumented for a high quality data acquisition. In addition, the input controls must be good enough for a reliable motion analysis. Recently, due to technological development, high quality instruments have become more accessible, which enables more accurate testing.

In this work, the data are used for aircraft dynamic motion analysis, which is done by using system identification techniques and other classical methods. For this purpose, the required measurements in flight are: linear acceleration, angular acceleration, control surfaces deflection, aircraft attitude angles (Euler angles, Section 2.4), wind angles related to the body axes (angle of attack and sideslip angle), and static and total pressure for relative velocity determination. Other quantities like throttle, other engine parameters and stick force, which are generally determined during flight tests, are not needed for the proposed analysis, thus they are out of the scope of this work.

3.1 Aircraft Instrumentation

The instrumentation system (or data acquisition system) is composed of a central computer, which receives data from the peripheral instruments (FIG. 3.1). These instruments can output digital or analog data; therefore, it is important to use an ADC (Analog-to-Digital Converter) for measurements to be sent to the central computer, which is responsible for storage for future analysis. Moreover, this central computer can also be connected to a telemetry system to send data to the ground station for real time data observation. One example of an acquisition system can be seen in (ISCOLD, 2008).

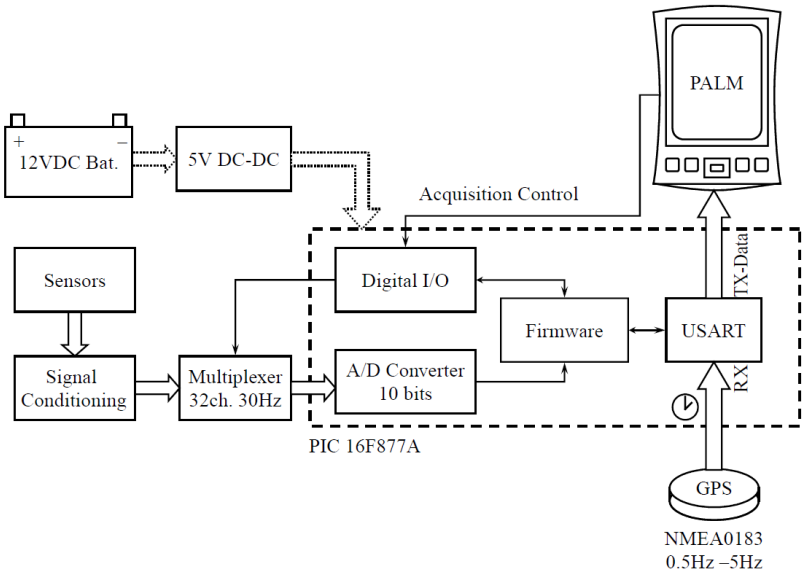

FIGURE 3.1 - Flight data acquisition system scheme
SOURCE - (ISCOLD, 2008)

According to JATEGAONKAR (2015), the rate of acquisition must be around 20-25 Hz for data analysis, when assuming a rigid-body model. In agreement with WARD (1998, p. 209), "the sampling theorem states that the sampling rate must be at least twice that of the highest frequency of interest", since the faster responses of general aircrafts have a frequency value far above 10 Hz. Furthermore, it is always preferable to record the raw data, since it can be properly observed and, if necessary, filtered before analysis.

Ideally, every data channel must have the same rate of acquisition, simplifying the application of the system identification methods. However, such techniques can also be applied for different data acquisition rate. Besides, it is important to have a synchrony between all data channel of the system. In addition, the sensors must by calibrated in laboratory for a higher quality measurement and noise reduction.

The quality of the data will depend on the availability of higher quality instruments, which is dependent on the available budget. However, due to the greater availability of technology in recent years, even more simple systems may provide data with a satisfactory quality. The instruments generally used to measure the relevant variables are described, as follows:

i. Inertial Measuring Unit (IMU): The linear accelerations and angular rates along the body axes X,Y,Z, generally are obtained using a inertial navigation system (INS), also called IMU, which is an integral unit that provides these measurements and also the aircraft attitude. The provided attitude angles from most of IMU's are calculated through internal integration of the measured angle rates. Some IMU's also uses a

magnetometer to improve the attitude estimation. This unit should be accurate enough to make sure that the raw data can be used in an accurate analysis of the aircraft motion. Since we are assuming a rigid-body model, only a single IMU is sufficient for the measurements (JATEGAONKAR, 2015). Generally, the angular acceleration are not measured directly but derived by numerical differentiation methods to be used in the system identification techniques.

ii. Linear Variable Differential Transducer (LVDT): This device is used to measure the linear displacement in the movement of an object along a direction. For flight tests, it is connected to control joints, cables or bars and in a fixed point into the aircraft to measure the surface deflections during flight.

For calibration, the surfaces are deflected and a digital inclinometer is used to measure its angle of deflection. Then, the obtained values are compared with the digital values read by the ADC in the central computer. An example of this procedure can be observed in DUTRA (2010). Besides the primary controls (ailerons, elevator and rudder), it is also important to measure other surfaces such as flaps, speed brakes, etc. In addition, all the calibration procedures and instruments installation must be done carefully, since it measure the inputs in the observed model, which affect directly the estimation results.

iii. Aerodynamic-probe: The aerodynamic probes are used to measure angle-of-attack, sideslip-angle and airspeed. The wind angles are commonly measured by using or mechanical vanes or multi-hole probes (JATEGAONKAR, 2015). In both devices, there are also a static and a total pressure intakes, which is necessary to measure the airspeed. The multi-hole probe must be carefully calibrated in a wind tunnel to determine the pressure difference between the ports for different flow angles (JATEGAONKAR, 2015). More details about these instruments can be found in (MALAQUIAS *et al,* 2012; BORGES, 2008; NCAR Bulletin 21, 2000).

3.2 Flight Procedures

During a flight test campaign with certification purposes, the maneuvers and measurements must be done for different flight situations, in agreement with the certification rules (United States Code of Federal Regulations, Title 14, Part 23) (United States Code of Federal Regulations, Title 14, Part 25). However, in this work, since only the method for flight dynamic analysis is under discussion, different aircraft data are analyzed for different flight situations. The flight tests consist of the following:

1. The pilot must put the airplane at the specified altitude and velocity. “It is recommended to start each maneuver from a trimmed level flight, and allow about 5-10 s of steady flight before applying specific control inputs” (JATEGAONKAR, 2015, p. 34). As a rule of thumb, if the aircraft is maintained within 0.5 KEAS and 20 feet during this time, then we assume a satisfactory trim condition;
2. The trim controls and stick are adjusted such that the aircraft reach the equilibrium condition with leveled wings and constant speed;
3. The pilot input controls with a specific maneuver to excite an aircraft mode (Section 3.3), returns and hold the stick in the equilibrium position and wait for the aircraft response. (If an stick-free analysis is required, the maneuvers are the same but after returning the control to equilibrium position, the pilot must be release them).

This sequence must be repeated more than once to obtain data both for analysis and validation, and can be scheduled for a single flight (DUTRA, 2010). It is recommended to verify the acquired data on-site to be sure that it is appropriate for analysis (JATEGAONKAR, 2015).

3.3 Maneuvers

For aircraft dynamic analysis, each mode must be excited for the pre-established flight conditions. In the analysis of a mode, it is important it to excite each of them for data observation, since the rule “If it is not in the data, it cannot be modeled” (JATEGAONKAR, 2015, p. 29) must be applied. This is a crucial step of the flight tests for a successful motion analysis, since, as shown, the non-correct excitation of a mode prevents its identification and analysis.

To excite the aircraft several different inputs could be used. However, it is interesting to have specific maneuver that excite each mode individually, which allows an easier observation of the aircraft motion and makes the analyses simpler. Further, it is recommended to use independent control inputs for each dynamic mode excitation, and maneuvers that can be executed manually by the pilot. The ideal inputs cannot be achieved by the pilot, even if using automatic flight control systems, since it is not possible to achieve an infinite rate of surface deflection. However, the exact execution of the motion is not a critical factor for dynamic motion excitation. Nevertheless, a smooth but rapid deflection is preferable for better results.
Techniques for aircraft dynamics excitation are presented by JATEGAONKAR (2015), KIMBERLIN(2003), WARD (1998) and in aeronautical regulatory documents (Advisory

Circular 23-8C Flight Test Guide for Certification of Part23 Airplanes, 2011; Advisory Circular 25-7C Flight Test Guide for Certification of Part25 Airplanes, 2012; UNITED STATES AIR FORCE, 1980). For each specific mode, common flight maneuvers are presented.

3.3.1 Short-Period excitation

The short-period frequency and damping have great influence on the pilot's rating about the aircraft flight quality, since he/she will sense these parameters through visual and tactile perceptions. The most common maneuver used to excite this dynamic mode is called doublet. However, JATEGAONKAR (2015) shows another maneuver to excite the fastest responding longitudinal mode, a multistep input with the elevator called "3-2-1-1", shown in FIG. 3.2.

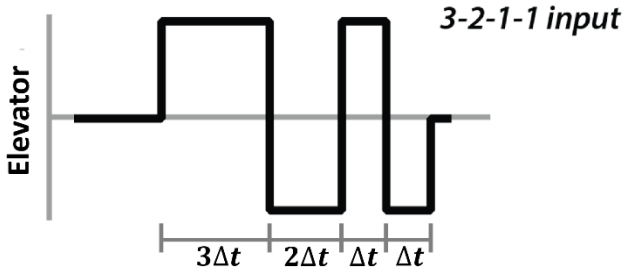

FIGURE 3.2 - "3-2-1-1" maneuver

The optimal value of Δt (for this maneuver we call it Δt_{3211}) is chosen for each aircraft to excite its natural frequency response. An estimate for Δt_{3211} is given by:

$$\Delta t_{3211} \approx \frac{2.1}{\omega_n} \approx \frac{1}{3}.period\ of\ oscillation \approx \frac{0.3}{f_c} \tag{3.1}$$

where ω_n and f_c are the frequency of the mode to be excited in $\mathrm{rad/s}$ and Hz, respectively. Eq. (3.1) can be used as rule of thumb, since its results is quite effective for most of aircrafts. The short-period frequency to use in Eq. (3.1) can be estimated based on aerodynamic coefficients obtained during the aircraft design. If these data are not available, data of similar aircraft can also be used. An estimation for $\omega_{n_{SP}}$ is based on short-period motion simplification (SCHMIDT, 1998) and is dependent of the aircraft's pitching moment due to the angle of attack (M_α) and is given by:

$$\omega_{n_{SP}} = (-M_\alpha)^{\frac{1}{2}} \tag{3.2}$$

Both Doublet and 3-2-1-1 are good inputs to excite the short period, since they are capable to excite this mode without exciting the phugoid mode. The time variation steps Δt for

both will change for different flight conditions (altitude and airspeed); however, in the 3-2-1-1 in spite of some deviations it is still capable to excite the natural frequency, which makes it simpler to execute the maneuver manually. Then, since the short-period is generally the fastest dynamic response of the aircraft, the 3-2-1-1 maneuver is preferable, and the Doublet is more indicated to excite the Dutch-Roll mode. More details about these maneuvers can be obtained in JATEGAONKAR (2015).

In practice, the pilot can use a technique to match the Δt repeatability for the several excitations. It can be done just by counting "twenty-one, twenty-two, twenty-three" to keep the stick in one side, "twenty-one, twenty-two" on the other side, "twenty-one" reverting stick position and finally "twenty-one" to bring stick back to the opposite position. The inputs amplitude must be chosen such as to result in a variation of about $\pm 3 \sim 4\ deg$ in the angle of attack about the trim, or of $\pm 0.4 \sim 0.5 g$ in the load factor. Typically, this maneuver and response has a duration of $15 \sim 20$ seconds. Moreover, if the pilot senses that the aircraft is not being excited using the estimated Δt_{3211}, he/she should try different frequencies, until the short period frequency is found.

3.3.2 Phugoid excitation

The slowest longitudinal response can be excited either by elevator pulse or thrust variation. Here we excite this mode using a pulse with the elevator. The surface must be displaced and held until reduce (or increase) the indicated airspeed approximately $5 \sim 10\%$ from trim airspeed. Then, the elevator is returned carefully to the trim position FIG. 3.3.

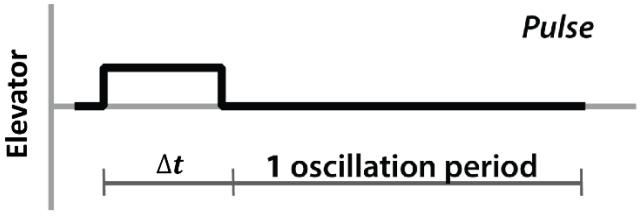

FIGURE 3.3 - Elevator pulse input

Another manner to estimate the time length for the pulse input is based on phugoid natural frequency value ($\omega_{n_{PH}}$) , given by:

$$\Delta t \approx \frac{2\pi}{\omega_{n_{PH}}} \approx \frac{6.3}{\omega_{n_{PH}}} \tag{3.3}$$

where the long period natural frequency can by estimated by a simplified model shown by KIMBERLIN (2003):

$$\omega_{n_{PH}} \approx \frac{\sqrt{2}g}{V_{P_1}} \tag{3.4}$$

where V_{P_1} is given in knots and g is the gravitational acceleration. In practice, due to the long time response of this mode, it is possible for the pilot to observe during the test if the mode has been excited. Further, after the pulse input the pilot must keep the elevator (or other longitudinal controls) as nearly as possible of the trim position; however, small lateral controls to keep the wings level are allowed during the oscillation, since avoiding bank angles higher than $5\sim10°$.

For the analysis based on system identification methods, only one full cycle of the phugoid is required (JATEGAONKAR, 2015), however, for other methods it is important to observe a larger part of the response, i.e., three or even four cycles.

3.3.3 Dutch Roll excitation

The lateral-directional oscillatory mode can by excited by different input forms, such as rudder pulse, rudder doublet and aileron pulse. The 3-2-1-1 maneuver can also be used here, however, the Dutch Roll is generally lightly damped when compared with the longitudinal Short Period mode. Thus, other inputs are preferable. The pulse input generally tends to excite the spiral mode causing a wing to drop. For aircrafts with large mass and inertias, the aileron pulse often result in a better Dutch Roll excitation. On the other hand, for general aircraft, the rudder doublet is the most common technique. The rudder doublet is applied by depressing the pedals in one direction holding by a pre-established time step, then depressing the pedals in the opposite side with the same magnitude holding by the same time step, and returning to the neutral position, as shown in FIG. 3.4.

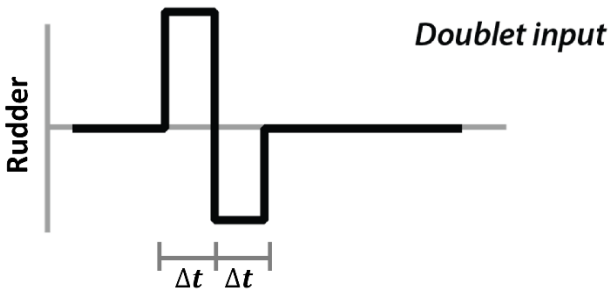

FIGURE 3.4 - Rudder doublet input

The time step for the doublet can be estimated by:

$$\Delta t \approx \frac{2.3}{\omega_n} \approx \frac{1}{2.7} \, . period \; of \; oscillation \tag{3.5}$$

In practice, a simpler factor of ½ is often used. A precise value for $\omega_{n_{SP}}$ can be calculated by wind tunnel test data and/or by semi-empirical estimative. However, if these are not available, Eq. (3.6) can be used for its estimation, which is based on simplified lateral-directional motion assumptions, where M is the Mach number, γ is the specific heat ratio, P_a is the absolute pressure in pounds per square foot, S is the wing are, b is the wing span, I_{zz} is the moment of inertia in yaw and C_{n_β} is the coefficient of yaw moment due to sideslip angle.

$$\omega_{n_{DR}} \cong M \sqrt{C_{n_\beta} \frac{\gamma P_a S b}{2 I_{zz}}} \tag{3.6}$$

Data of similar aircraft can be useful for a first assumption of natural frequency. Since this mode is easier to sense by the pilot, he/she can change the time step until feel that the Dutch Roll has been excited. Typically, the maximum peak-to-peak in the sideslip angle is on the order of $\pm 4°$, which is a reference to estimate the input amplitudes.

3.3.4 Roll Subsidence excitation

The rolling motion corresponds to a first-order system, thus the maneuvers applied here are used to observe the time constant of its response. Further, these inputs are used to observe the maneuverability of the aircraft. This mode is most often excited by application of a bank-to-bank maneuver (FIG. 3.5).

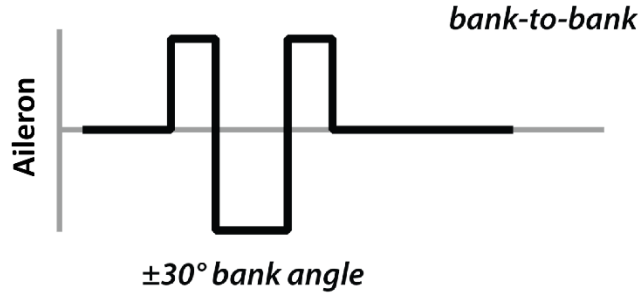

FIGURE 3.5 - Aileron bank-to-bank input

Procedurally, from a steady-state level flight, an aileron step input is applied until reach a chosen bank angle, then, another step with the same magnitude is applied to the opposite side; once stabilized at this bank angle the stick is moved to return the wings to the leveled condition.

Generally, an initial choice of 30° for the bank angle is reasonable. However, if the airplane presents a fast response, different bank angles (45° and 60°) must be tested. According to (JATEGAONKAR, 2015), this maneuver has a typical duration of 30-40s.

3.3.5 Spiral excitation

This mode is the one with the higher response time and for several aircrafts is slightly divergent. To excite it, the pilot must carefully trim the aircraft. Then, using ailerons or rudder (it is important to use only one of the controls at time), the aircraft is banked to an angle of approximately 10°. After step input, the control must return to neutral position and the dynamic response is observed. (FIG.3.6)

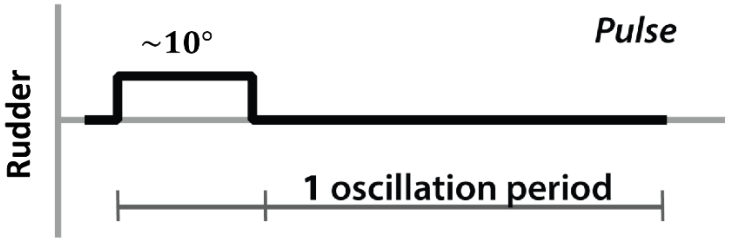

FIGURE 3.6 - Rudder pulse input

During the spiral response the elevator must be slightly deflected to maintain a constant airspeed. The maneuver must be recorded time enough to observe how long the spiral takes to double its amplitude (for divergent motion) or to half the amplitude (for convergent motion). During these tests, it is also important to avoid bank angles higher than 20°, since the linearized assumptions for the aircraft model are no more valid for these situations. In a flight test campaign, the spiral must be observed for both flight directions. For multi-engine aircraft, “care must be taken to ensure that all engines are producing the same thrust; otherwise, the asymmetric moment produced by engines will overpower the spiral mode behavior” (WARD e STRGANAC, 1998).

4 DATA REDUCTION METHODS

A flight data acquisition system is used during the maneuver execution to record the aircraft motion, as mentioned in Section 3.1. For data reduction, several classical methods can be used, which are based on simplification assumptions for the aircraft motion and graphical interpretation. Here other different techniques for data analysis are shown, which are based on system identification methods. In addition, the Nonlinear Least Squares method is proposed as an alternative for a fast data analysis.

4.1 Classical Methods

Some simple methods are proposed by WARD (1998), KIMBERLIN (2003) and CHALK (1969) for data reduction. These basic tools are described by several graphical interpretations to determine the parameters for each dynamic mode. They are simple to use and can be easily implemented for a faster analysis. These methods assume that the oscillatory motions can be described as a damped sinusoid, representing a second-order system. The range of applicability of the most often used graphical methods are described in TAB. 4.1.

TABLE 4.1 - Graphical Methods for Data Reduction

Method	**Range of Applicability**
Transient Peak Ratio (TPR)	$-0.5 < \zeta < 0.5$
Modified TPR (MTPR)	$-0.5 < \zeta < 0.5$
Time-Ratio (TR)	$0.5 < \zeta < 1.2$
Maximum Slope (MS)	$0.5 < \zeta < 1.2$

SOURCE - (WARD e STRGANAC, 1998)

4.1.1 Transient Peak Ratio method (TPR)

The TPR, also known as Log Decrement Method (YECHOUT, MORRIS, *et al.*, 2003), is the most usable method for oscillatory motions of damping coefficient ζ value between -0.5 and 0.5. As rule of thumb, this method can be applied to transient responses that has three or more overshoots, which is common to observe in the Phugoid, Short-Period and Dutch-Roll modes. It assumes that any of the oscillatory responses of an aircraft can be isolated and interpreted as a second order response. In addition, it is considered that the data being analyzed begins with zero slope at the initial time.

FIG. 4.1 shows the parameters that must be measured from the aircraft response data, i.e., the distance of the peaks from the steady state condition, and the half time of the period

$T/2$, which can also be measured as the time between local maximum and minimum peaks. From these values the transient peak ratios must be determined.

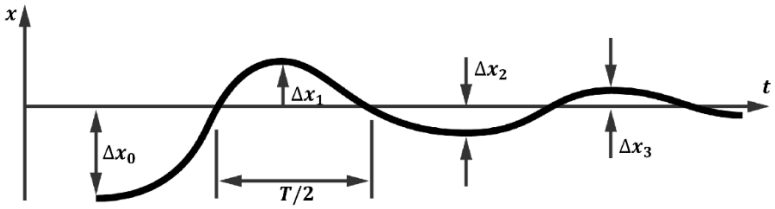

FIGURE 4.1 - Parameter for Transient Peak Ratio Analysis

$$TPR = \frac{\Delta x_1}{\Delta x_0} = \frac{\Delta x_2}{\Delta x_1} = \frac{\Delta x_3}{\Delta x_2} = \cdots \tag{4.1}$$

Based on the TPR, the chart of FIG. 4.2 is used to determine the damping ratio value. The natural frequency ω_n is obtained from the damping ratio and period using the relation in Eq. (4.2), where it is assumed a 2nd order model:

$$\omega_n = \frac{2\pi}{T\sqrt{1-\zeta^2}} \tag{4.2}$$

Another way to use this method is known as Modified Transient Peak Ratio (MTPR), where the transient response peaks also must be determined, but it is not necessary the determination of the equilibrium. The MTPR is quite similar to the TPR, and more details of it can be found in WARD (1998). Typically, the ratios obtained are not identical when measured from flight data, thus, its average is often used.

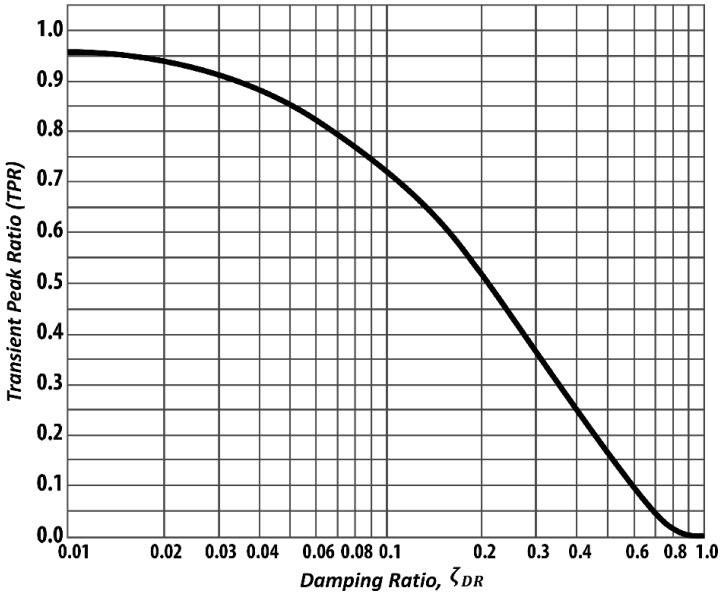

FIGURE 4.2 - Chart for Transient Peak Ratio Analysis. Adapted from WARD (1998)

4.1.2 Time-Ratio method (TR)

The TR is used for determining the response characteristics of relatively most damped modes, such as Short-Period and Dutch-Roll. From the transient response data, three values at specific points must be measured, as shown in FIG. 4.3. These points are located in the transient response in $0.736\Delta x$, $0.406\Delta x$, and $0.199\Delta x$ below the final steady state value, which must be previously measured.

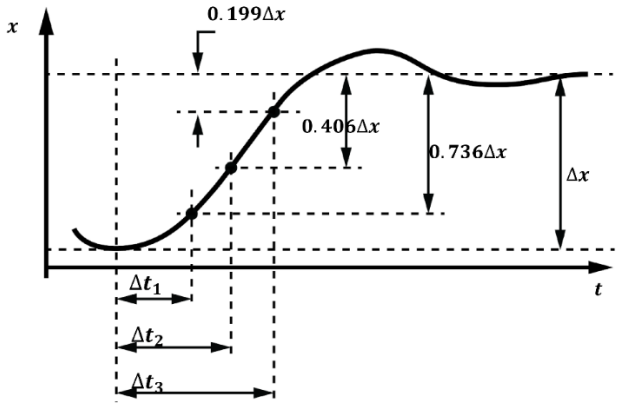

FIGURE 4.3 - Parameter for Time Ratio Analysis

The ratios $\Delta t_2/\Delta t_1$, $\Delta t_3/\Delta t_1$ and $(\Delta t_3 - \Delta t_2)/(\Delta t_2 - \Delta t_1)$ are calculated and used to enter the chart shown in FIG. 4.4, which results in three estimation of damping ratio ζ. Based on these values, the natural frequencies can be obtained in the same way as for damping. The test team "should use some engineering judgment in considering which damping ratio to choose" (WARD e STRGANAC, 1998), or if an average of the values are more plausible.

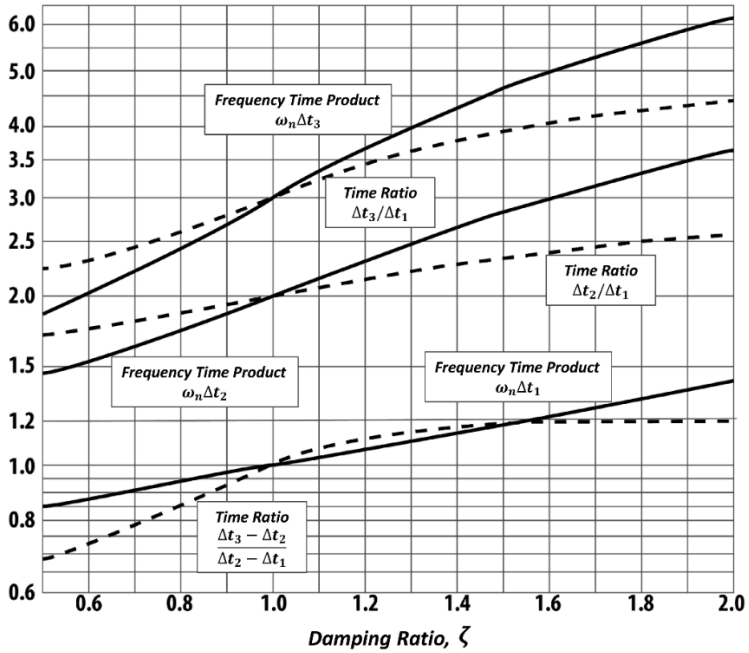

FIGURE 4.4 - Chart for Time Ratio Analysis. Adapted from WARD(1998)

4.1.3 Maximum Slope method (MS)

The MS is an alternative for the Time-Ratio Method. It is also used for relatively highly damped oscillatory motions, with a damping ratio between 0.5 and 1.2. These characteristics are generally observed in fast response aircrafts like the aerobatic ones, and commonly represents the Short-Period response behavior. The parameters shown in FIG. 4.5 must be measured from flight data, which are the peak amplitude of the motion response Δx, the maximum slope of the tangent in the transient rise motion and fraction of period ΔT.

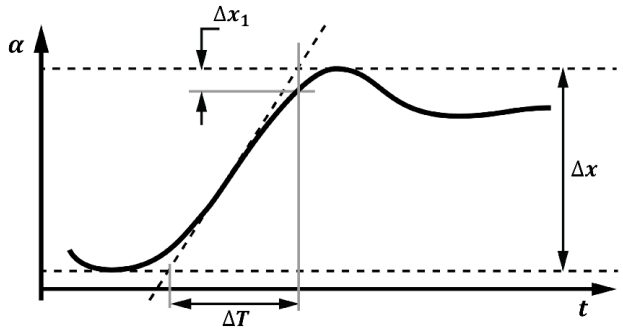

FIGURE 4.5 - Parameter for Maximum Slope Analysis

Using these values the ratio $\Delta x_1/\Delta x$ is calculated and used in the chart of FIG. 4.6 to determine ζ and $\omega_n \Delta T$. The value of Δx_1 is very small and difficult to be measured from flight data, hence it is an error source for this method.

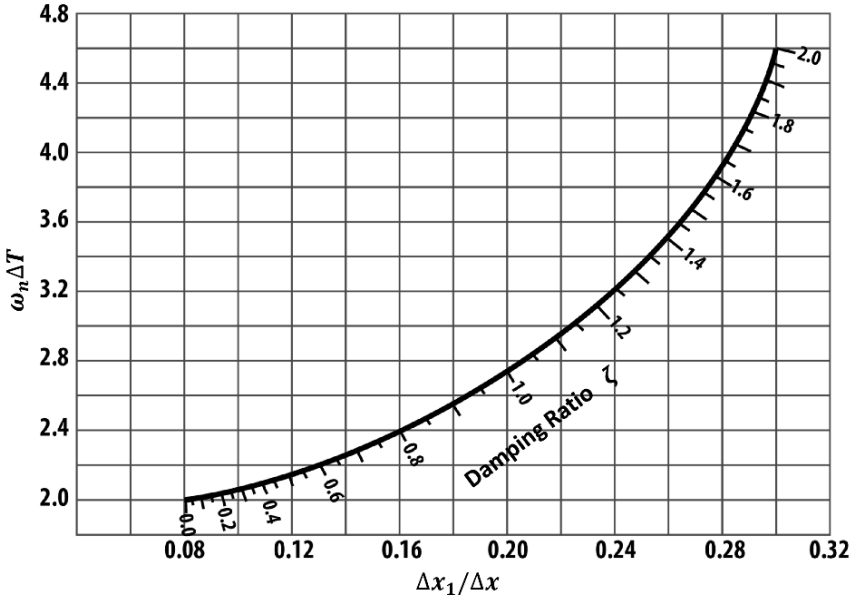

FIGURE 4.6 - Chart for Maximum Slope Analysis. Adapted from WARD (1998)

4.2 System Identification Methods

System identification methods can be described as an inverse problem, where they aim to obtain a description of a given dynamic system based on the observation of its behavior. It is mainly concerned with modeling from experimental data, where different dynamic models are compared and a detailed parameter estimation is performed intending to determine the most adequate for the system description. These techniques have been widely used in the analysis of flight test data (MAINE e ILIFF, 1986; ILIFF e MAINE, 1985; JATEGAONKAR, FISCHENBERG e GRUENHAGEN, 2004; DUTRA, 2010).

In this work, we use the linearized mathematical models for the aircraft dynamics description to determine its parameters, which are related with the characteristics of each of the dynamic modes.

The Equation Error Method is also based on the least squares. It is used for the estimation of the parameters in linearized models, assuming that there is a linear dependence between the parameters and the independent variables.

The Output Error Method is a more robust method with several statistical properties and is based on the principle of maximum likelihood. In this method, the system is assumed deterministic and the optimum parameters are obtained by an iterative process.

At last, the Filter Error Method is applied for the analysis. This technique assumes a stochastic system, and a Kalman filter is used to correct the estimations in the iterative process.

Those three last mentioned methods, intend to estimate the matrices $[A]$ and $[B]$. From these results, the eigenvalues of the plant matrix can be calculated to obtain the characteristics of each dynamical mode of the aircrafts motion.

4.2.1 Maximum Likelihood Principle

The likelihood is a statistical concept that measures the probability of a realization given an event; in a general view, the likelihood is the probability for an already realized event (DUTRA, 2010). The theory of maximum likelihood is based on the probabilistic aspect of random variables, defining a process to estimate the parameters that most likely produce the model responses and that closely match the measurements (KLEIN e MORELLI, 2006). In this process a function of the measurements (or observations) $(z_1, z_2, \dots, z_N)$ and of the unknown parameters $\boldsymbol{\theta}$ called likelihood function is defined. Mathematically, the likelihood of the measurements given the parameters is the same as its conditional probability, i.e.,

$$L(z|\boldsymbol{\theta}) = p(z|\boldsymbol{\theta}) \tag{4.3}$$

Given the samples of N random independent measurements $(z_1, z_2, \dots, z_N)$ from time t_0 to t_N in the same population, the likelihood function is defined as:

$$p(z|\boldsymbol{\theta}) = p(z_1|\boldsymbol{\theta})\,.\,p(z_2|\boldsymbol{\theta}) \dots\ p(z_N|\boldsymbol{\theta}) = \prod_{k=0}^{N} p(z(t_k)|\boldsymbol{\theta}) \tag{4.4}$$

The parameters $\boldsymbol{\theta}$ are estimated to maximize the likelihood function, which represents the probability of the observed variables given the parameters. In practice, we use the logarithm of the likelihood function for the optimization process, since for computational solution it does have a better numerical behavior. Then, the maximum likelihood is obtained when:

$$\frac{\partial \ln p(z|\boldsymbol{\theta})}{\partial \boldsymbol{\theta}} = 0 \tag{4.5}$$

Eq. (4.5) can be solved by linear expansion of the logarithmic likelihood equation about a first approximation θ_0 to be solved by successive approximations (JATEGAONKAR, 2015). Then, the increment for each step of the solution can be obtained solving:

$$\frac{\partial^2 \ln p(z|\boldsymbol{\theta_0})}{\partial \boldsymbol{\theta^2}} \Delta\boldsymbol{\theta} = -\frac{\partial \ln p(z|\boldsymbol{\theta_0})}{\partial \boldsymbol{\theta}} \tag{4.6}$$

To apply the maximum likelihood principle to the dynamical models proposed in Section 2.7 we assume that the measurements noise are zero-mean, white Gaussian, and that $\boldsymbol{R}$ is the covariance matrix of this noise. The assumption of whiteness of the measurement noise is very used in many practical engineering analyses. The probability density function for n_y dimensional measurement vector at N discrete time points is

$$p(z|\boldsymbol{\theta}, \boldsymbol{R}) = \{(2\pi)^{n_y}|\boldsymbol{R}|\}^{-N/2} \exp\left[-\frac{1}{2}\sum_{k=1}^{N}[z(t_k) - y(t_k)]^T \boldsymbol{R}^{-1}[z(t_k) - y(t_k)]\right] \tag{4.7}$$

where $y(t_k)$ are the model outputs, which are also dependent of the parameters $\boldsymbol{\theta}$. The maximization of the likelihood function for an unbounded search is the same as the minimization of its opposite (DUTRA, 2010). Then, to the optimization problems, we minimize the negative of the logarithm of the likelihood function, given by:

$$\ell(z|\boldsymbol{\theta},\boldsymbol{R}) = \frac{1}{2}\sum_{k=1}^{N}[z(t_k) - y(t_k)]^T \boldsymbol{R}^{-1}[z(t_k) - y(t_k)] + \frac{N}{2}\ln[\det(\boldsymbol{R})] + \frac{Nn_y}{2}\ln(2\pi) \tag{4.8}$$

The obtained optimum values for the parameters $\widehat{\boldsymbol{\theta}}$ are the most plausible, because it gives highest probability to the measurements (JATEGAONKAR, 2015).

4.2.2 Equation Error Method (EEM)

The EEM is based on a special case of the maximum likelihood estimator. For linear systems parameter estimation the EEM uses the classical ordinary least squares method (OLS). It assumes that there is only process noise and no measurement noise, moreover the system is considered deterministic. In practice, there will always be measurement noise, and is the role of the engineer to decide if the available data has enough low noise level to use with this technique. Another important detail is that several variables, such as angular acceleration, are determined by using finite differences, which can add other difficulties to the problem, such as the differentiation process. Thus, we observe that the applicability of the EEM is strongly influenced by the data quality (KLEIN e MORELLI, 2006).

Basically, the least squares technique minimizes the sum of the squares of the errors between the measurements and model response given a set of parameters, where the independent variables are noise free and the dependent variables are corrupted by uniformly zero mean, white and Gaussian noise (JATEGAONKAR, 2015).

In the OLS, each dependent variables (also known as "observations") $y_j(k)$, at each discrete time t_k is assumed to be linearly dependent on the independent variables (also termed as "regressors") $x_n(k)$. For N discrete data samples, we have

$$y_j(t_k) = \theta_1 x_1(t_k) + \theta_2 x_2(t_k) + \cdots + \theta_n x_n(t_k) + \varepsilon(t_k); \qquad t_k = 1,2,\ldots,N \tag{4.9}$$

where $\boldsymbol{\theta} = [\theta_1\ \theta_2\ \cdots\ \theta_n]^T$ denotes the vector of unknown parameters and ε is the equation error in the independent variable. In this work, these parameters are the unknown coefficients of matrices in Eq. (2.36) and Eq. (2.41) for longitudinal and lateral-directional motion, respectively. They are assumed constant along the data acquisition, i.e., the aircraft motion is assumed quasi stationary during measurement period (RAOL, GIRIJA e SINGH, 2004).

Furthermore, the independent variables, represented here by angular rates, attitude angles, linear velocities, flow angles and control inputs are assumed to be error-free.

In Eq. (2.36) and Eq. (2.41), there is more than one dependent variable for multiple independent variables, however, when the noise in each channel is independent each other, it is not necessary to know the noise variance, therefore, the estimation can be done independently for each measurement (DUTRA, 2010). Eq. (4.9) can be rewritten in matrix notation, for each dependent variable been modeled separately as

$$Y = X\boldsymbol{\theta} + \varepsilon \tag{4.10}$$

where $Y = [y(1)\ y(2)\ ...\ y(N)]^T$ is the observation vector and $\varepsilon = [\varepsilon(1)\ \varepsilon(2)\ ...\ \varepsilon(N)]^T$ is the equation error vector. The matrix of regressors is represented by

$$X = \begin{bmatrix} x_1(1) & x_2(1) & \cdots & x_n(1) \\ x_1(2) & x_2(2) & \cdots & x_n(2) \\ \vdots & \vdots & & \vdots \\ x_1(N) & x_2(N) & \cdots & x_n(N) \end{bmatrix} \tag{4.11}$$

This is an over determined problem, since in practice $N > n$, where "the larger the number of such redundant data, the better will be the averaging out process, yielding more reliable estimates" (JATEGAONKAR, 2015). In Eq. (4.10), the error is assumed to be white noise process with zero mean and variance σ^2.

$$\varepsilon \sim \mathcal{N}(0, \sigma^2) \tag{4.12}$$

From Eq. (4.10), the residuals can be written as

$$\varepsilon = Y - X\hat{\boldsymbol{\theta}} \tag{4.13}$$

Since the least squares estimates are obtained by minimizing the sum of the squares of the residual, the cost function is defined as

$$J(\boldsymbol{\theta}) = \frac{1}{2}\sum_{k=1}^{N} \varepsilon^2(k) = \frac{1}{2}\varepsilon^T\varepsilon = \frac{1}{2}[Y - X\boldsymbol{\theta}]^T[Y - X\boldsymbol{\theta}] \tag{4.14}$$

The minimum is obtained by setting the gradient of $J(\boldsymbol{\theta})$ with respect to the unknown parameters $\boldsymbol{\theta}$ to zero, i.e.,

$$\frac{\partial J(\boldsymbol{\theta})}{\partial \boldsymbol{\theta}} = -Y^T X + \boldsymbol{\theta}^T(X^T X) = 0 \tag{4.15}$$

Assuming ($X^T X$) to be invertible, the parameter that minimize the least squares cost function (estimates), are given by

$$\widehat{\boldsymbol{\theta}} = (X^T X)^{-1} X^T Y \tag{4.16}$$

The major limitation of EEM is that they result on inconsistent estimates in the presence of noise in the measurements. However, this problem can be solved by using high-quality sensors and instrumentation system, which, in turn, is more expensive. Flight path reconstruction techniques can also be used as a data-preprocessing step, reducing more reliable data, and, consequently, better estimates.

The OLS can be easily implemented on a personal computer. It also does not depend on initial estimate, and it is not an iterative process. Thus, it is generally used to find an initial estimate for iterative methods shown in the following sections. The aircraft model used in this work is linear in the parameters, which is an adequate condition to use the OLS. However, the EEM can also be adapted to be used with nonlinear models, where the problem is solved iteratively.

4.2.3 Output Error Method (OEM)

The "Output Error Method is the most widely applied time-domain method to estimate aircraft parameters from flight data" (JATEGAONKAR, 2015, p. 97). It is a maximum likelihood estimator which assumes that there is only noise in the measurements of the system. In this method, there is no process noise, i.e., the system is assumed deterministic, which depends only of the initial states, inputs and parameters. The OEM can also be called response curve fitting, where the main idea is to adjust the model parameters iteratively, comparing the simulated response for a set of parameters with the measured variables. The method intends to minimize the error between the measured variables (system output) and the estimated responses (model prediction), where the optimum set of parameters is the one that maximizes the likelihood function.

Thus, the dynamic system can be represented here by:

$$\begin{aligned} \dot{x}(t) &= f[x(t), \delta(t), \boldsymbol{\theta}], \quad x(t_0) = x_0 \\ y(t) &= g[x(t), \delta(t), \boldsymbol{\theta}] \\ z(t_k) &= y(t_k) + G\, v(t_k) \end{aligned} \tag{4.17}$$

where x are denoted the vector of the state variables, y are the model outputs, δ are the control input variables, z are the measured variables at the discrete time t_k, G is the additive

measurement noise distribution matrix, and v is the measurement noise, which is a white noise represented by a Gaussian distribution with zero mean, i.e.,

$$v \sim \mathcal{N}(0, \boldsymbol{R}) \tag{4.18}$$

In Eq. (4.18), $\boldsymbol{R}$ is the measurement noise covariance matrix. The dynamic system in Eq.(4.17) can be linear or non linear; Here, we used the aircraft linearized models for parameter estimation.

The minimization of the cost function J, which is represented by the negative of the logarithm of the likelihood function (Eq. (4.8)), leads to a nonlinear optimization problem. To estimate the system parameters we depend on the measurements noise covariance matrix and vice versa. To solve this problem, JATEGAONKAR (2015) proposes the use of relaxation strategy, which is carried out in two steps. First, for any given set of parameters $\boldsymbol{\theta}$, differentiating the maximum likelihood equation with respect to $\boldsymbol{R}$ and setting it to zero we have that:

$$\boldsymbol{R} = \frac{1}{N}\sum_{k=1}^{N}[z(t_k) - y(t_k)][z(t_k) - y(t_k)]^T \tag{4.19}$$

Then, substituting Eq. (4.19) in the maximum likelihood function, we have the cost function:

$$J(\boldsymbol{\theta}) = \frac{1}{2}n_y N + \frac{N}{2}\ln[\det(\boldsymbol{R})] + \frac{Nn_y}{2}\ln(2\pi) \tag{4.20}$$

The estimation procedure is summarized in the following (REIS, DUTRA e PINTO, 2016):

1. An initial set of values for the parameters $\boldsymbol{\theta}_0$ are chosen. Here, we obtain these values from Equation Error Method.
2. System outputs y and the residuals $(z - y)$ are computed; then, the measurement noise covariance matrix $\boldsymbol{R}$ is also estimated by Eq. (4.19).
3. The cost function $J(\boldsymbol{\theta})$ is minimized with respect to the parameters by applying a nonlinear optimization method.
4. Return to step 2 and iterate until the convergence of the cost function.

Any optimization method can be applied to minimize the cost function in step 3. In this work, we used Gauss-Newton Algorithm, also known as Newton-Raphson method. This

algorithm shows that for minimizing the cost function, the step increment in the parameters for each iteration is given by (JATEGAONKAR, 2015):

$$\Delta\boldsymbol{\theta} = -\left[\left(\frac{\partial^2 J}{\partial \boldsymbol{\theta}^2}\right)_i\right]^{-1}\left(\frac{\partial J}{\partial \boldsymbol{\theta}}\right)_i \tag{4.21}$$

where $\Delta\boldsymbol{\theta} = \boldsymbol{\theta}_{i+1} - \boldsymbol{\theta}_i$ is the parameter change; $(\partial J/\partial\boldsymbol{\theta})_i$ is the cost function gradient, also known as Jacobian matrix and $(\partial^2 J/\partial\boldsymbol{\theta}^2)_i$ is the second gradient for the ith iteration. The second gradient is also known as Hessian matrix. To obtain the Jacobian and the Hessian for the cost function we differentiate the likelihood function in the parameters, then:

$$\begin{aligned}\frac{\partial J}{\partial \boldsymbol{\theta}} &= -\sum_{k=1}^{N}\left[\frac{\partial y(t_k)}{\partial \boldsymbol{\theta}}\right]^T \boldsymbol{R}^{-1}[z(t_k) - y(t_k)] \\ \frac{\partial^2 J}{\partial \boldsymbol{\theta}^2} &= \sum_{k=1}^{N}\left[\frac{\partial y(t_k)}{\partial \boldsymbol{\theta}}\right]^T \boldsymbol{R}^{-1}\frac{\partial y(t_k)}{\partial \boldsymbol{\theta}} + \sum_{k=1}^{N}\left[\frac{\partial^2 y(t_k)}{\partial \boldsymbol{\theta}^2}\right]^T \boldsymbol{R}^{-1}[z(t_k) - y(t_k)]\end{aligned} \tag{4.22}$$

The computation of the Jacobian matrix is relatively simple, however the Hessian is more time consuming, since it requires the calculation of the second gradient of the response. Thus, a simplification for the Hessian calculation is assumed, since the second term in the right-hand side tends to zero as the process converges. It occurs due to the fact that this term depends on the error $[z(t_k) - y(t_k)]$, which is canceled over a sufficient amount of data point, in agreement with the noise assumptions. This simplification is largely used in practice (ILIFF e MAINE, 1986), where the second gradient of the cost function is:

$$\frac{\partial^2 J}{\partial \boldsymbol{\theta}^2} \approx \sum_{k=1}^{N}\left[\frac{\partial y(t_k)}{\partial \boldsymbol{\theta}}\right]^T \boldsymbol{R}^{-1}\frac{\partial y(t_k)}{\partial \boldsymbol{\theta}} \tag{4.23}$$

To calculate the cost function gradients it is possible to use an implicit analytical formulation or finite differences. Several techniques can be used to solve these gradients by calculating them analytically, such as using symbolic computation. However, in this work, we use finite differences calculation. This method is indicated by JATEGAONKAR (2015) and KLEIN (2006), since they are simpler to work with and yield a more flexible code, where the model structure can be changed without software modifications.

The finite differences method must be carefully used, since it depends on the magnitude of parameters perturbation. For a good gradient calculation, the perturbations must be as small as possible, but not too small, since truncation errors can be add due to computer numerical

precision. Techniques for an adequate parameter perturbation can be observed in JATEGAONKAR (2015).

4.2.4 Filter Error Method (FEM)

The Filter Error Method is based on the Principle of Maximum Likelihood and assumes a stochastic system under investigation, thus its parameter estimation process accounts for both process and measurement noise. Among the system identification methods presented in this work, this is the most general approach to parameter estimation problem (JATEGAONKAR, 2015).

In a more general view, the FEM is a combination of the Output Error Method and the Kalman Filter, which is a tool used for the correction of the predicted states. In the OEM the error is accounted from the beginning to the end of the acquisition interval, on the other hand, the error is accounted at each prediction step in the Filter Error Method, which attempts to minimize it by using the filter corrections. In summary, reliable parameters are that which give a better prediction, in other words, they require a lower correction level.

The dynamic system is represented by:

$$\begin{aligned} \dot{x}(t) &= f[x(t), \delta(t), \boldsymbol{\theta}] + F\, w(t), \qquad x(t_0) = x_0 \\ y(t) &= g[x(t), \delta(t), \boldsymbol{\theta}] \\ z(t_k) &= y(t_k) + G\, v(t_k) \end{aligned} \tag{4.24}$$

where F represents the process noise distribution matrix. It is assumed that both process and measurement noise affect the dynamic system linearly. The process noise $w(t)$ and the measurement noise $v(t_k)$ are characterized by a zero-mean, Gaussian and white noise.

Since this method is also based on the Principle of Maximum Likelihood the cost function is given by

$$J(\boldsymbol{\theta}) = \frac{1}{2}\sum_{k=1}^{N}[z(t_k) - \tilde{y}(t_k)]^T \boldsymbol{R}^{-1}[z(t_k) - \tilde{y}(t_k)] + \frac{N}{2}\ln[\det(\boldsymbol{R})] + \frac{Nm}{2}\ln(2\pi) \tag{4.25}$$

where $\tilde{y}$ is the system output based on the predicted states, which depends of the estimated parameters $\boldsymbol{\theta}$, and $\boldsymbol{R}$ is the covariance matrix of the residual. As it will be shown, $\boldsymbol{R}$ is a function of the Kalman gain matrix ($\boldsymbol{K}$), which exact equation is complex, thus an asymptotic approximation proposed by JATEGAONKAR (2015) is given by:

$$\boldsymbol{R} = \frac{1}{N}\sum_{k=1}^{N}[z(t_k) - \tilde{y}(t_k)][z(t_k) - \tilde{y}(t_k)]^T \tag{4.26}$$

The fist step in the evaluation of the cost function is to compute the model outputs. Since the system is no longer deterministic, it is not possible a simple integration of the states, as it was used for the OEM. Rather, we use now a state estimator, which is the Kalman Filter. In this work we use an extended Kalman Filter, which has a broader application also for nonlinear filtering. This filter consists of two steps: the prediction and the correction. They are represented as follows:

Prediction step:

$$\tilde{x}(t_{k+1}) = \hat{x}(t_k) + \int_{t_k}^{t_{k+1}} f\left[\hat{x}(t), \bar{\delta}(t_k), \boldsymbol{\theta}\right]dt, \qquad \hat{x}(t_0) = x_0 \tag{4.27}$$

$$\tilde{y}(t_{k+1}) = g[\tilde{x}(t_{k+1}), \delta(t_{k+1}), \boldsymbol{\theta}] \tag{4.28}$$

Correction step:

$$\hat{x}(t_{k+1}) = \tilde{x}(t_{k+1}) + \boldsymbol{K}[z(t_{k+1}) - \tilde{y}(t_{k+1})] \tag{4.29}$$

where $\tilde{x}$ and $\hat{x}$ denote the predicted and corrected state vector respectively, $\tilde{y}$ is the predicted system outputs, $\bar{\delta}$ is the average of the control inputs at the two discrete time points, and $\boldsymbol{K}$ is the Kalman gain matrix. In this work we assume that the aircraft's motions is time-invariant during the time interval under analysis. Besides this, we consider that the system under investigation has a small deviation from its nominal trajectory. Therefore, it is adequate to use a steady-state filter for the estimation process, where the Kalman gain is constant all over the time interval, and is given by:

$$\boldsymbol{K} = \boldsymbol{P}C^T\boldsymbol{R}^{-1} \tag{4.30}$$

where $\boldsymbol{P}$ is the covariance matrix of the state-prediction error, obtained by the solution of the Riccati equation (RAOL, GIRIJA e SINGH, 2004) ; and C is the observation matrix of the linearized system, which is given by

$$C = \left[\frac{\partial g[x(t), u(t), \boldsymbol{\theta}]}{\partial x}\right]_{t=t_0} \tag{4.31}$$

Here, such as in the OEM, the Gauss-Newton algorithm is adopted for the minimization problem. The first and second gradients to calculate the cost function are given by Eq. (4.32).

$$\frac{\partial J}{\partial \boldsymbol{\theta}} = -\sum_{k=1}^{N} \left[\frac{\partial \tilde{y}(t_k)}{\partial \boldsymbol{\theta}}\right]^T \boldsymbol{R}^{-1}[z(t_k) - \tilde{y}(t_k)]$$
$$\frac{\partial^2 J}{\partial \boldsymbol{\theta}^2} \approx \sum_{k=1}^{N} \left[\frac{\partial \tilde{y}(t_k)}{\partial \boldsymbol{\theta}}\right]^T \boldsymbol{R}^{-1} \frac{\partial \tilde{y}(t_k)}{\partial \boldsymbol{\theta}} \tag{4.32}$$

The estimation used in FEM for the minimization is much like that of OEM; however, here the estimates must be corrected at each iteration by the calculation of the Kalman gain.

Although it is a more complex method, it is possible to evaluate the flight data obtained in a turbulent atmosphere, since the system is no more assumed deterministic. This often occurs due to the rigid schedule of the airplane development program, which must be complied to avoid financial losses. Nonetheless, this method can be used in the estimation of open-loop unstable systems, since there is a feedback step during the integration using the values corrected by the filter. In addition, this technique is not only necessary to analyze data obtained in turbulent atmosphere, but also to provide better estimations for data acquired in an atmosphere seemly smooth.

4.3 Nonlinear Least Squares Method (NLS)

The NLS method is based on least squares principle and is presented here as an alternative method to obtain the characteristics of the aircraft flight dynamics. Unlike OLS, here the method is developed to fit data in a model where there is nonlinear dependence between the independent variables and the parameters (STRUTZ, 2011). This nonlinear relation can be observed for each aircraft dynamic mode. In agreement with Section 2, we observe that the Phugoid, Short-Period and Dutch Roll can be simplified by a second-order natural response. For the Roll Subsidence and Spiral a first-order natural response is observed.

Generally, the following variables are used to observe each dynamic mode:

- Phugoid → u (linear speed in the X axis)
- Short-Period → α (angle of attack)
- Dutch-Roll → β (sideslip angle)
- Roll Subsidence → p (roll rate)
- Spiral → ϕ (roll angle)

A second-order natural response for these modes are assumed as a damped sinusoidal form (NISE, 2011), given by:

$$y(t) = Ke^{\zeta\omega_n t}\cos\left(\omega_n\sqrt{1-\zeta^2}t + \varphi\right) + y_{eq} \tag{4.33}$$

where $y(t)$ represents u, α or β depending on each mode is over analysis, K, φ and y_{eq} are parameters that define the sinusoid amplitude, phase and equilibrium value, respectively; ζ and ω_n are the sinusoid damping and natural frequency respectively. Then, the vector of parameters is $\boldsymbol{\theta} = [K\ \phi\ y_{eq}\ \zeta\ \omega_n]$.

The form of a first-order natural response can be represented by

$$y(t) = K\left(1 - e^{-\frac{t}{\tau}}\right) \tag{4.34}$$

where $y(t)$ represents p or ϕ depending on each mode is over analysis, K is a curve scale parameter and τ is the system time constant. The time constant is an important parameter for a first-order system observation, since it defines the behavior of the transient response. The vector of parameters is represented by $\boldsymbol{\theta} = [K\ \tau]$.

In the least squares sense, for a set of N data points during the aircraft response, the parameters $\boldsymbol{\theta}$ that best fits the given data in the model is the one which minimizes the sum of the squares of the residuals, i.e., the difference between the output and the measurements.

$$\min \quad J = \sum_{k=1}^{N} \varepsilon_k^2 \tag{4.35}$$

where the residuals ε_k are the difference between the measurement z_k and the model value at each discrete time t_k. Then,

$$\varepsilon_k = z_k - [y(t_k, \boldsymbol{\theta})] \tag{4.36}$$

As observed in Section 4.2.2, the minimum of the least squares cost function with respect to the unknown parameters occurs when its gradient is zero. In the NLS the model is not linear, thus the cost function minimization is done iteratively. The Gauss-Newton algorithm, used to solve the OEM, can also be used here. To calculate the parameter step size for each iteration we must calculate the first and second gradients of the cost function, which, in the least squares sense, are given by

$$\frac{\partial J}{\partial \boldsymbol{\theta}} = 2\sum_{k=1}^{N} \varepsilon_k \frac{\partial \varepsilon_k}{\partial \boldsymbol{\theta}}$$
$$\frac{\partial^2 J}{\partial \boldsymbol{\theta}^2} \approx 2\sum_{k=1}^{N} \left[\frac{\partial \varepsilon_k}{\partial \boldsymbol{\theta}}\right]^T \left[\frac{\partial \varepsilon_k}{\partial \boldsymbol{\theta}}\right] \tag{4.37}$$

In Eq. (4.37) the second order derivatives of the Hessian are neglected. For the iterative solution, the NLS requires an initial guess for the parameters. Then, the optimal parameters will represent the model function that best fits the aircraft motion data. NLS implementations are readily available in many different programing languages, including Python, Matlab and C++.

5 RESULTS

Data from two different aircrafts were used in this work to evaluate the respective dynamic characteristics. The aircrafts analyzed here have different characteristics: one is a small two-seater general aircraft (ACS-100 Sora) and the other is a jet aircraft with a capacity for more than 40 passengers (VFW-Fokker 614). Given these characteristics, it is possible to observe how the use of the methods (for the excitation or data reduction) varies in each case. It is expected to obtain fairly different values for the dynamical behavior of each aircraft, which contributes to the assessment of the methods employed. The measurements have been acquired during flight test campaigns, where the aircrafts were submitted to maneuvers for excitation of several modes. Then, the obtained data were treated for the analysis and each of the proposed reduction methods were used.

5.1 VFW-Fokker 614

The VFW-Fokker 614/ATTAS (Advanced Technologies Testing Aircraft System) is an aircraft from DLR (German Aerospace Center). It was conceived to be the first jet passenger plane develop in the Federal Republic of Germany, with many technological innovations that are still used during the developments of new aircrafts today (JORDAN, 2000). One unit of VFW 614 was owned by the DLR and was used until the end of 2012 for experimental and research purposes. The data used here was kindly ceded by JATEGAONKAR (2015), and it is available as a supplementary material from its book. FIG. 5.1, FIG. 5.2 and TAB. 5.1 show some dimensional and performance details about this aircraft.

TABLE 5.1 - VFW-Fokker 614/ATTAS Dimensions and Performance Data

Dimensions		
Span	21.50 m	70.5 ft
Wing Area	64 m²	5.95 ft²
Length	20.60 m	67.6 ft
Cabin Height	1.92 m	6.3 ft
Performance		
Max. takeoff weight	19950 kg	43980 lb
Range (40 passengers)	1200 km	746 mi
Max. operating speed (21000 ft)	700 km/h	434.9 mph
Engine	Rolls-Royce/SNECMA M45H Mk 501	
Thrust	2x 33.2 kN	2x 7.46 lbf

SOURCE - (JORDAN, 2000)

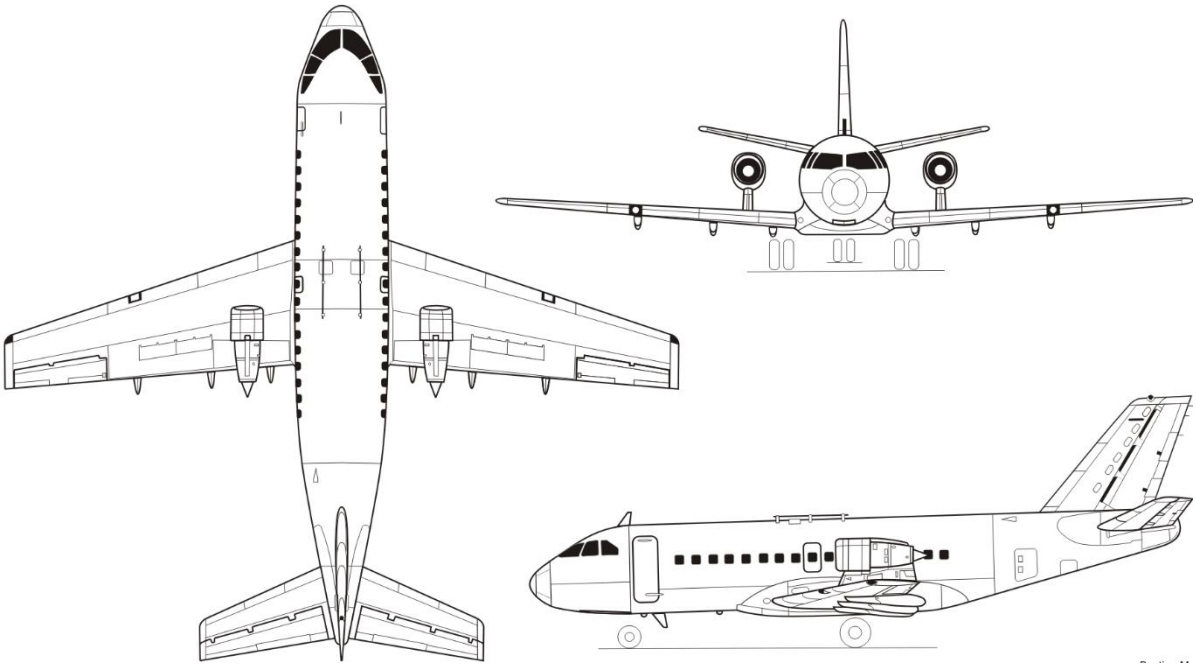

FIGURE 5.1 - VFW-Fokker 614/ATTAS 3 view
SOURCE - (WIKIWAND, 2001)

FIGURE 5.2 - VFW-Fokker 614/ATTAS picture
SOURCE - (AVIATION FAN CLUB, 2014)

5.1.1 Lateral-Directional motion analysis

For the Lateral-Directional motion of VFW 614, two different maneuvers were used for analysis: the rudder doublet and the bank-to-bank. We assessed each response separately and for a final check they were used together for the analysis with the system identification methods.

The rudder doublet is used to excite the Dutch Roll motion, as can be seen in the first dataset (FIG. 5.3), used for estimation.

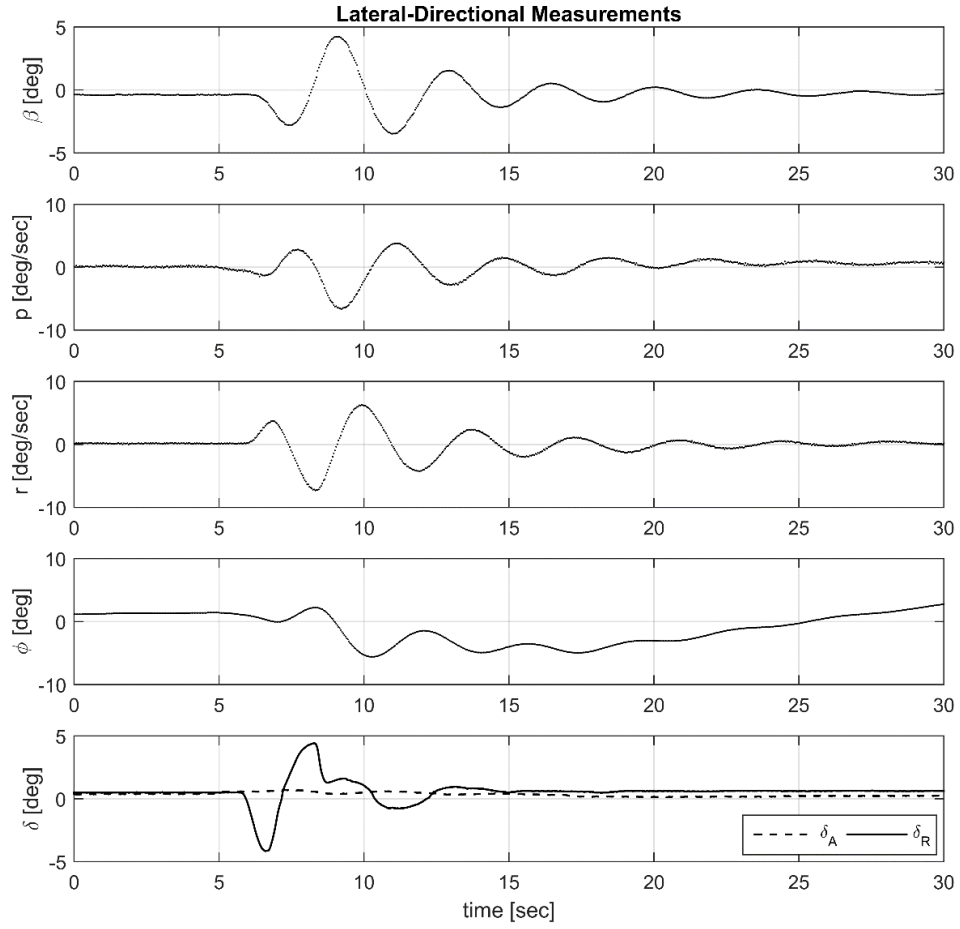

FIGURE 5.3 - Lateral-directional measurements for a doublet input (VFW 614)

After the pilot input we can observe the Dutch Roll response, mainly through the sideslip angle (β). It is almost fully damped within 15 seconds with almost four complete oscillations, thus, as expected, this lateral-directional response is a lightly damped motion. We can observe that, for the doublet, a Δt of approximately 1.7 seconds has been applied by the pilot and no corrections were used by the autopilot, since it must be turned off for the evaluation of the aircrafts natural motion. Other important observation is that even with an input slightly different from the ideal (see the obtained results for the natural frequency in the end of this section), the mode is successfully excited.

Due to Dutch-Roll characteristic, the Transient Peak Ratio (or MTPR) has been used for determining the natural frequency and the damping coefficient during this oscillatory response. The measured peaks in the sideslip response are shown in FIG. 5.4. The peak ratios and the period T are graphically obtained from these measurements. Then, the damping coefficient is obtained with the chart in FIG. 4.2. From these values the natural frequency is calculated from Eq. (4.2). The estimates using this method are: $\omega_{n,DR} = 1.739$ rad/s and $\zeta = 0.079$.

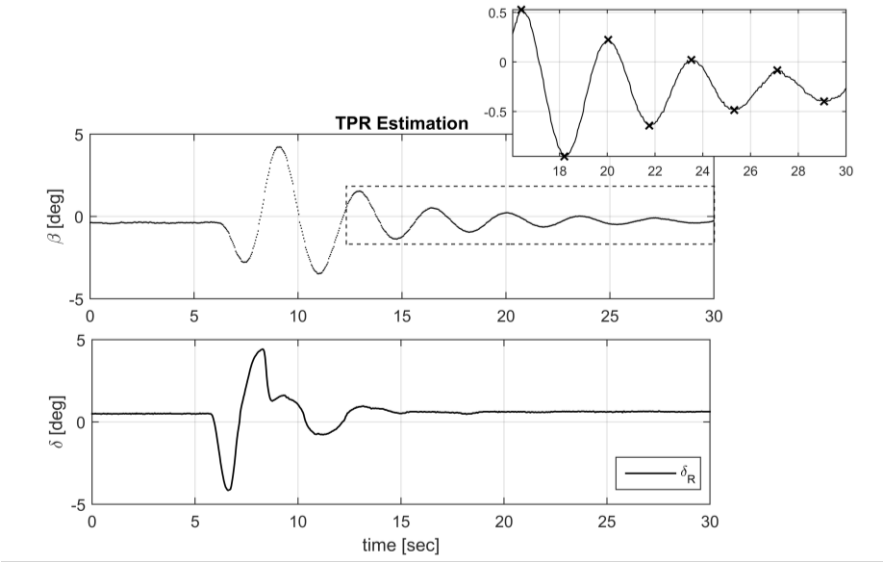

FIGURE 5.4 - TPR estimation (VFW 614 rudder doublet)
with selected peaks emphasized in the box.

A second method used for the motion analysis is the Nonlinear Least Squares. For this mode it is assumed that after the input the aircraft response is a damped sinusoid, in the form of Eq. (4.3). The initial parameters required for the iterative process are assumed the same obtained from the TPR method. The estimated values by the NLS are: $\omega_{n,DR} = 1.7627$ rad/s and $\zeta = 0.0826$, and the obtained optimum curve fitting is shown in FIG. 5.5.

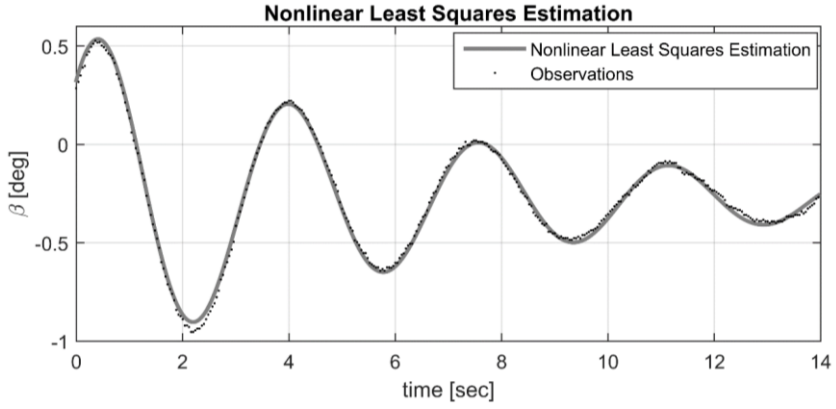

FIGURE 5.5 - NLS estimation (VFW 614 rudder doublet)

For system identification techniques, we first tried to estimate the parameters for the Dutch Roll mode assuming a 4th order system. The estimated outputs by using the Equation Error Method are shown in FIG.5.6.

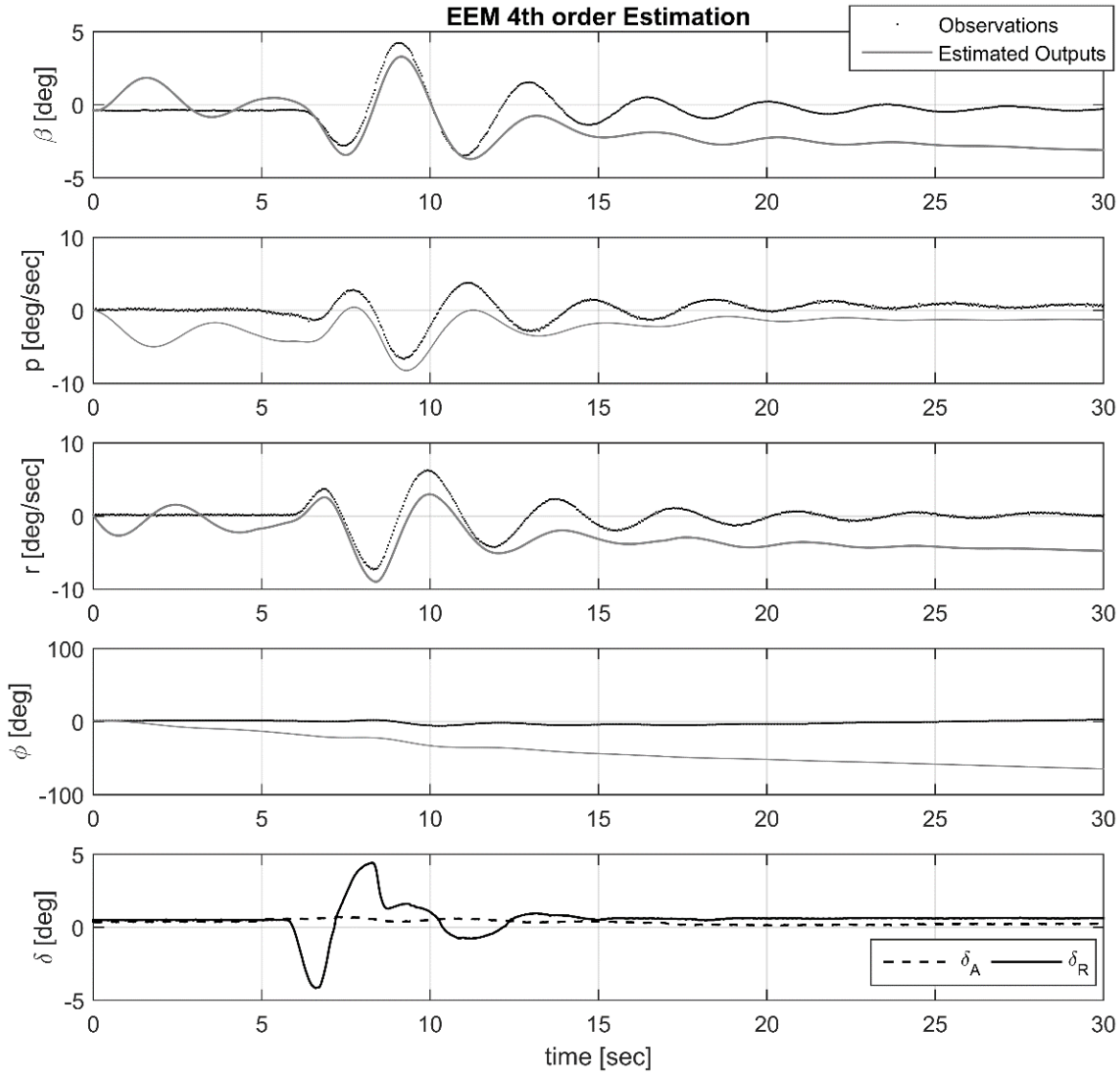

FIGURE 5.6 - EEM 4th order model estimation (VFW 614 rudder doublet)

We can observe that the estimated responses are fairly different from the measurements, making it inconsistent. However, the obtained parameters with the EEM can be used as initial guess for the Output Error Method. Therefore, the OEM is used for the estimation process and the estimated outputs are shown in FIG. 5.7. From the plant matrix $[\boldsymbol{A}]$ we obtain the following values for the Dutch Roll characteristics: $\omega_{n,DR} = 1.8065$ rad/s and $\zeta = 0.0851$.

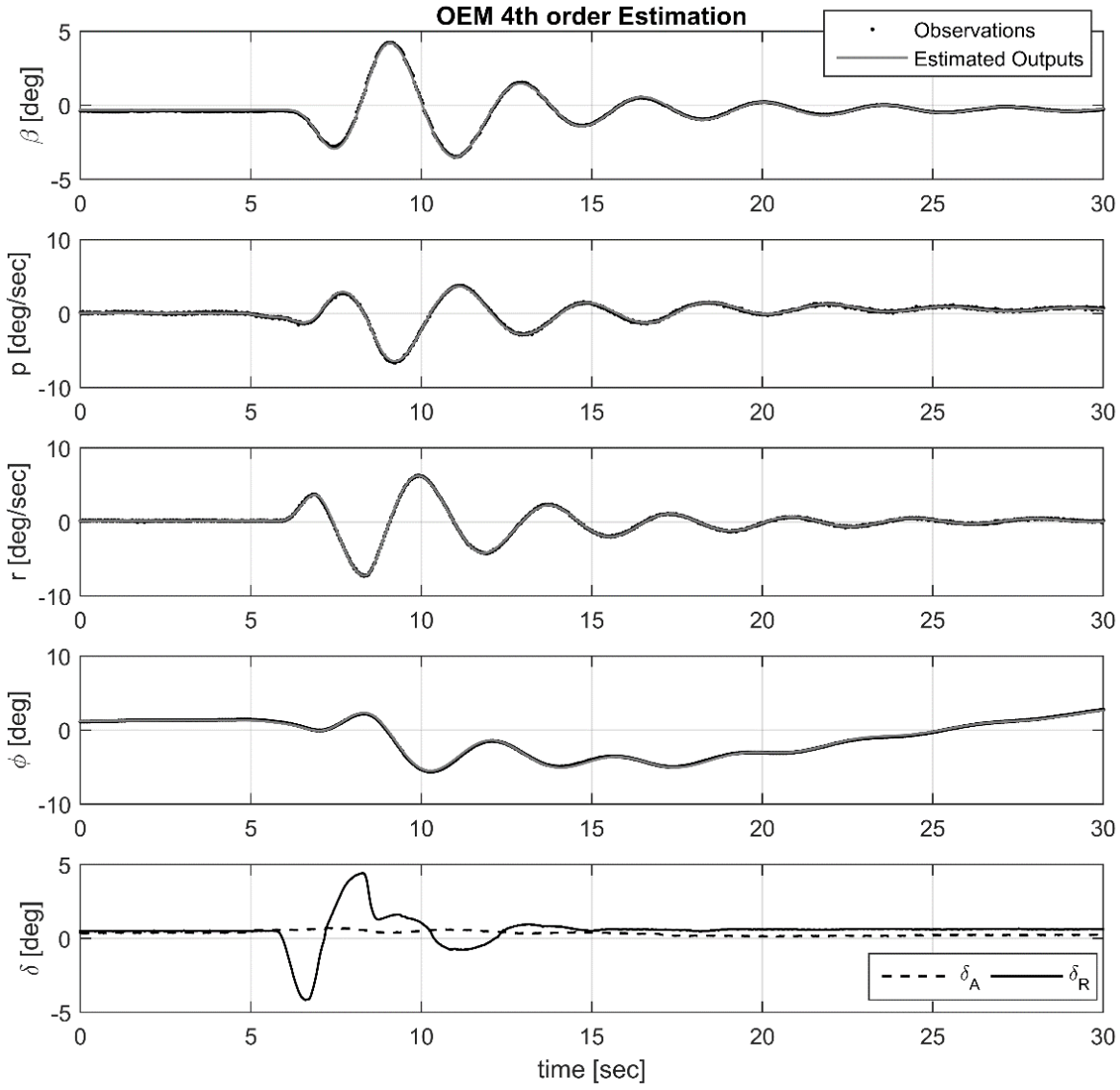

FIGURE 5.7 - Output Error Method 4th order model estimation (VFW 614 rudder doublet)

In the present data, it is known that the tests has been performed with a low turbulence level, allowing us to assume that the aircraft motion can be seen as a deterministic system. Thus, we can assume that the analysis by using the OEM, given its statistical properties, is sufficient for the given data. Nevertheless, we used the Filter Error Method for comparison. The free simulation from the estimated parameters are shown in FIG. 5.8, and the values for the natural frequency and damping are: $\omega_{n,DR} = 1.7933$ rad/s and $\zeta = 0.0890$.

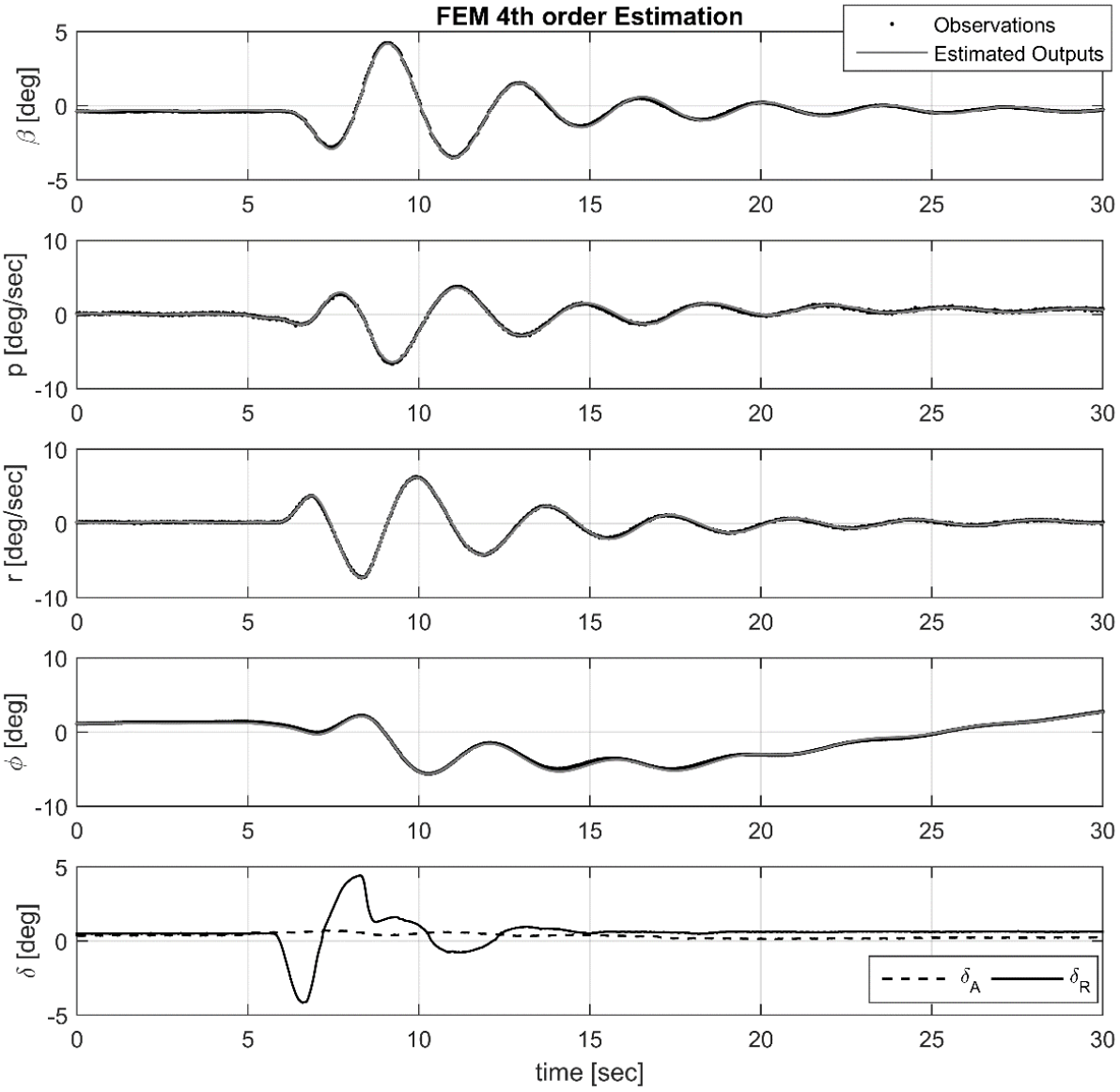

FIGURE 5.8 - Filter Error Method 4th order model estimation (VFW 614 rudder doublet)

The same estimation process using system identification techniques were repeated assuming a simplified motion for the Dutch Roll as a 2nd order system. The EEM presented inconsistent responses, and its parameters were used for the OEM and FEM estimation process. The obtained results are shown if FIG. 5.9 and FIG. 5.10, where the following results were obtained for the OEM and FEM, respectively: $\omega_{n,DR} = 1.7983\ \text{rad/s},\ \zeta = 0.0876$ and $\omega_{n,DR} = 1.7913\ \text{rad/s}, \zeta = 0.0888$.

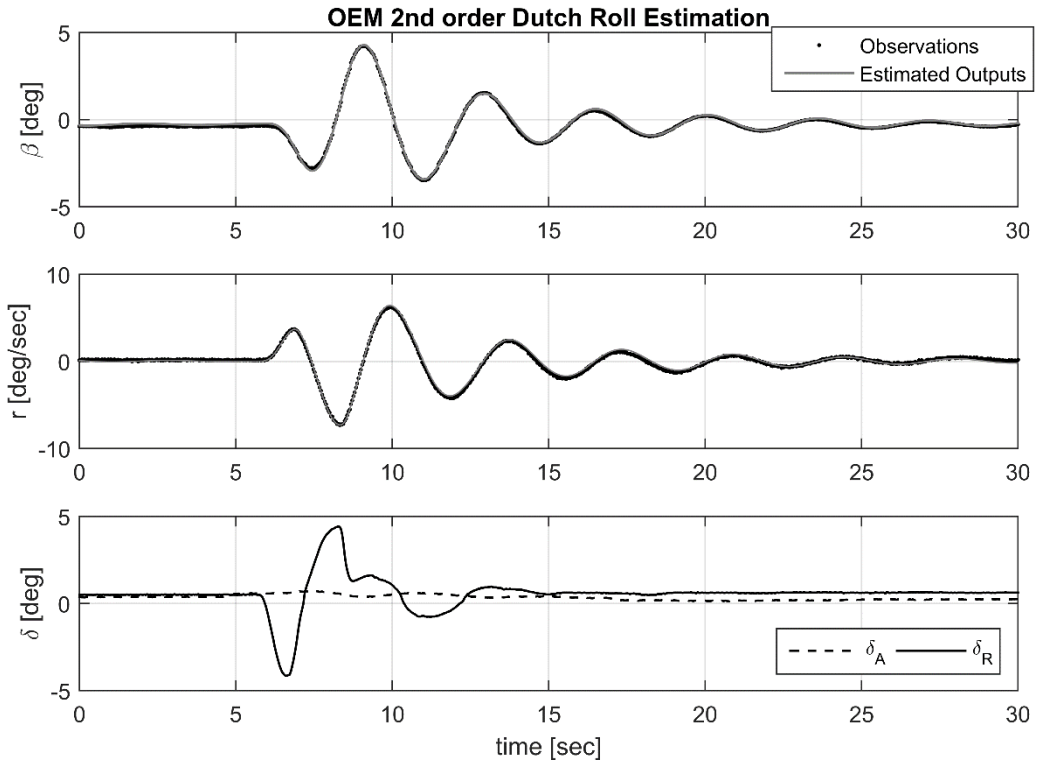

FIGURE 5.9 - Output Error Method 2nd order model estimation (VFW 614 rudder doublet)

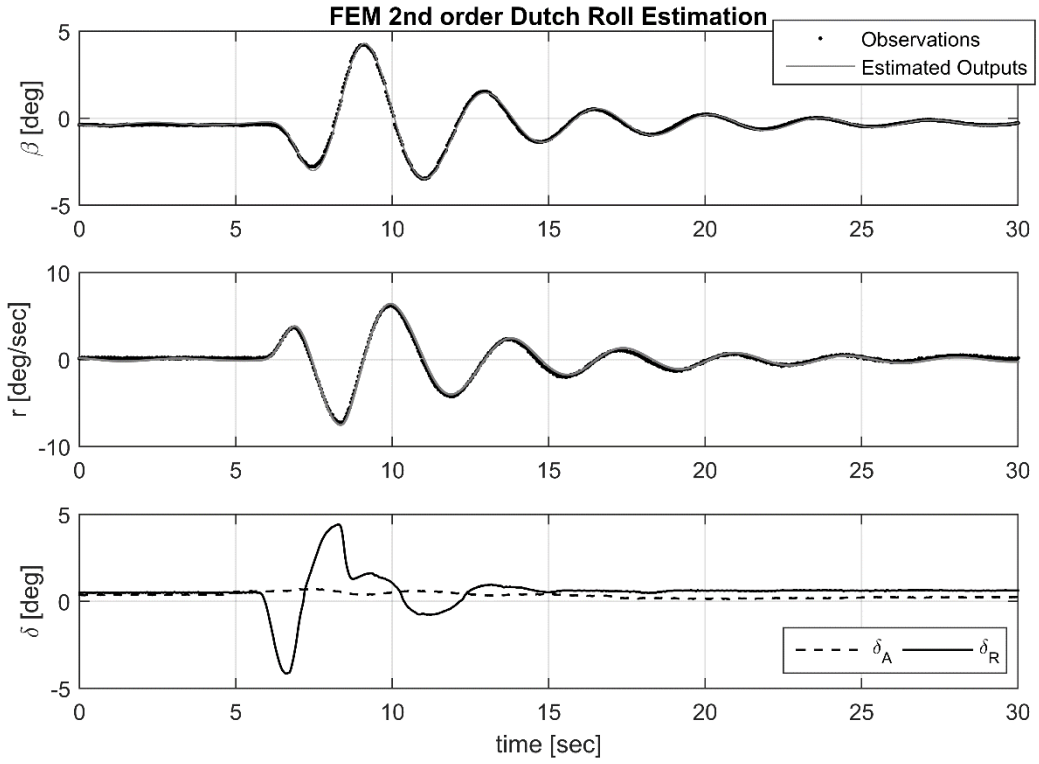

FIGURE 5.10 - Filter Error Method 2nd order model estimation (VFW 614 rudder doublet)

The estimated parameters for each different method are summarized in TAB. 5.2.

TABLE 5.2 - Estimation for each method based on rudder doublet input

	$\omega_{n_{DR}}\ [rad/s]$	ζ_{DR}
TPR	1.739	0.079
NLS	1.7627	0.0826
OEM 2nd	1.7983	0.0876
OEM 4th	1.8065	0.0851
FEM 2nd	1.7913	0.0888
FEM 4th	1.7933	0.0890

One interesting characteristic of system identification methods is that they only require one full cycle response of the Dutch Roll for its characterization. For a better perspective of this property, we applied the OEM technique using a 2nd and a 4th order models, where a minor part of the data were used, containing only one cycle of the Dutch Roll after the rudder doublet, as shown in FIG. 5.11 and FIG. 5.12. The obtained results are shown in TAB. 5.3. Comparing these results with the full data estimation we can note that for the 2nd order model the obtained results for the natural frequency and the damping vary only 0.34%. For the 4th order model the natural frequency and damping variation are also a small value.

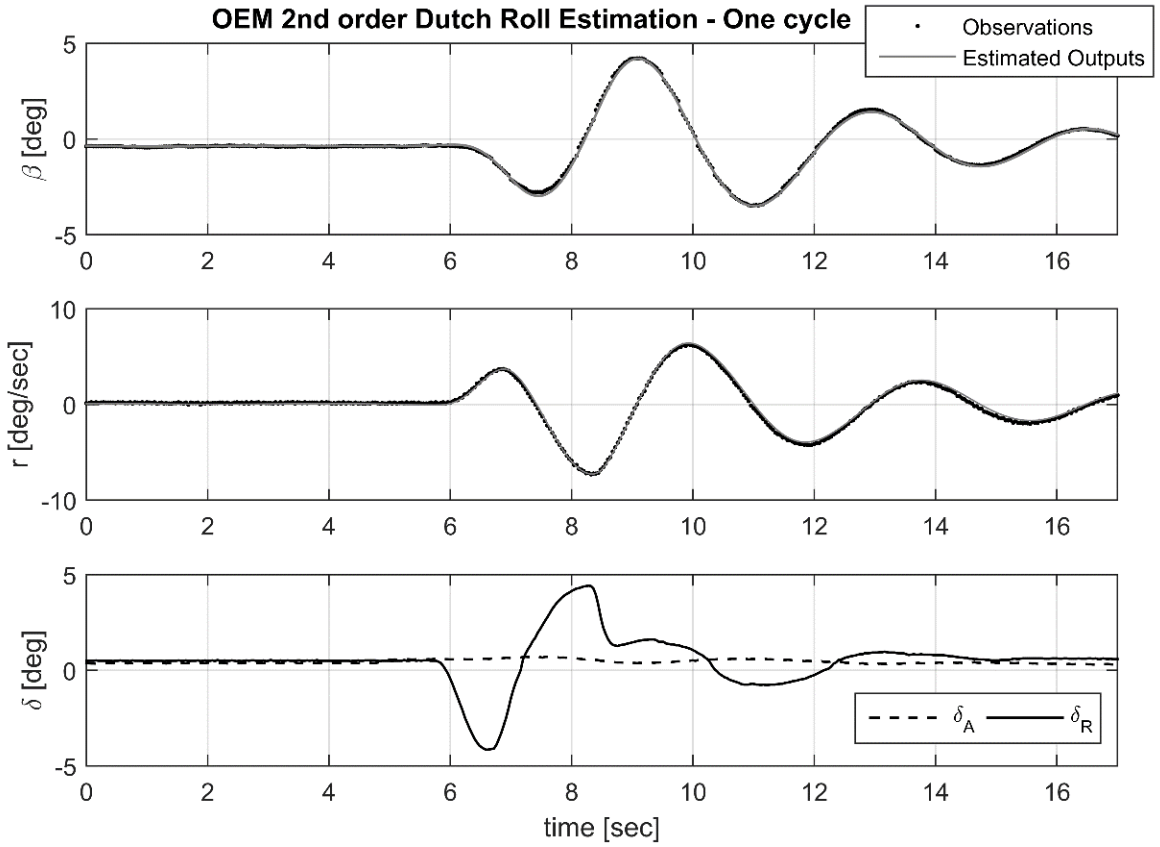

FIGURE 5.11 - OEM 2nd order model estimation in one cycle (VFW 614 rudder doublet)

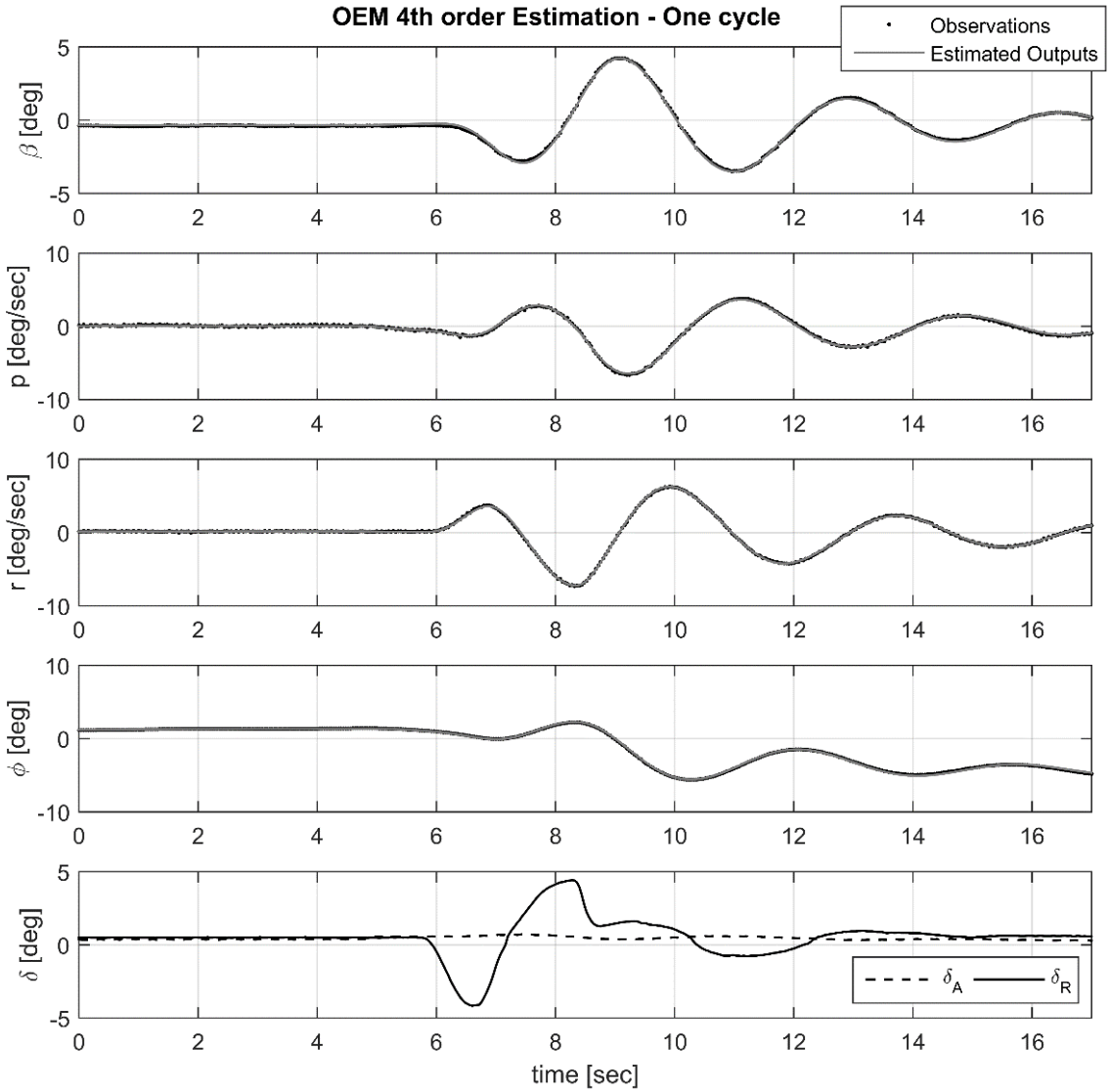

FIGURE 5.12 - OEM 4th order model estimation in one cycle (VFW 614 rudder doublet)

TABLE 5.3 - Rudder doublet input estimation in one cycle

	$\omega_{n_{DR}}$ [rad/s]	ζ_{DR}
OEM 2nd (one cycle)	1.7922	0.0879
OEM 4th (one cycle)	1.8009	0.0834

A second dataset for the rudder doublet maneuver was used to compare and validate the obtained parameters. The input has been performed over the same flight conditions, i.e., airspeed and altitude. Since the maneuver is applied in time step after the first dataset acquisition, we assume that the center of gravity and the aircraft weight are also the same. Thus, it is expected that the Dutch Roll characteristics do not change. For the validation of the TPR and NLS estimates, the obtained values of natural frequency $\omega_{n,DR}$ and damping coefficient ζ_{DR} are maintained, and new values for the amplitude K, the phase angle φ and equilibrium β_{eq} are estimated by minimizing the least squares function. This methodology is used, since we are

assuming that the Dutch-Roll characteristics are not changing but only the other parameters between each execution of the rudder doublet maneuver. The root mean squared (RMS) error between the predicted curve and the measurements of the sideslip angle for this second dataset is used as a metric of comparison. To compare the OEM with the TPR and NLS techniques, the previously estimates for matrices [$\boldsymbol{A}$] and [$\boldsymbol{B}$] were kept constant and a new estimation for the equilibrium and bias parameters were estimated for the new dataset. The RMS error is calculated over the same time interval as for the other two methods, and both the 4th and 2nd order have been used in this validation process. The calculated values for the RMS error are shown in TAB. 5.4 and FIG. 5.13 shows the validation responses.

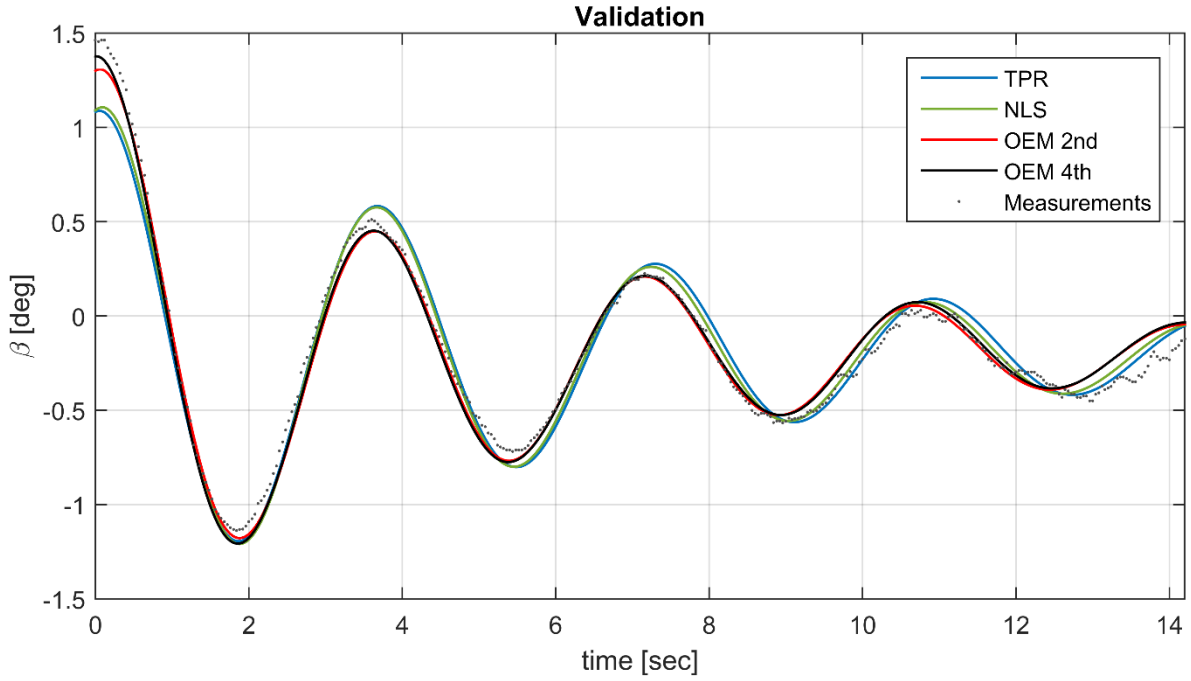

FIGURE 5.13 - Validation of the methods (VFW 614 rudder doublet)

TABLE 5.4 - RMS error obtained in validation process

	RMS error [deg]
TPR	0.1030
NLS	0.0901
OEM 2nd	0.0730
OEM 4th	0.0735

A second maneuver (bank-to-bank) was applied to observe how the aircraft respond due to aileron controls. The measurements used in estimation process are shown in FIG. 5.14.

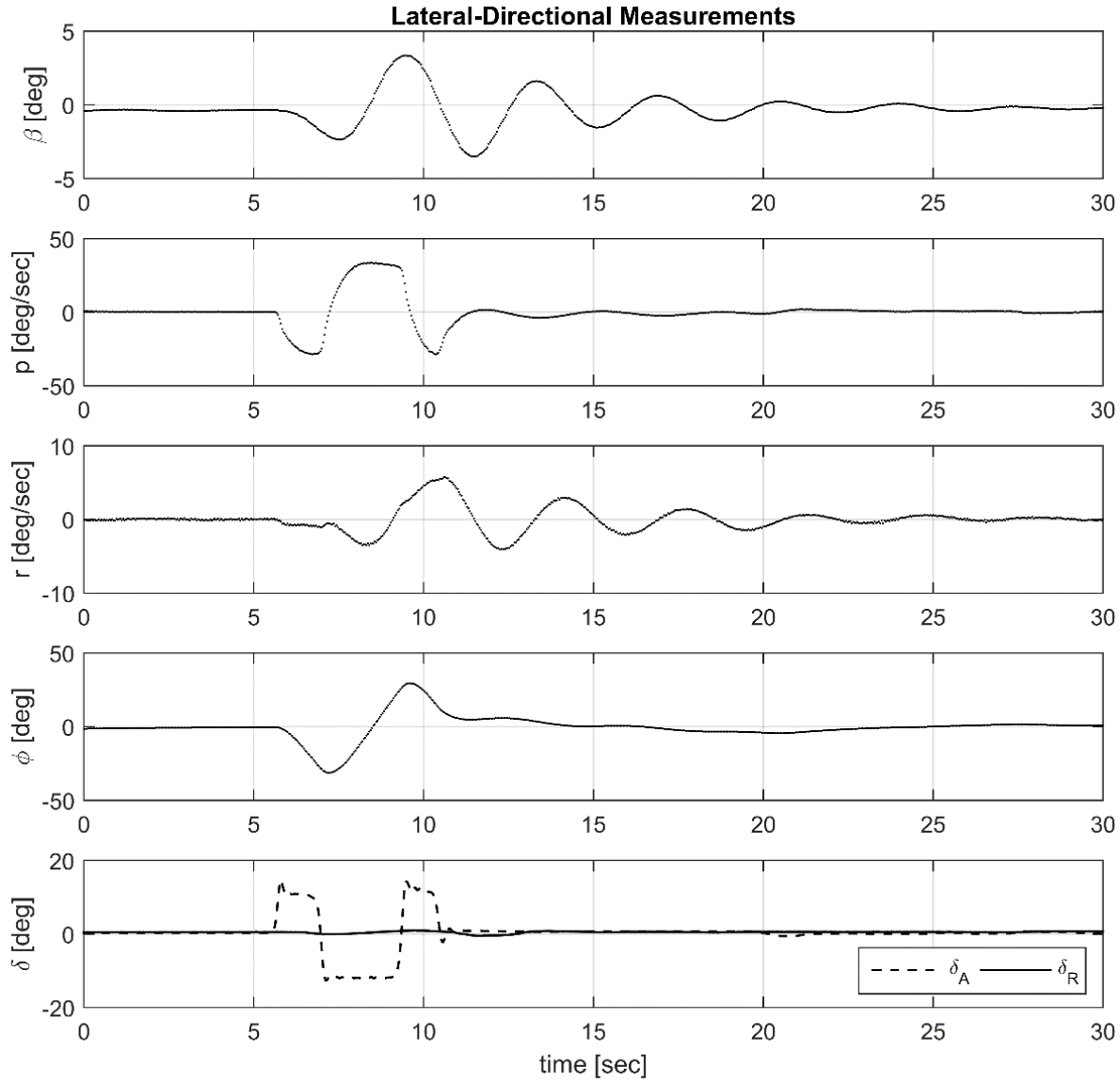

FIGURE 5.14 - Lateral-directional measurements for a bank-to-bank input (VFW 614)

By using the ailerons, the pilot made the aircraft go from $-30°$ to $+30°$ in bank angle and, then, returned it to neutral position. In this maneuver we can observe the roll rate (p) transient response, allowing us to evaluate the maneuverability of the aircraft in roll. It is important to note that the bank-to-bank maneuver had also the capability to excite the Dutch Roll mode in this aircraft.

To evaluate the Dutch Roll motion, the same techniques used with the rudder doublet were applied here. The estimated responses are presented from FIG. 5.15 to FIG. 5.19, and the parameter values are shown in TAB. 5.5.

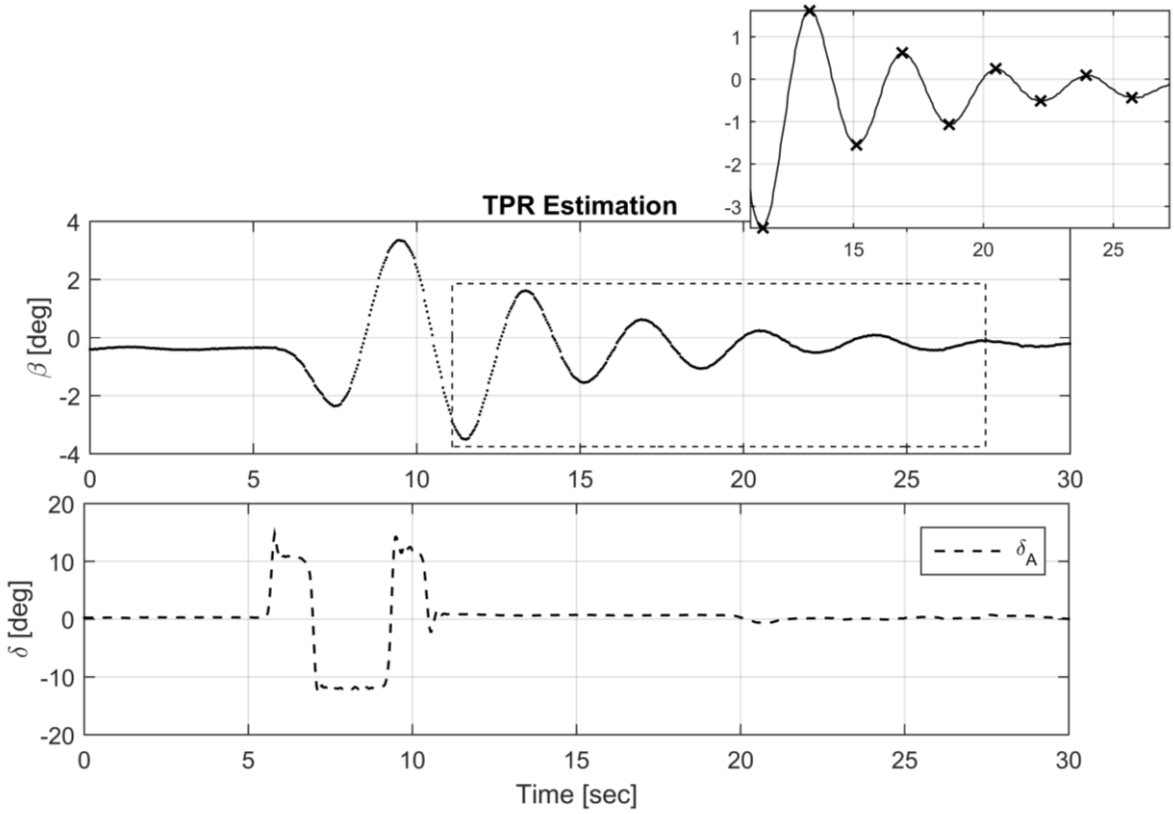

FIGURE 5.15 - TPR Dutch Roll estimation (VFW 614 bank-to-bank)
with selected peaks emphasized in the box.

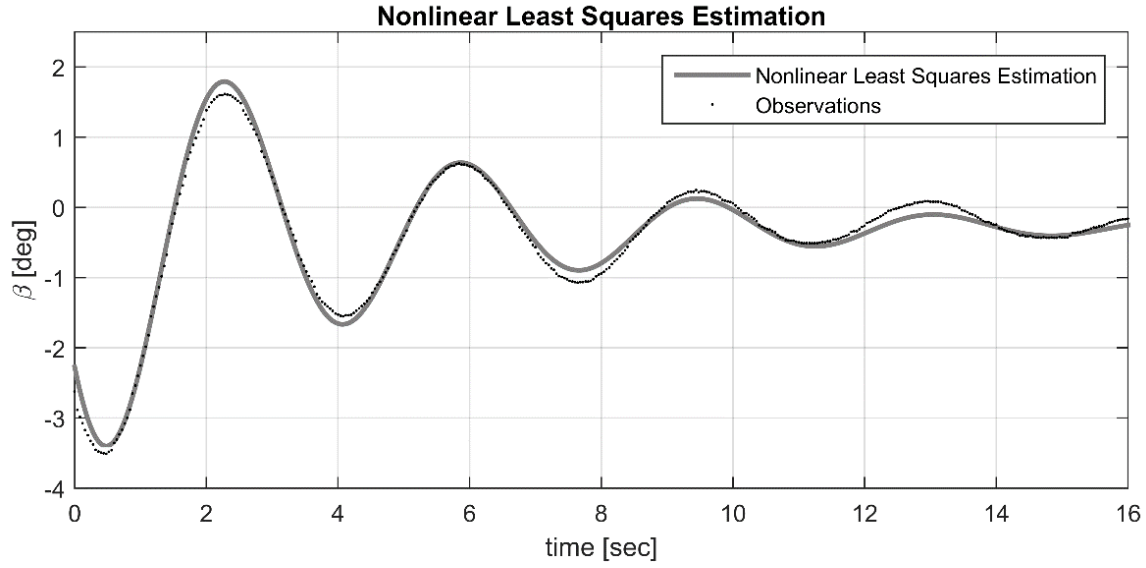

FIGURE 5.16 - NLS Dutch Roll estimation (VFW 614 bank-to-bank)

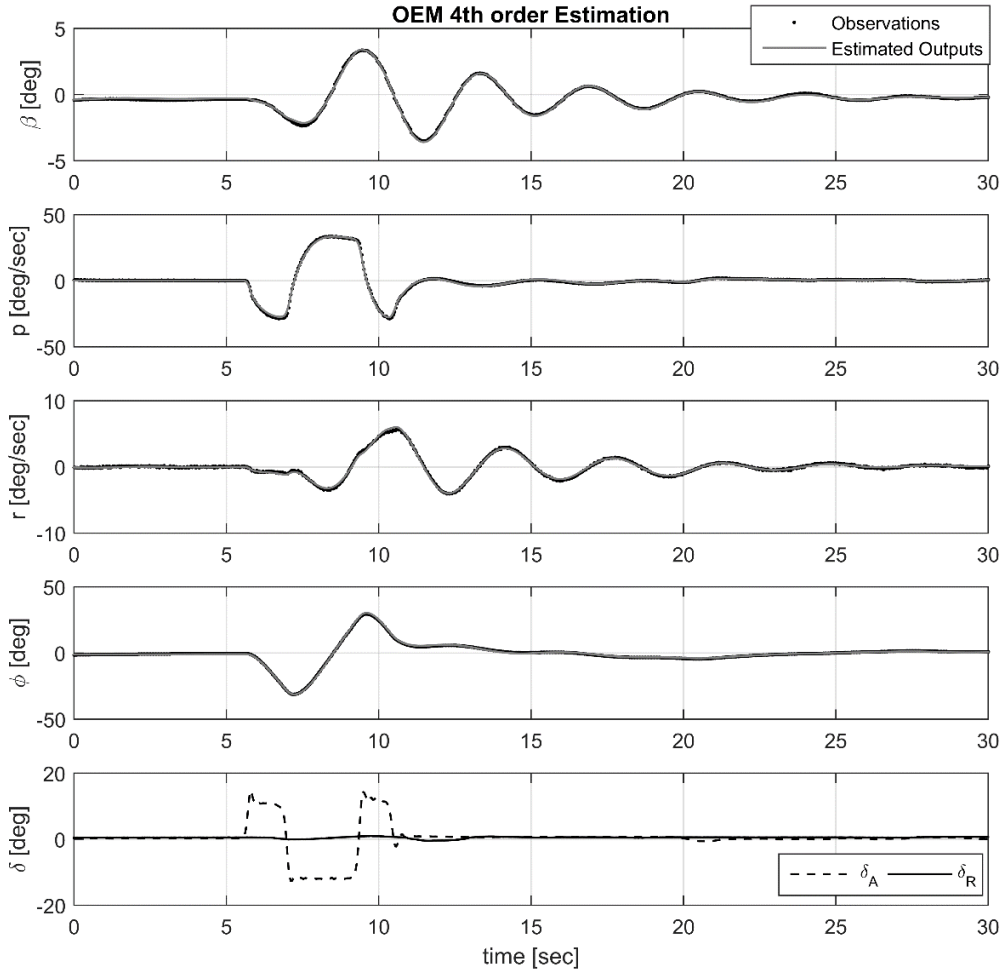

FIGURE 5.17 - OEM 4th order model estimation (VFW 614 bank-to-bank)

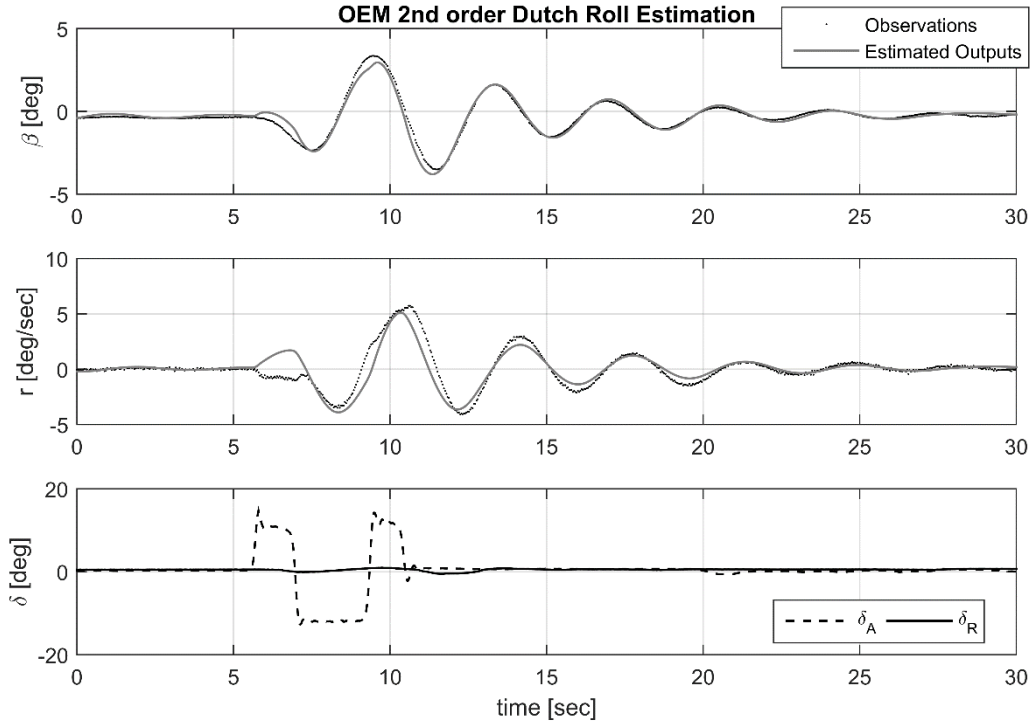

FIGURE 5.18 - OEM 2nd order model estimation (VFW 614 bank-to-bank)

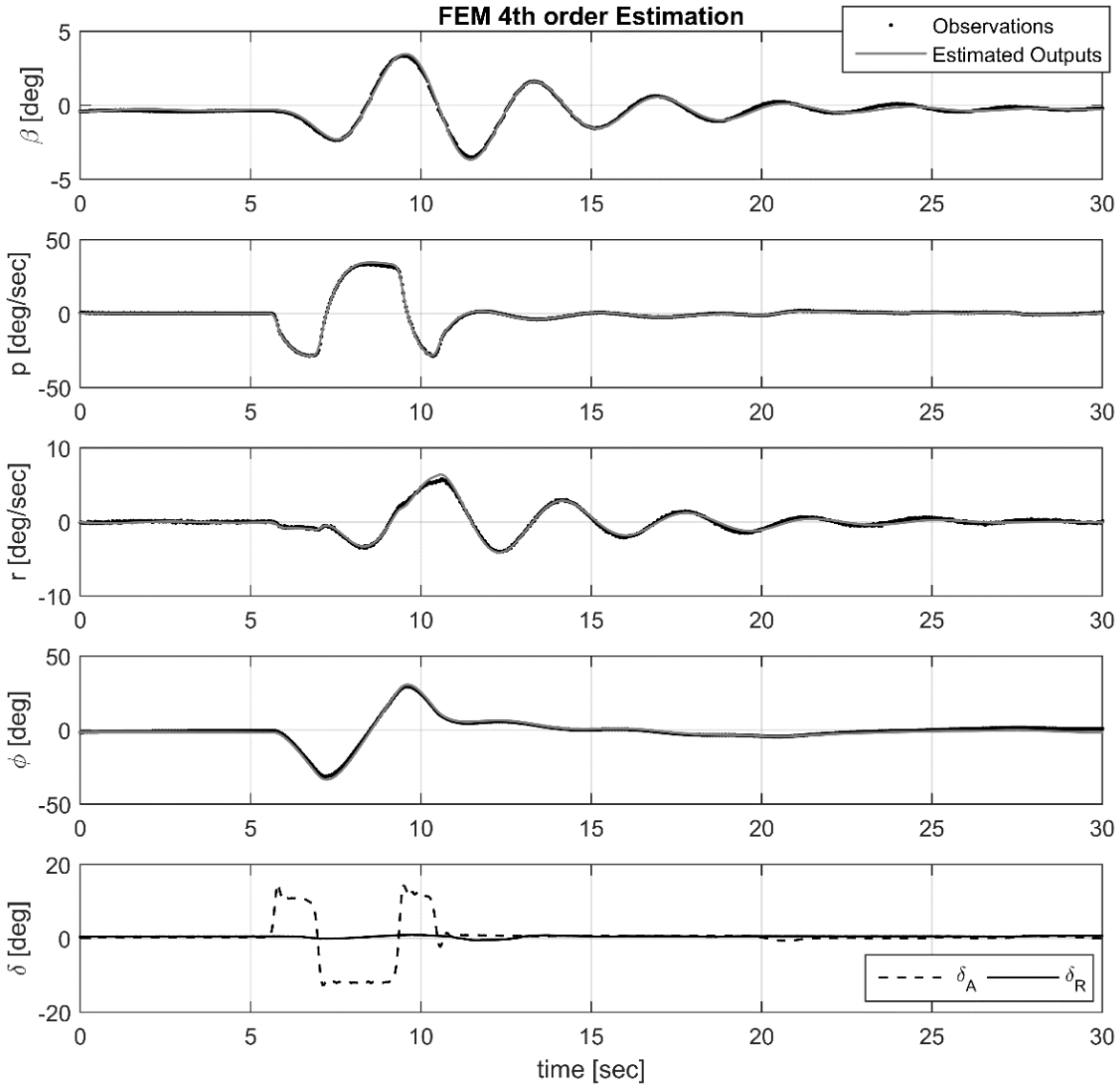

FIGURE 5.19 - FEM 4th order model estimation (VFW 614 bank-to-bank)

TABLE 5.5 - Estimation for each method based on bank-to-bank input

	$\omega_{n_{DR}}$ [rad/s]	ζ_{DR}
TPR	1.780	0.100
NLS	1.7649	1.1283
OEM 2nd	1.8041	0.0988
OEM 4th	1.8026	0.0949
FEM 4th	1.7604	0.1076

For the Roll motion analysis, it is assumed that it is a first order response in the roll rate (p) (Eq. (4.34)) in the interval approximately between 6 and 7 seconds. Thus, to obtain the Roll time constant value we used the Nonlinear Least Squares method, where both the roll time constant and roll steady state are estimated. The obtained response is shown in FIG. 5.20. The values for the estimated parameters for the Roll and Spiral motion by using the NLS, OEM and FEM from the bank-to-bank maneuver data are shown in TAB. 5.6.

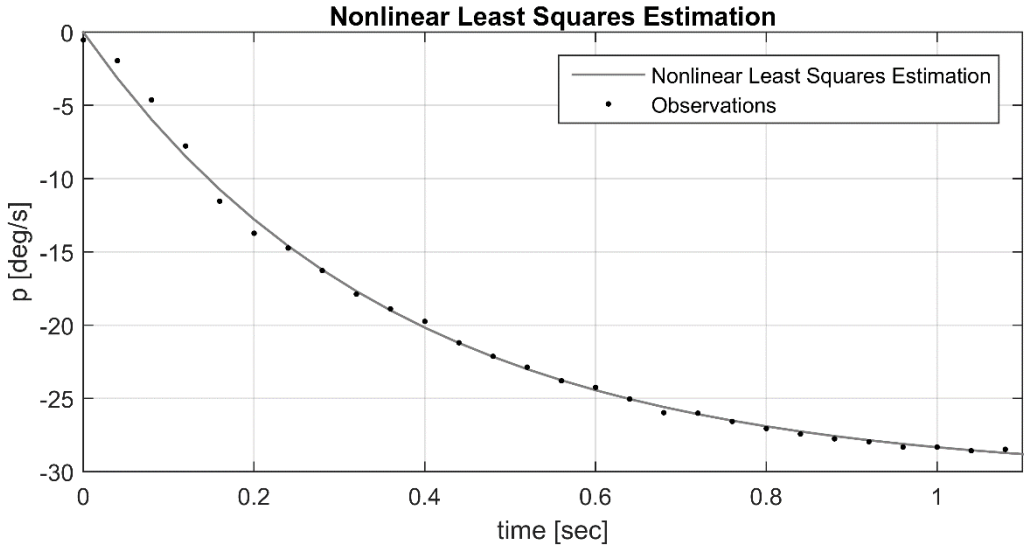

FIGURE 5.20 - NLS 1st order model estimation (VFW 614 bank-to-bank)

TABLE 5.6 - Estimation of Roll and Spiral based on bank-to-bank input

	τ_R [s]	τ_S [s]
NLS	0.365	-
OEM 4th	0.462	132.535
FEM 4th	0.4759	57.1324

A validation process was applied in this maneuver for the comparison of the NLS and OEM, where the RMS error was measured in the same time interval for the Roll Subsidence analysis. The results are shown in FIG. 5.21, and the RMS error values are presented in TAB.5.7.

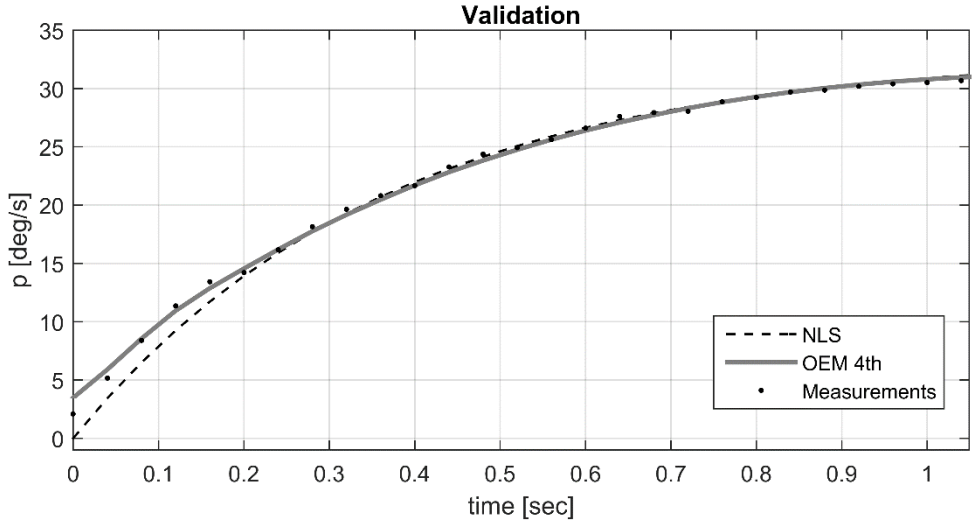

FIGURE 5.21 - Validation of the methods used for Roll estimation (VFW 614)

TABLE 5.7 - *RMS* error obtained in validation process (Roll motion)

	RMS error [deg/s]
NLS	0.8335
OEM 4th	0.4082

A most complete analysis of the lateral-directional motion for this aircraft was performed by joining both the rudder doublet and the bank-to-bank maneuver in a single dataset, which were analyzed over OEM and FEM perspective, assuming a 4th order model. This strategy is adopted to obtain the optimum parameters by the observation of the effects due to the ailerons and rudder inputs on the aircraft response in a single motion. These maneuvers are concatenated in a point where the variables at the end of the first maneuver with the beginning of the second maneuver are quite similar and is used for analysis in JATEGAONKAR (2015), thus, the analysis can be simplified here. An alternative would be by assuming that the initial conditions in each maneuver are parameters to be estimated. The free simulation of the OEM and FEM based on the optimum parameters are shown in FIG. 5.22 and FIG. 5.23. TAB. 5.8 contains the obtained parameters for each mode.

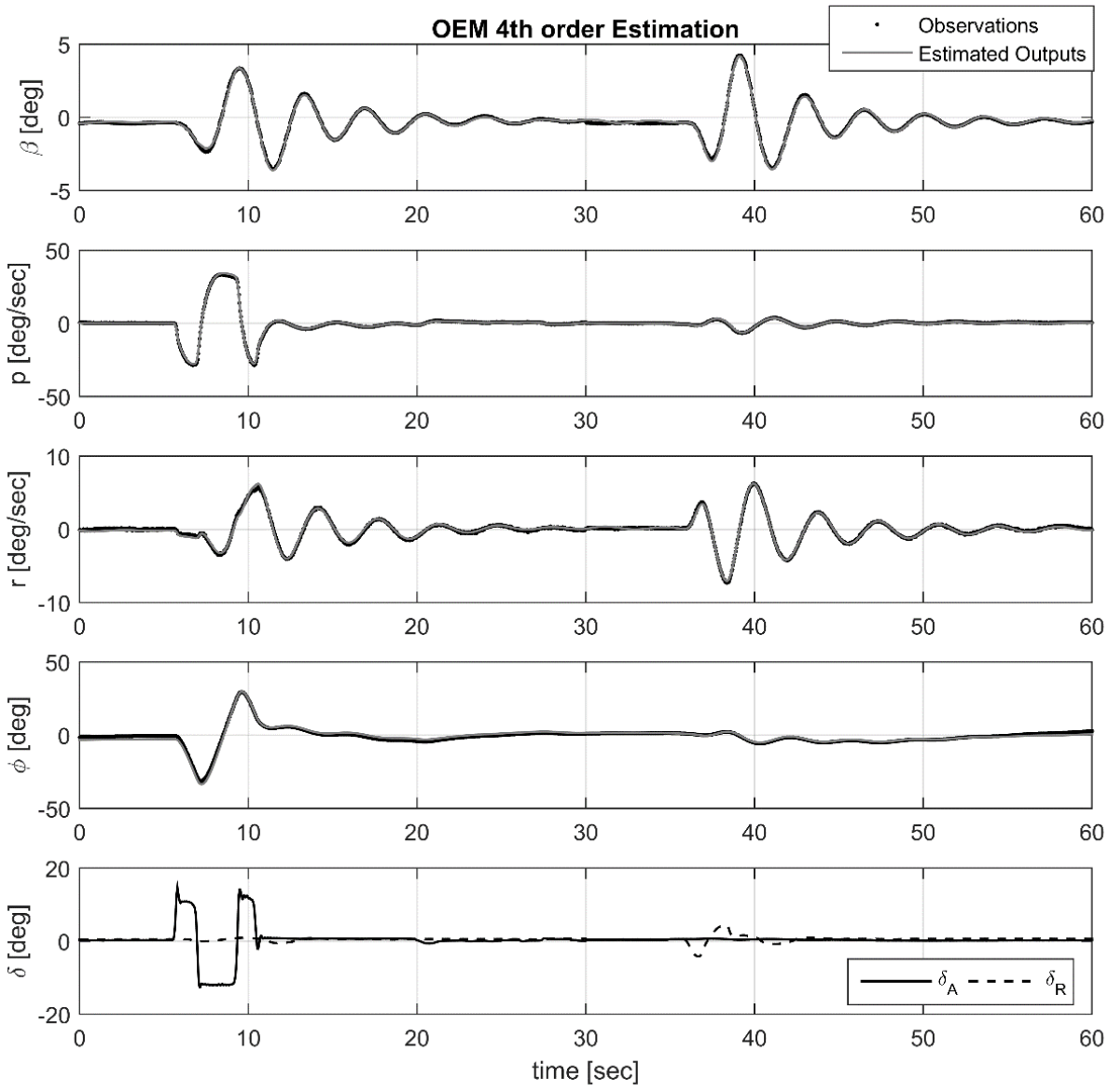

FIGURE 5.22 - OEM 4th order model estimation (VFW 614 both maneuvers)

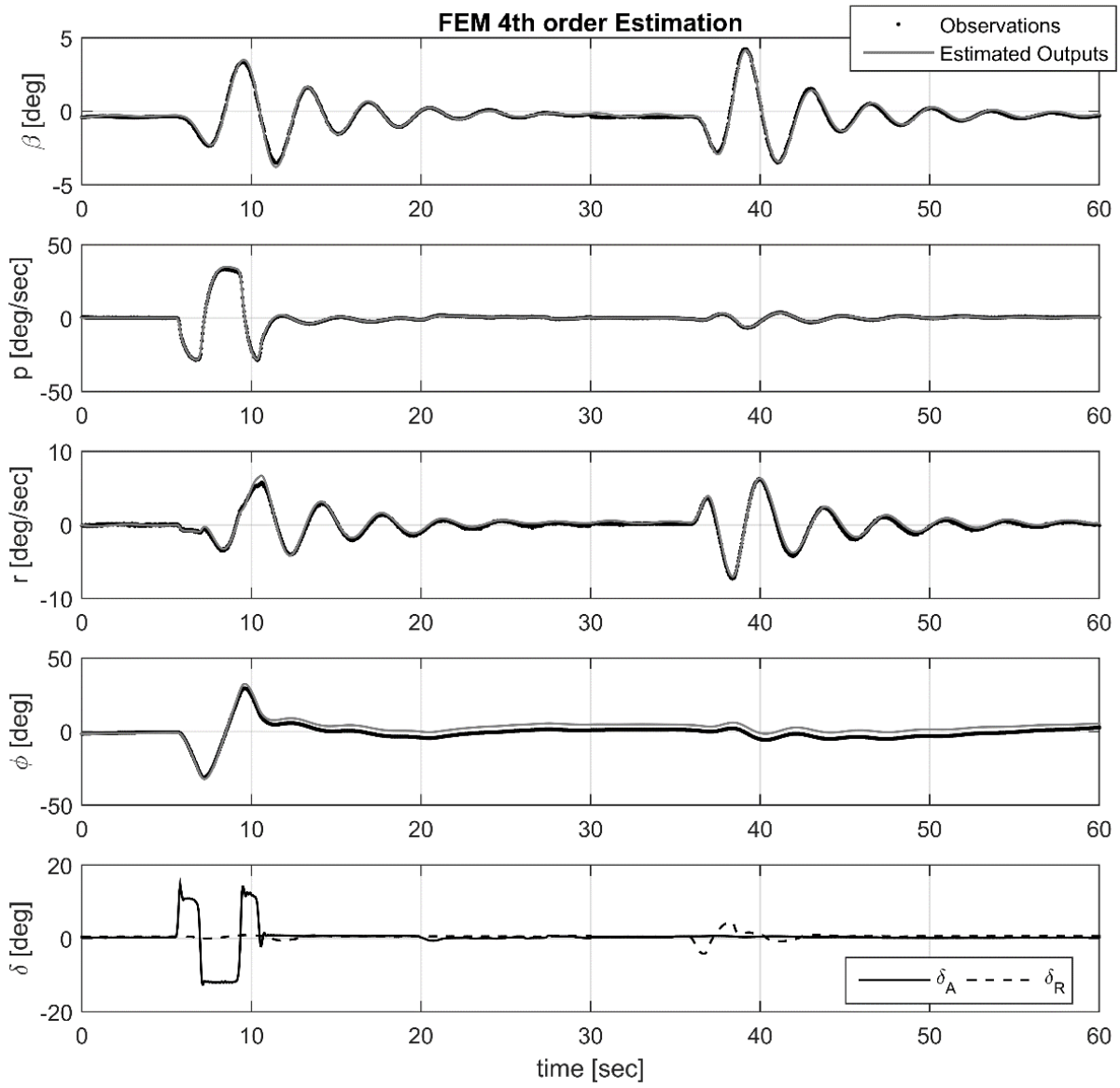

FIGURE 5.23 - FEM 4th order model estimation (VFW 614 both maneuvers)

TABLE 5.8 - Lateral-Directional estimation for both maneuvers (VFW 614)

	$\omega_{n_{DR}}$ [rad/s]	ζ_{DR}	τ_R [s]	τ_S [s]
OEM 4th	1.8011	0.0845	0.4741	65.493
FEM 4th	1.7947	0.0877	0.4797	58.4112

Since the VFW 614 is a twin jet engine aircraft, we must carefully observe the engine thrust along the responses. FIG. 5.24 shows the thrust of each engine and the difference between them for the first rudder doublet maneuver.

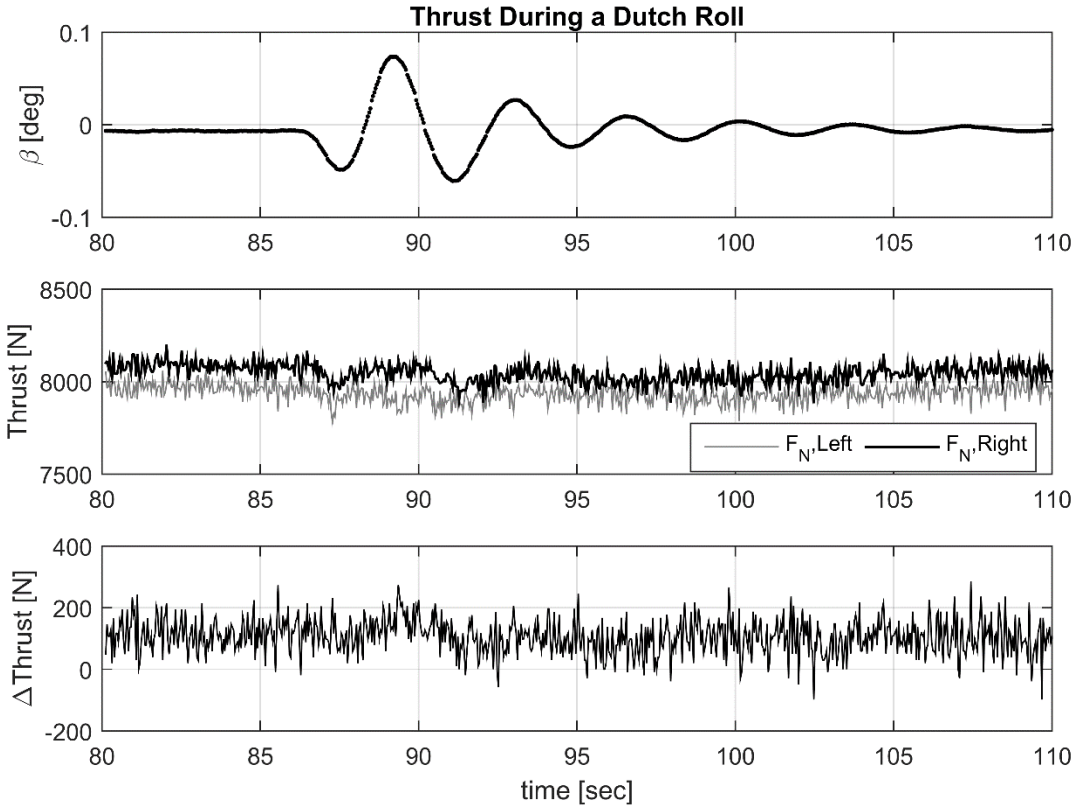

FIGURE 5.24 - VFW 614 thrust during the Dutch Roll

During the maneuver the right engine has a thrust value around 100 N higher than the left engine. This difference is probably used as a manner to trim the aircraft in its vertical axis. Any difference in the thrust value much higher than this can create a yaw moment, inducing the aircraft in a Spiral motion. It is possible to observe from FIG. 5.3 that the Spiral mode is slightly unstable since the bank angle (ϕ) tends to increase along time, which is a usual property in most of the aircrafts. In addition, we note that the rudder doublet was not capable to suppress the spiral in these tests, which is not an easy task for the pilot. An another interesting observation of the Spiral can be done by the chart of $\beta \; x \; \phi$, which shows the aircraft motion after the doublet maneuver (FIG. 5.25). While the sideslip angle tends to return to the equilibrium, the bank angle tends to slowly increase along time. It is a hard task to determine what is the right value for the Spiral time constant, because the available data have only a small part of its response. However, the obtained values with the FEM in the full dataset and in the bank-to-bank are very close one each other, which is due to the fact that this method is capable to estimate unstable modes. Thus, we can assume that the Spiral time constant is: $\tau_S \approx -57\text{sec}$.

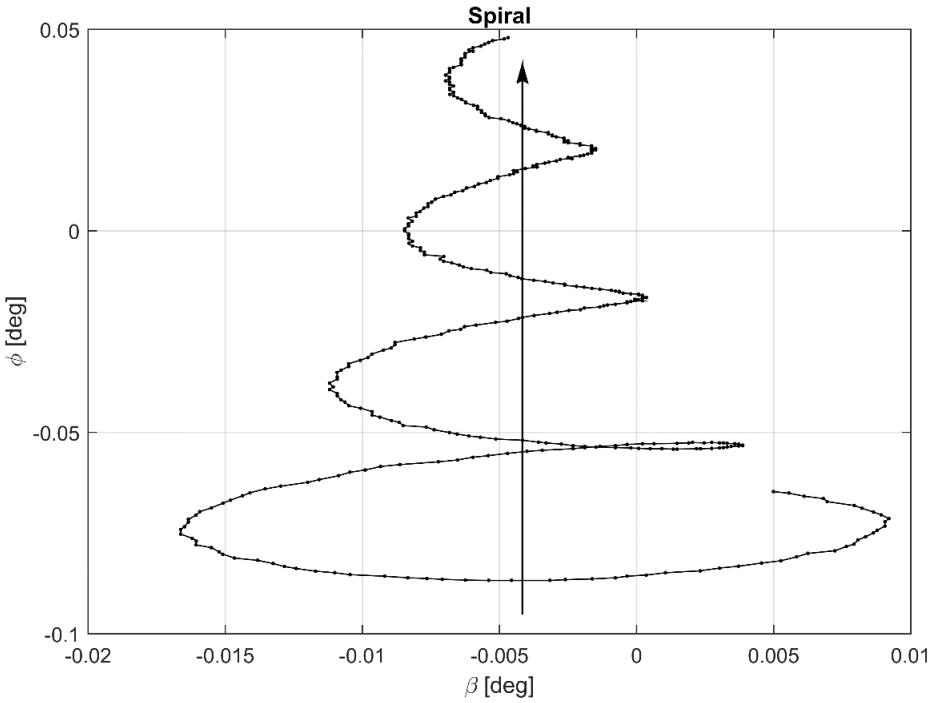

FIGURE 5.25 - VFW 614 Spiral behavior

From the values shown from TAB. 5.2 to TAB. 5.5, we realize that there is a small variation between the obtained parameters in the doublet and in the bank-to-bank. This can be explained due to the fact that the flight conditions are not exactly the same. The aircraft weight changes in time due to fuel consumption, and, thus, the trim conditions. Anyway, the most recommended maneuver for the Dutch Roll excitation is the rudder doublet, since it tries to do not excite any of the other lateral-directional modes, which is one of the primary requirements by the classical data reduction methods for a good estimation. In spite of the higher RMS error for the TPR method, we observe that its estimation are very consistent when compared with the other methods. The NLS shows to be a good alternative to the TPR method, since it uses only the sideslip observations for estimation process. In addition, all the points are used for estimation, while the TPR only use the peaks. The Dutch Roll characteristics obtained with the OEM and FEM using the 2^{nd} order model are very close to that obtained with a 4^{th} order model, showing that this is a satisfactory assumption. It is interesting to note that the analysis by using only the doublet maneuver and the analysis with the two lateral-directional maneuvers, results in a very close values for the Dutch-Roll natural frequency and damping, which we assume here as the much reliable results, due to statistical properties of the system identification methods used here.

In the Roll motion analysis, we observe that the NLS value is quitely different from the values obtained with the OEM and FEM. This can be explained due to the fact that in the bank-

to-bank roll, the pilot bring the stick to the opposite side very quickly, then, there is not the observation of the pure roll motion in only one direction. To improve the NLS estimative a degree input in the ailerons could be applied. The obtained values for the Roll time constant with the OEM and FEM are very close one each other, and are assumed most reliable estimative.

5.1.2 Longitudinal motion analysis

For the longitudinal motion analysis of the VFW 614, a "3-2-1-1" maneuver has been applied with the elevator to excite the short-period, which is the fastest longitudinal mode. A step time Δt of around 1 second is observed. We observe that the short-period motion was successfully excited, as shown in the first dataset, used for estimation process (FIG. 5.26). As expected on the Short-Period response, there is a low variation of the aircrafts airspeed, and the motion is mainly characterized by the variation of the angle of attack (α).

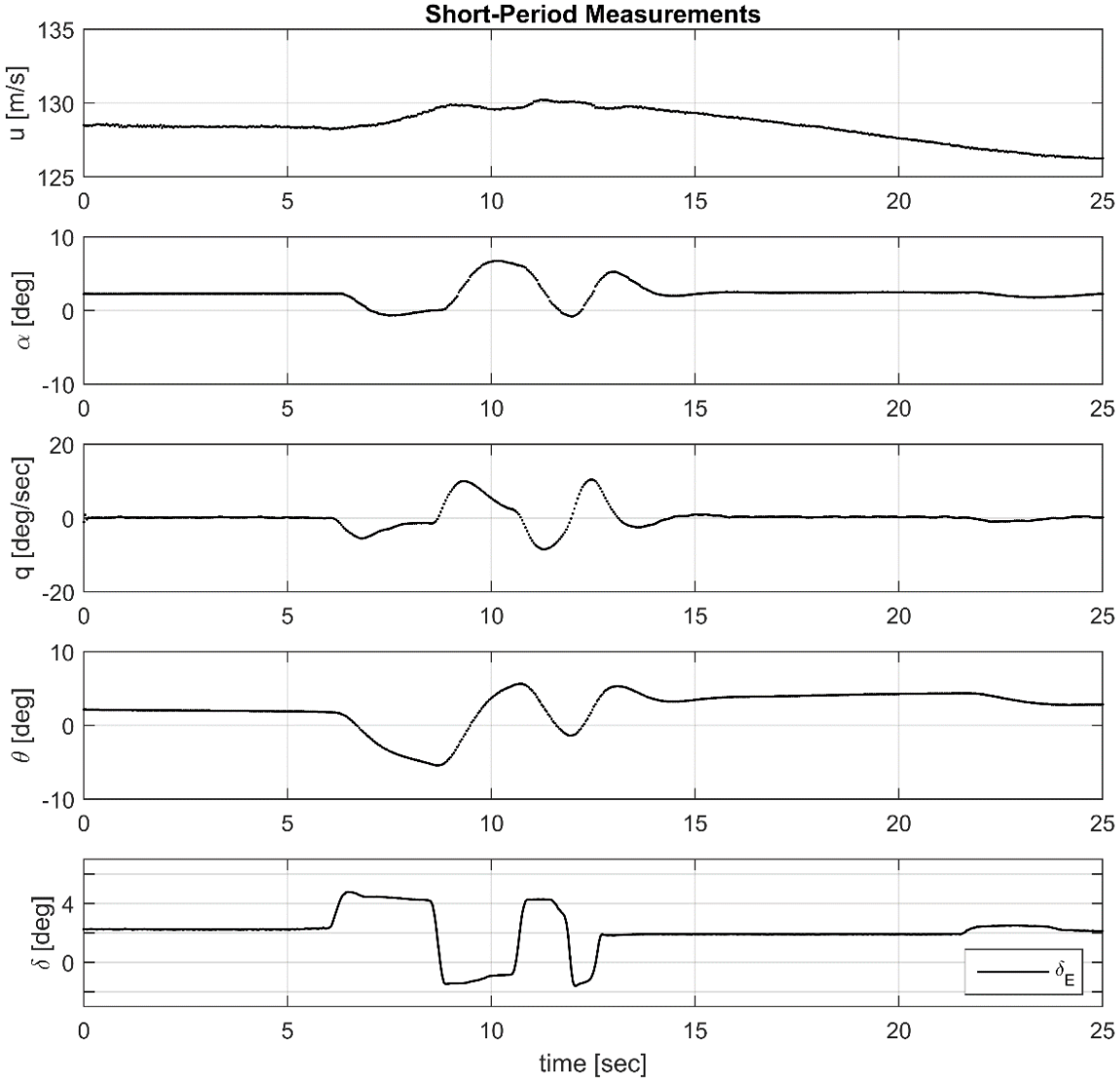

FIGURE 5.26 - Longitudinal measurements for a 3-2-1-1 input (VFW 614)

Two classical methods were used here for the short-period analysis. The graphical measurements for the Maximum Slope are shown in FIG. 5.27. These measurements depend on the engineer interpretation. Even with low noise data, it is not a simple task to implement on a computer an automatic determination of the required parameters for this analysis, thus, a manual measurement of the parameters are preferable. From the obtained parameters, we used the chart of FIG. 4.4 to obtain the damping coefficient ($\zeta = 0.48$) and the natural frequency ($\omega_{n,SP} = 2.33\ \mathrm{rad/s}$).

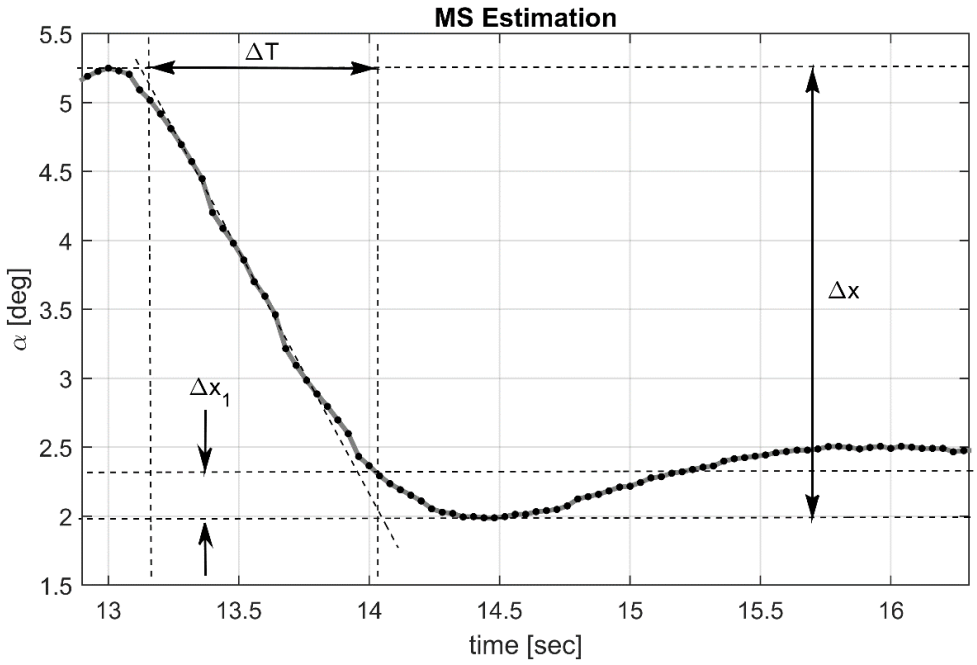

FIGURE 5.27 - MS estimation for a 3-2-1-1 input (VFW 614)

The Time Ratio method is also used here, where it is necessary to guess the equilibrium condition. Then, tree points on the transient response curve must be calculated as shown in Section 4.1.2 and, thus, the three time ratio values (FIG. 5.28). For each of these ratios, a damping and a natural frequency values are obtained by using the chart in FIG. 4.6. The first ratio is lower than 0.6, therefore, it cannot be used for the estimation process, then. The estimative for the second ratio is $\zeta_2 = 0.63$ and $\omega_{n2} = 2.484\ \mathrm{rad/s}$; and for the third ratio we obtain $\zeta_3 = 0.54$ and $\omega_{n3} = 2.382\ \mathrm{rad/s}$. The mean of these values are assumed as the Short-Period characteristics, which are: $\zeta = 0.585$ and $\omega_n = 2.433\ \mathrm{rad/s}$.

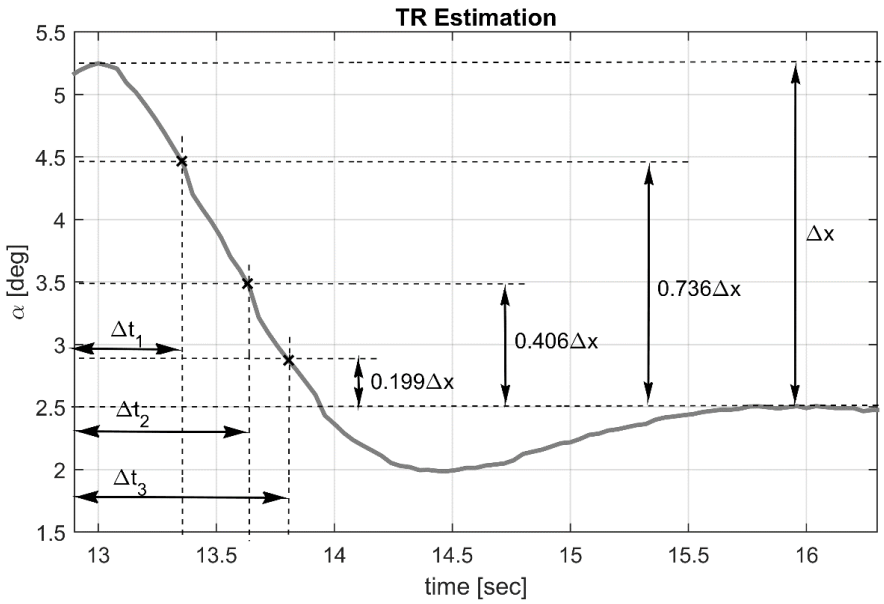

FIGURE 5.28 - TR estimation for a 3-2-1-1 input (VFW 614)

Observing the angle of attack measurements, we used here the same assumptions for the Nonlinear Least Squares estimation as that used in lateral-directional motion. The curve fit is shown in FIG. 5.29, and the motion parameters are: $\zeta_{SP} = 0.5078$ and $\omega_{n,SP} = 2.4706\ \mathrm{rad/s}$.

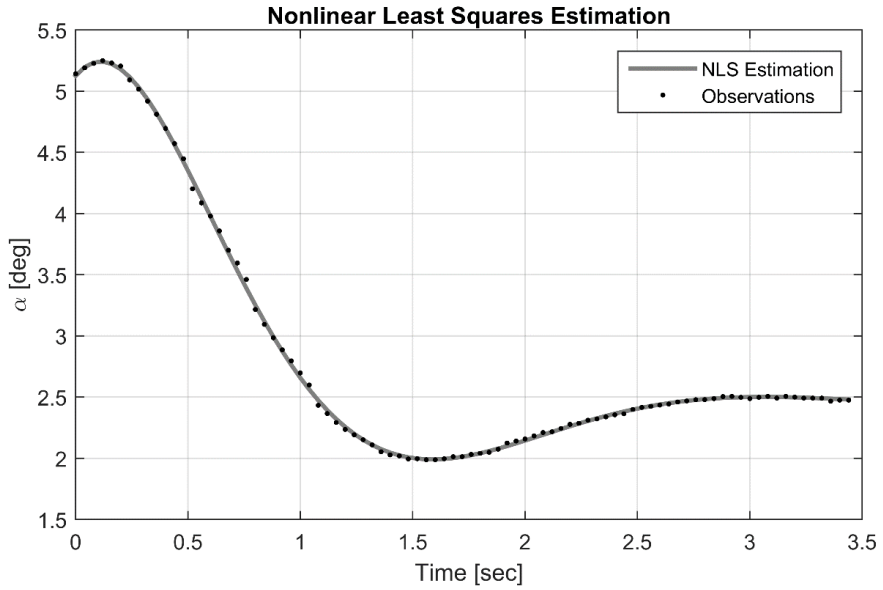

FIGURE 5.29 - NLS estimation for a 3-2-1-1 input (VFW 614)

The estimated responses for the Equation Error Method based on the 4th order model (FIG. 5.30) is quite better than that obtained in the analysis of the lateral-directional motion and are a good initial estimative for the OEM method. Nevertheless, the quality of the EEM curves are not enough for a reliable estimative of the short-period parameters.

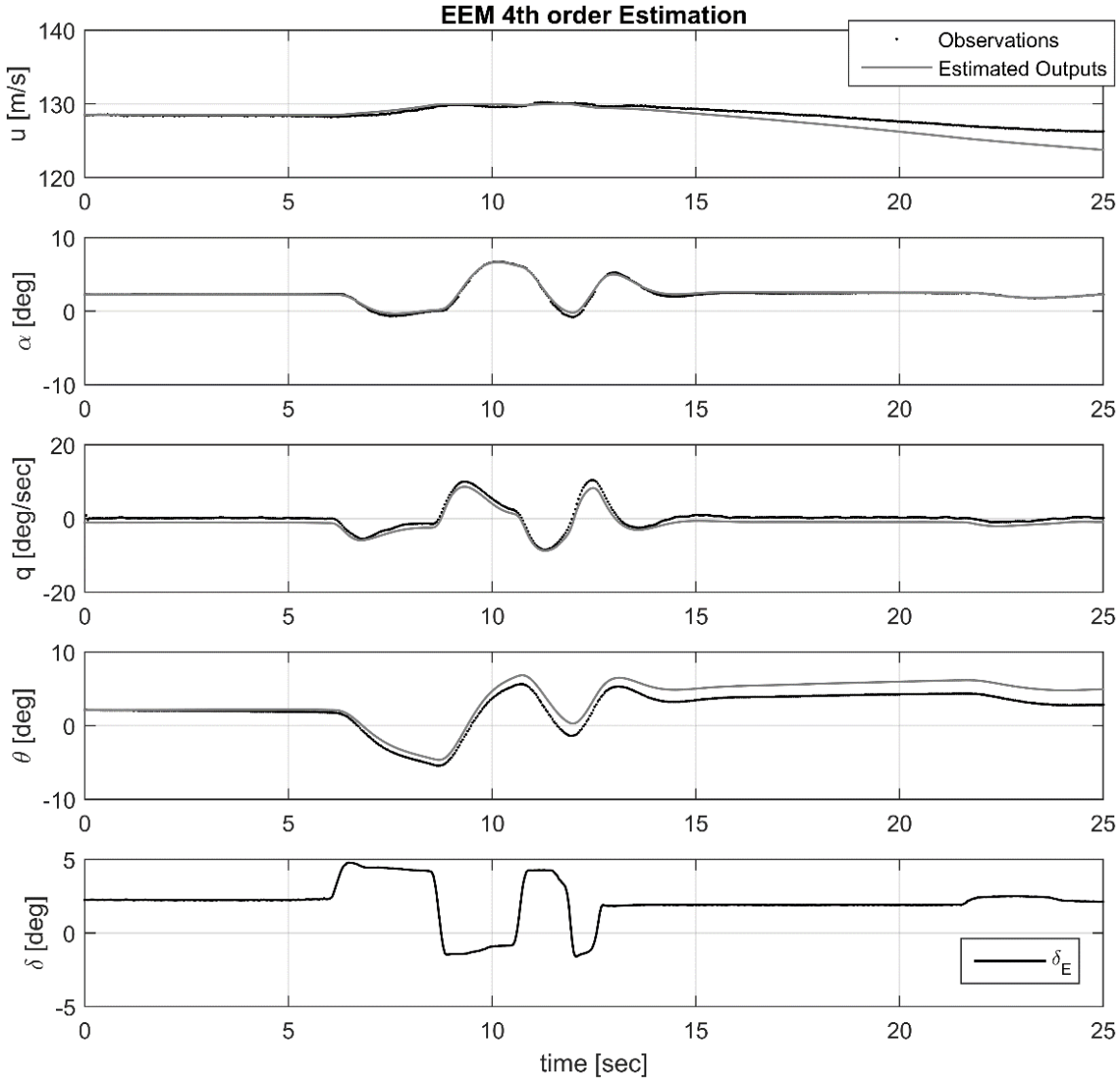

FIGURE 5.30 - EEM 4th order model estimation for a 3-2-1-1 input (VFW 614)

The estimation process has been done using the Output Error Method, assuming the 2nd and 4th order models. The obtained responses are shown in FIG. 5.31 and FIG. 5.32. For both cases a reliable model is obtained, given its simplifications. The parameters obtained for the all methods are summarized in TAB. 5.9.

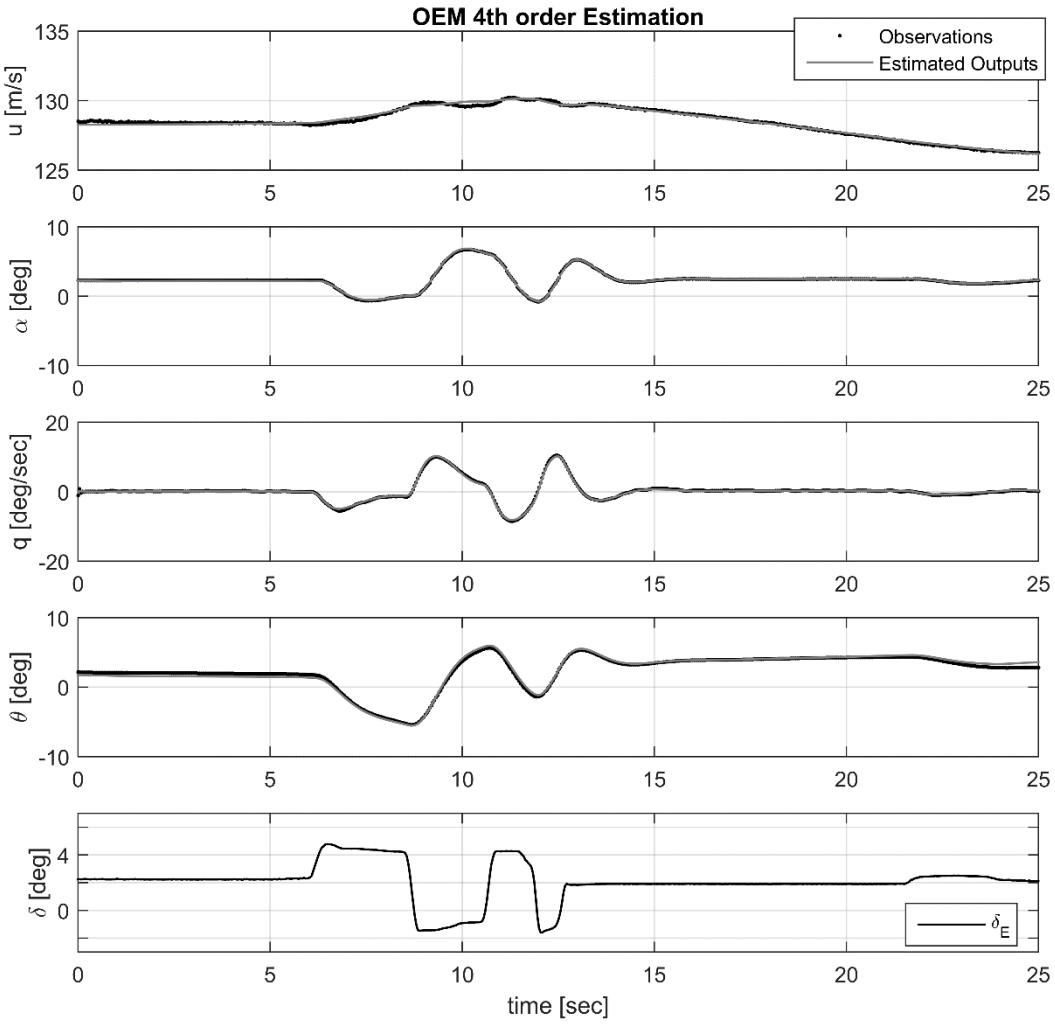

FIGURE 5.31 - OEM 4th order model estimation for a 3-2-1-1 input (VFW 614)

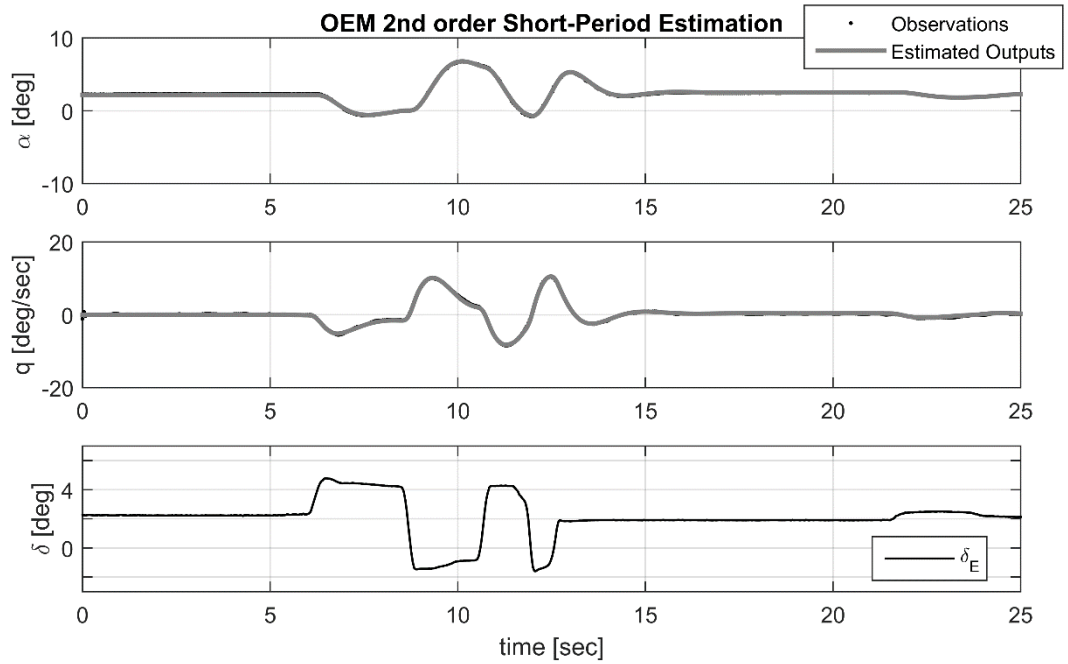

FIGURE 5.32 - OEM 2nd order model estimation for a 3-2-1-1 input (VFW 614)

TABLE 5.9 - Longitudinal estimation for a 3-2-1-1 maneuver

	$\omega_{n_{SP}}$ [rad/s]	ζ_{SP}
MS	2.33	0.48
TR	2.433	0.585
NLS	2.4706	0.5078
OEM 2nd	2.5387	0.4988
OEM 4th	2.5405	0.5111

To compare the methods, a new dataset with a "3-2-1-1" maneuver is used. The MS, TPR and NLS methods are evaluated by the minimization of least squares function, keeping the same values for the natural frequency and damping obtained in the estimation process. For the OEM, parameters of matrices [$\boldsymbol{A}$] and [$\boldsymbol{B}$] are maintained, while new values for the equilibrium and bias parameters are estimated, since it is different dataset. Thus the RMS error, is calculated for each method over the same time interval, as shown in FIG. 5.33 and TAB. 5.10.

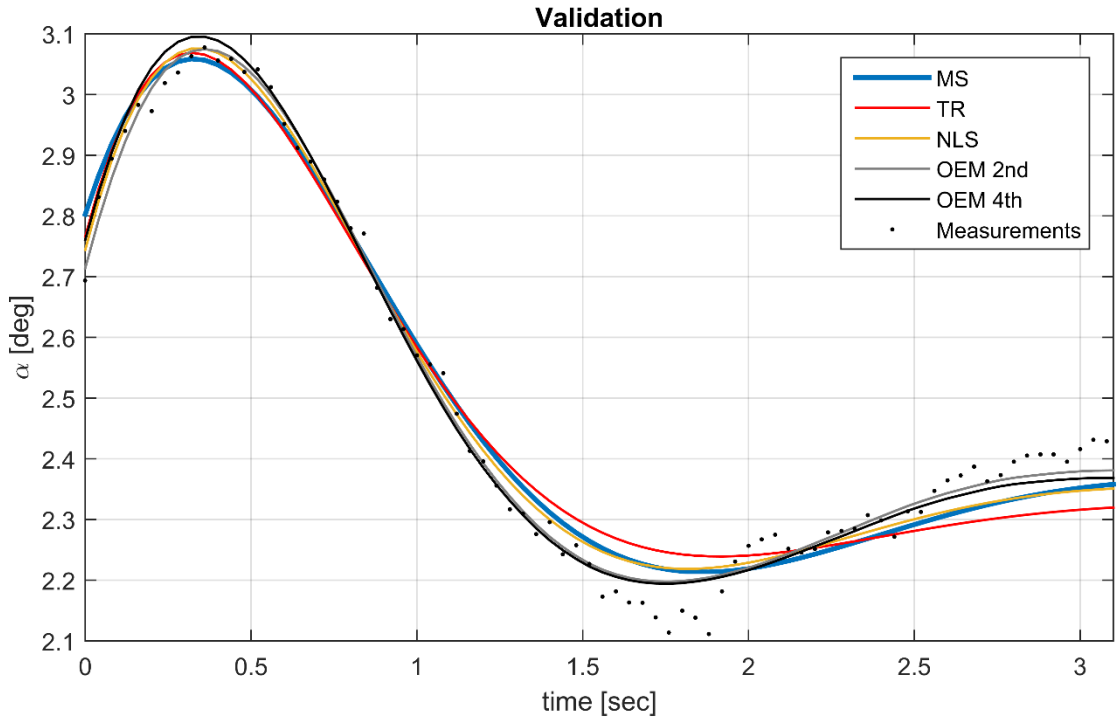

FIGURE 5.33 - Validation of the methods (VFW 614 / 3-2-1-1 maneuver)

TABLE 5.10 - RMS error obtained in validation process (Short-Period motion)

	RMS error [deg]
MS	0.047
TR	0.061
NLS	0.0430
OEM 2nd	0.0295
OEM 4th	0.0341

We note that there is significant difference between the values obtained by the Maximum Slope and Time Ratio methods when compared with the NLS and the OEM results. They has also a higher value of RMS error. These differences observed are due to the difficult in the application of such methods, which are very sensitive due to the engineer judgment. Even with a well filtered data, there is still noise in the signal, interfering during the graphical interpretation. Other difficult task is to determine the equilibrium value after the short-period response, since small variations in the input can generate significant perturbations in the angle of attack during such analysis. Nonetheless, the obtained parameters with the MS and TR present a great proximity in order of magnitude when compared with the other methods. Here, the OEM results are assumed as the most reliable ones, not only because of its lower RMS error values, but also due to its properties, and the good estimates observed in FIG.5.31 and FIG.5.32.

5.2 ACS-100 Sora

The ACS-100 Sora was designed and built by the Advanced Composite Solution (ACS) Company (ACS AVIATION, 2006). Its project is based in the CEA-306 CB.10 Thriatlon, designed by Professor Cláudio Barros from the Center for Aeronautical Studies (CEA) of Federal University of Minas Gerais (UFMG), Brazil. It is a two-seater passenger airplane and with structure built in composite materials. Some dimensional and performance details can be observed in FIG. 5.34, FIG. 5.35 and TAB. 5.11.

TABLE 5.11 - ACS-100 Sora Dimensions and Performance Data

Dimensions		
Span	7.5 m	24.6 ft
Wing Area	8.7 m^2	93.2 ft^2
Length	6.5 m	21.3 ft
Cabin Height	1.1 m	42 in
Performance (100 HP)		
Cruise Speed	250 km/h	155 mph
Stall Speed	83 km/h	52 mph
Never exceed Speed	340 km/h	211 mph
Climb Rate	7 m/s	1377 ft/min
Take-off distance	190 m	623 ft
Landing distance	250 m	819 ft
Load Factors	+6g / -4g	

SOURCE - (ACS AVIATION, 2006)

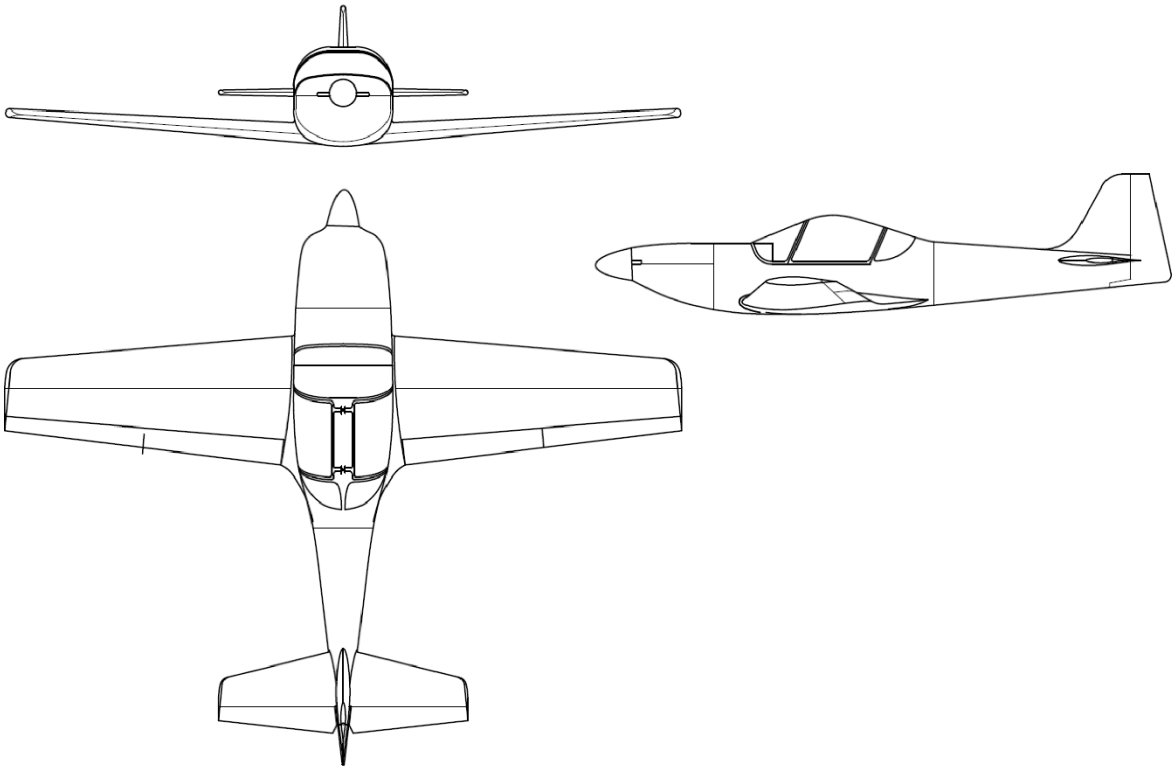

FIGURE 5.34 - ACS-100 Sora 3 view
SOURCE - (ACS AVIATION, 2006)

FIGURE 5.35 - ACS-100 Sora picture

A Flight Data Acquisition System (CEA-FDAS) was mounted in Sora for data acquisition (DUTRA, 2010). This system is composed by a central computer for data processing and storage, an analog acquisition board, an inertial platform AHRS-400, a GPS (Global

Positioning System) and a aerodynamic probe for the measurements of the angles of the wind relative to the body frame. Linear transducers and other sensors were connected to the analog board for the data acquisition, as shown from FIG. 5.36 to FIG. 5.38. The CEA-FDAS has a synchronous code which interrupts the analog channels sampling for 210 ms at every 2 second, to waits for the GPS message transmission. Because of it, during the analysis, several intervals can be observed in the data set. This aspect is an important consideration during the estimation process.

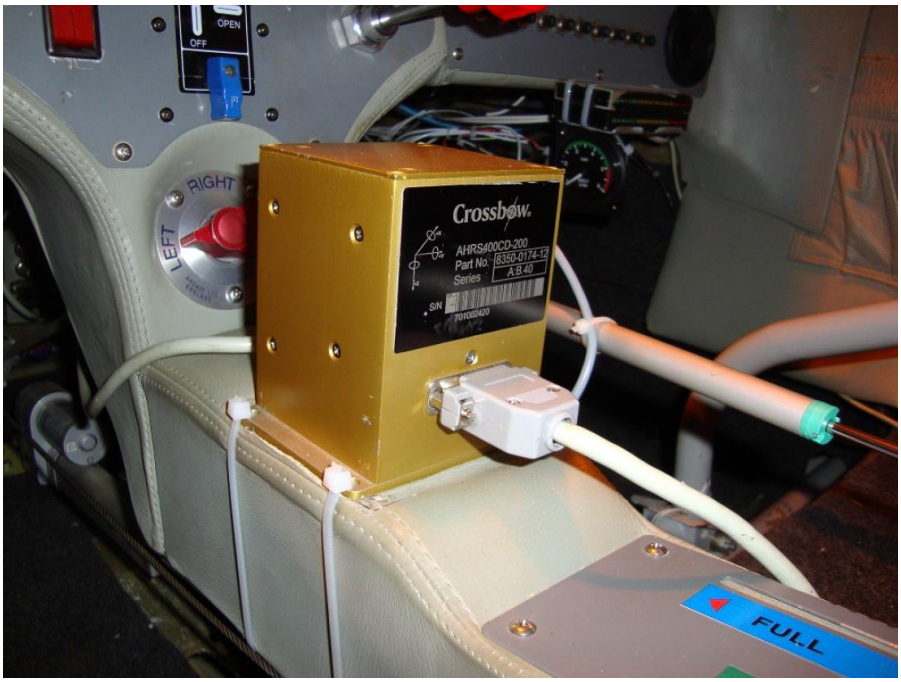

FIGURE 5.36 - ARS-400 used for Sora flight test
SOURCE - (DUTRA, 2010)

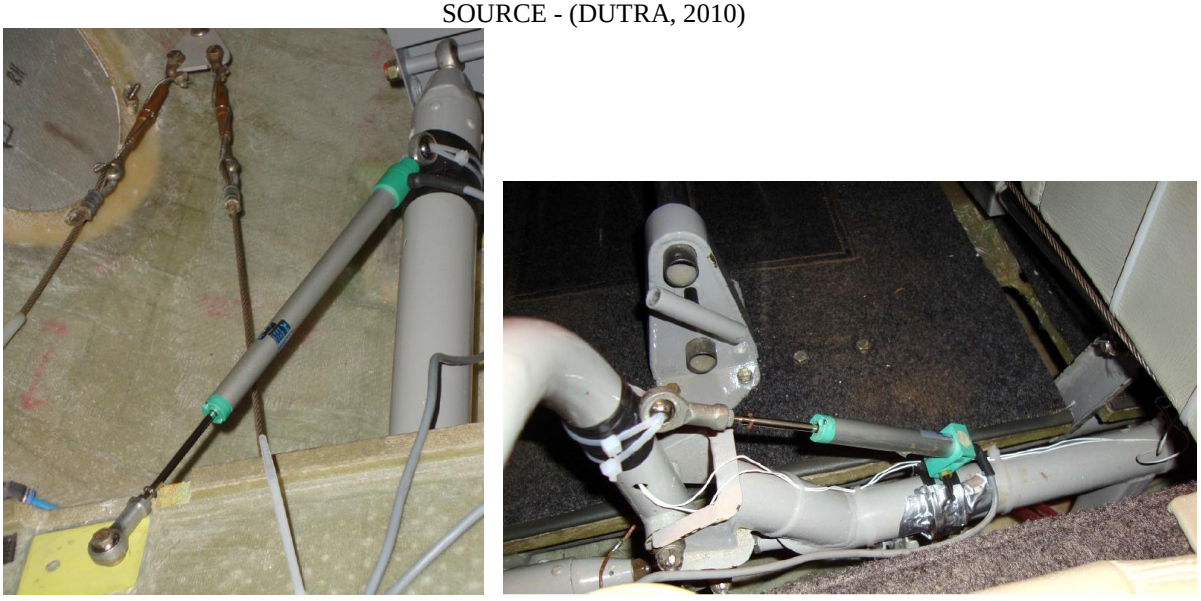

(a) (b)

FIGURE 5.37 - Some of the linear transducers installed to measure commands deflections. (a)elevator, (b)aileron.
SOURCE - (DUTRA, 2010)

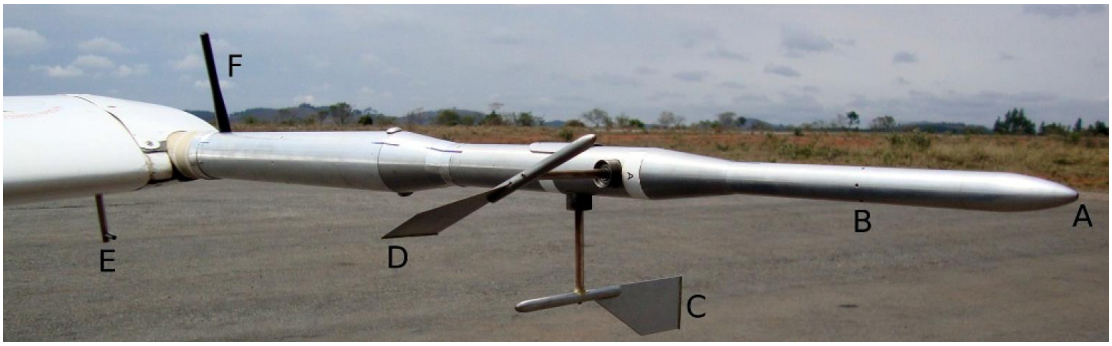

FIGURE 5.38 - Aerodynamic probe used for Sora flight tests. A) total pressure intake, B) static pressure intake, C) sideslip angle flag, D) angle of attack flag, E) temperature sensor and F) antenna
SOURCE - (DUTRA, 2010)

5.2.1 Lateral-Directional Motion Analysis

During Sora flight test campaign, several maneuvers have been performed to analyze each dynamical mode. To observe the Dutch Roll oscillation a rudder doublet input was used. The measurements after the input, shown in FIG. 5.39, were used here as a dataset for the estimation process.

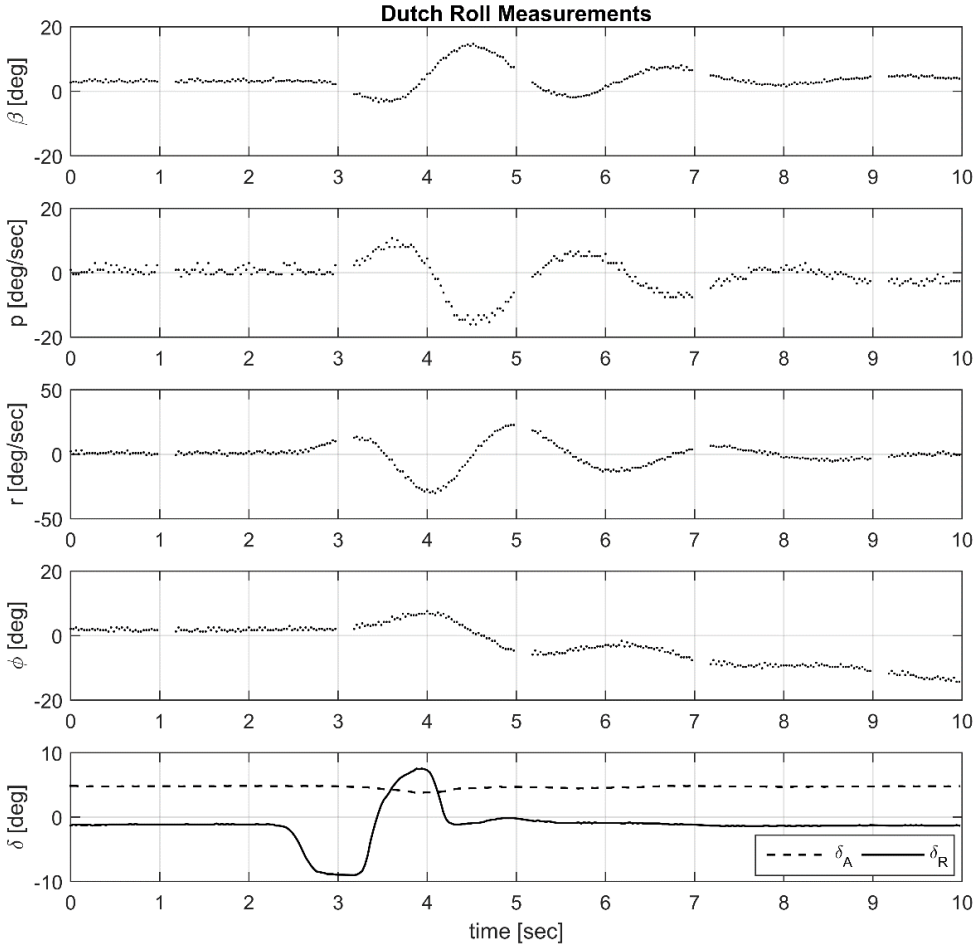

FIGURE 5.39 - Lateral-directional measurements for a doublet input (Sora)

We observe that Sora has a faster response than the VFW 614, however, its Dutch Roll mode is still observed as damped sinusoid, which reaches its steady state with a little more than 6 seconds. This is an expected behavior since this is a smaller aircraft than the VFW 614, thus its aerodynamic, inertial and propulsive properties tends to a faster response. The time step Δt used by the pilot for the input was of about 1 sec, and quite symmetric.

The graphical method used to evaluate this mode was the Transient Peak Ratio (or the MTPR). Due to the high noise level in the available data, it was required to use a low pass filter for such analysis, since the noise creates interferences in the engineer interpretation, making it a harder task. FIG. 5.40 shows the raw and the filtered data, and the selected peaks. From these ratios and the measurement of the period T, the chart of FIG. 4.4 is used to determine the natural frequency and the damping coefficient, which obtained values are: $\omega_{n,DR} = 2.599$ rad/s and $\zeta_{DR} = 0.171$.

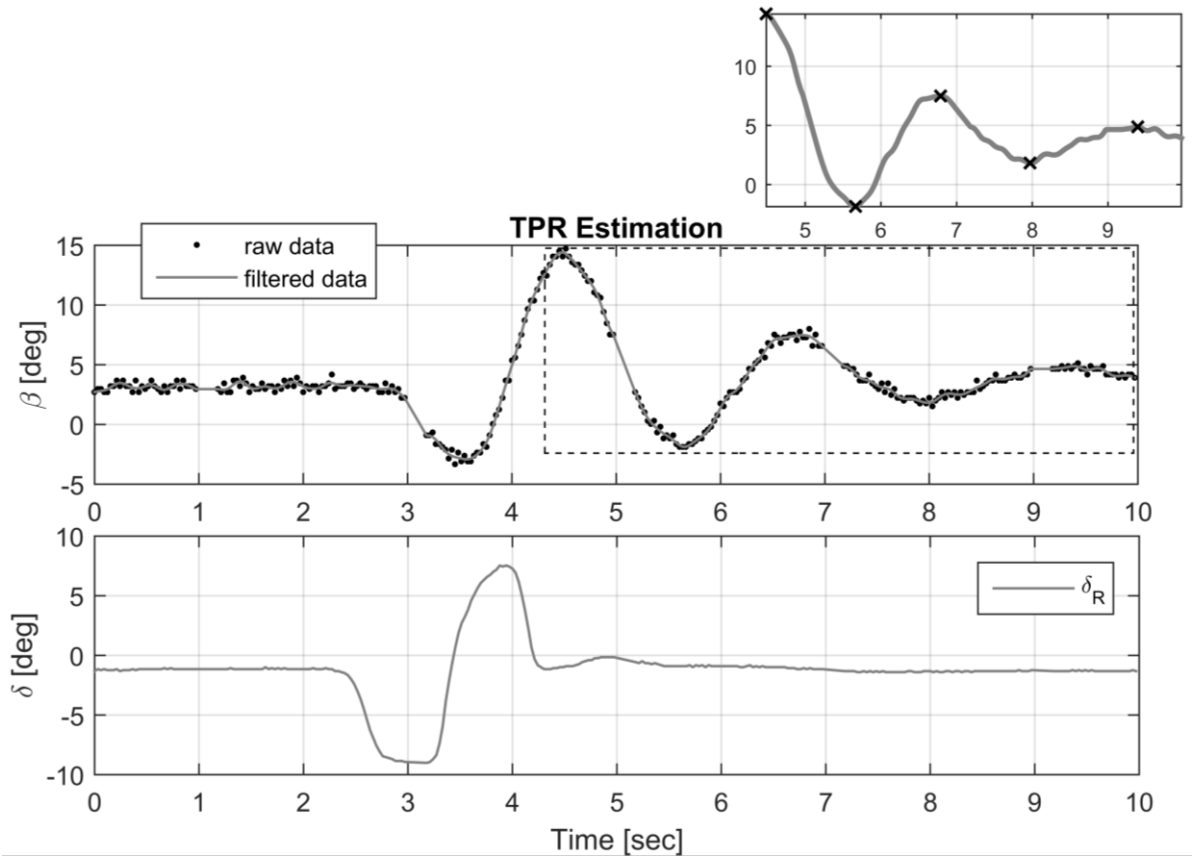

FIGURE 5.40 - TPR estimation for a doublet input (Sora)

The Nonlinear Last Squares method was also used for the analysis of the motion, where the initial guess for the parameters were obtained from the TPR results. Here, it was also used filtered data for the estimation. The obtained response curve is shown in FIG. 5.41, and the optimum parameters obtained are: $\omega_{n,DR} = 2.7767$ rad/s and $\zeta_{DR} = 0.1816$.

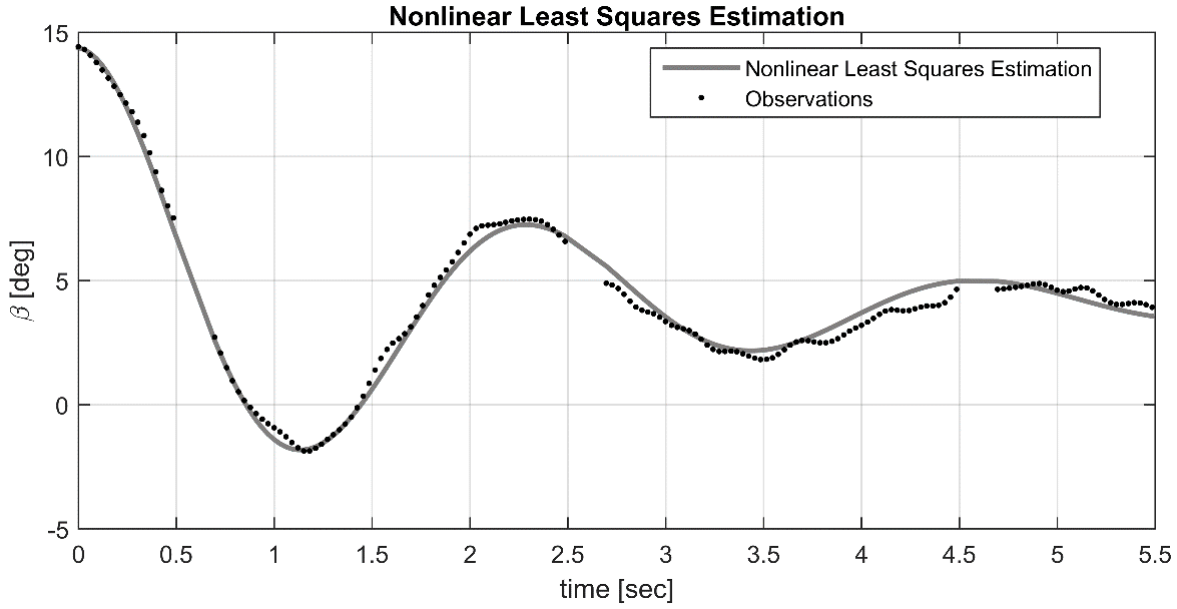

FIGURE 5.41 - TPR estimation for a doublet input (Sora)

The 4th order model was initially used for the system identification analysis. In the application of this method, we used the filtered dataset, since EEM does not assume noise in the measurements. Non-satisfactory results were obtained with the EEM, a reason for the poor quality for the results can be explained due to two main issues: i) a simple method of finite differences were used to obtain the differentiation for the states, which can be an imprecise technique for such analysis; ii) the intervals on the data set can generate problems in the finite differences. Nonetheless, the obtained parameters were used as an initial guess for the OEM technique. The obtained results for this method are shown in FIG. 5.42.

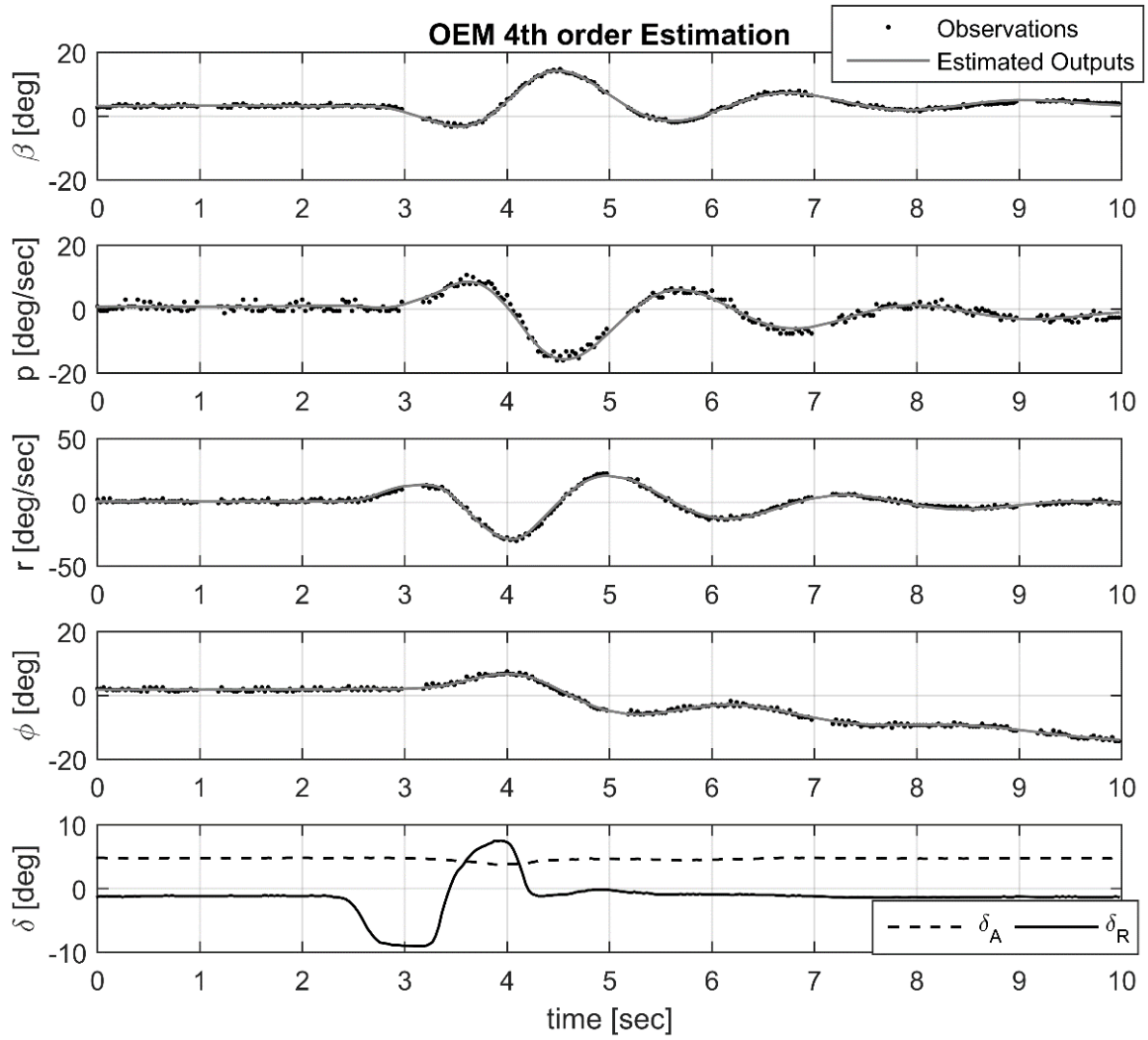

FIGURE 5.42 - Output Error Method 4th order model estimation (Sora rudder doublet)

The pair of complex conjugate roots of matrix $[\boldsymbol{A}]$, results in the following properties for the mode: $\omega_{n,DR} = 2.7960$ rad/s and $\zeta_{DR} = 0.1567$. The flight tests were performed with a low level of turbulence, in the attempt to avoid interferences from these unpredictable effects in the measurements. Based on it, it is known that the OEM is a satisfactory method for such analysis. However, we also used the FEM to observe its behavior in the determination of the Dutch Roll properties. From the optimum parameters of matrices $[\boldsymbol{A}]$ and $[\boldsymbol{B}]$ obtained with the FEM, a free simulation is realized, as shown in FIG. 5.43, and the characteristics of the Dutch Roll are: $\omega_{n,DR} = 2.8244$ rad/s and $\zeta_{DR} = 0.1811$.

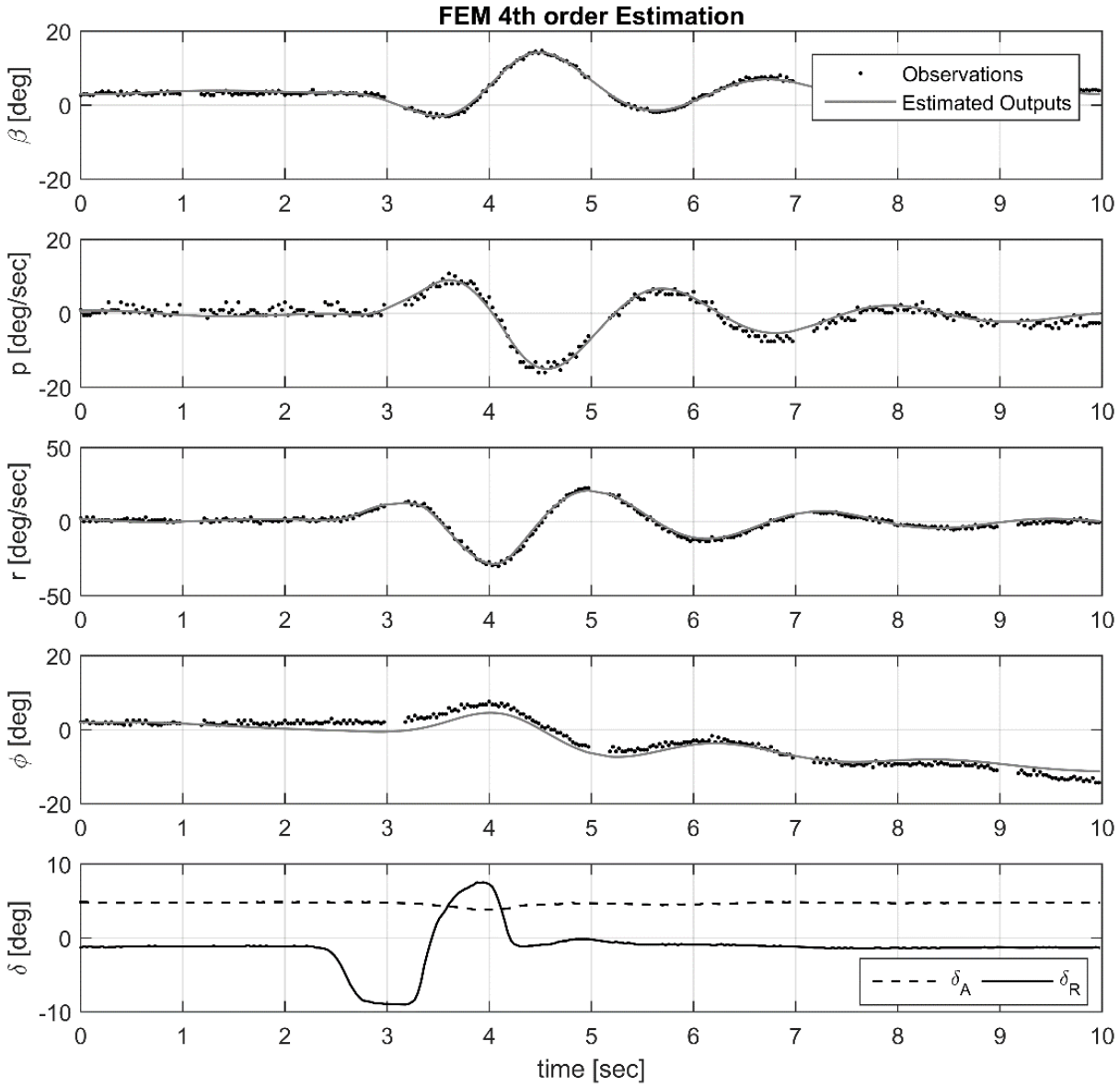

FIGURE 5.43 - Filter Error Method 4th order model estimation (Sora rudder doublet)

An interesting property of the OEM and FEM methods is that both these are capable to deal with the noise in the measurements, thus its estimation process were not done by using filtered data. The 2nd order model was also used for the estimation with both the OEM and FEM methods. The obtained curves are shown in FIG. 5.44 and FIG. 5.45.

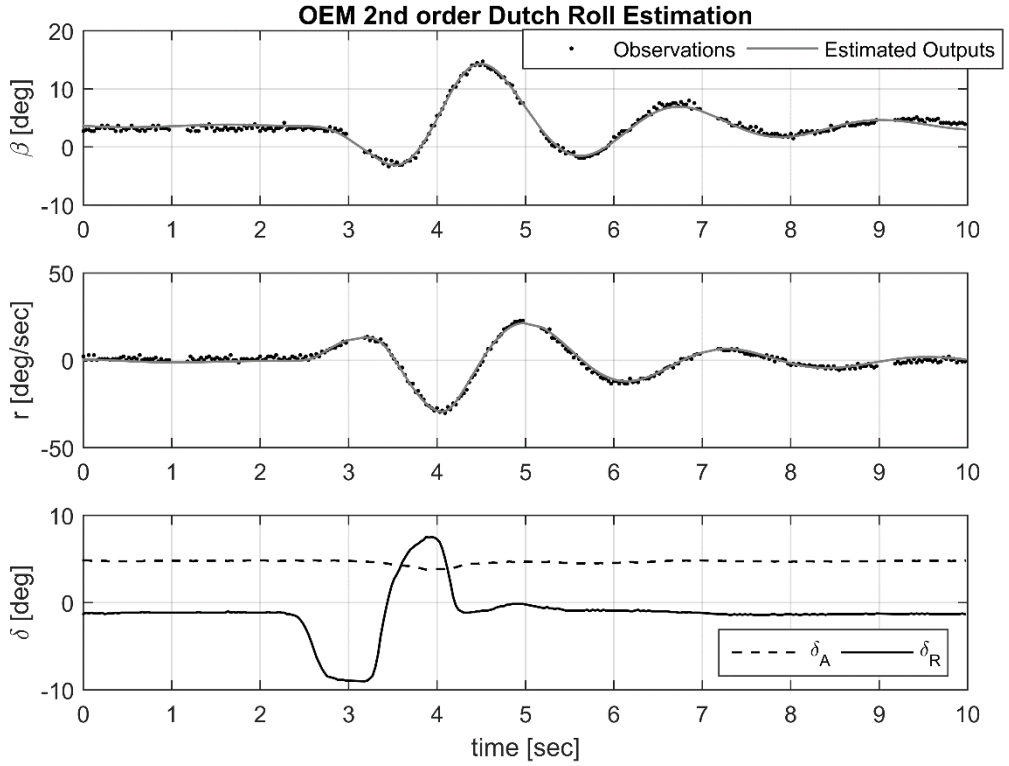

FIGURE 5.44 - Output Error Method 2nd order model estimation (Sora rudder doublet)

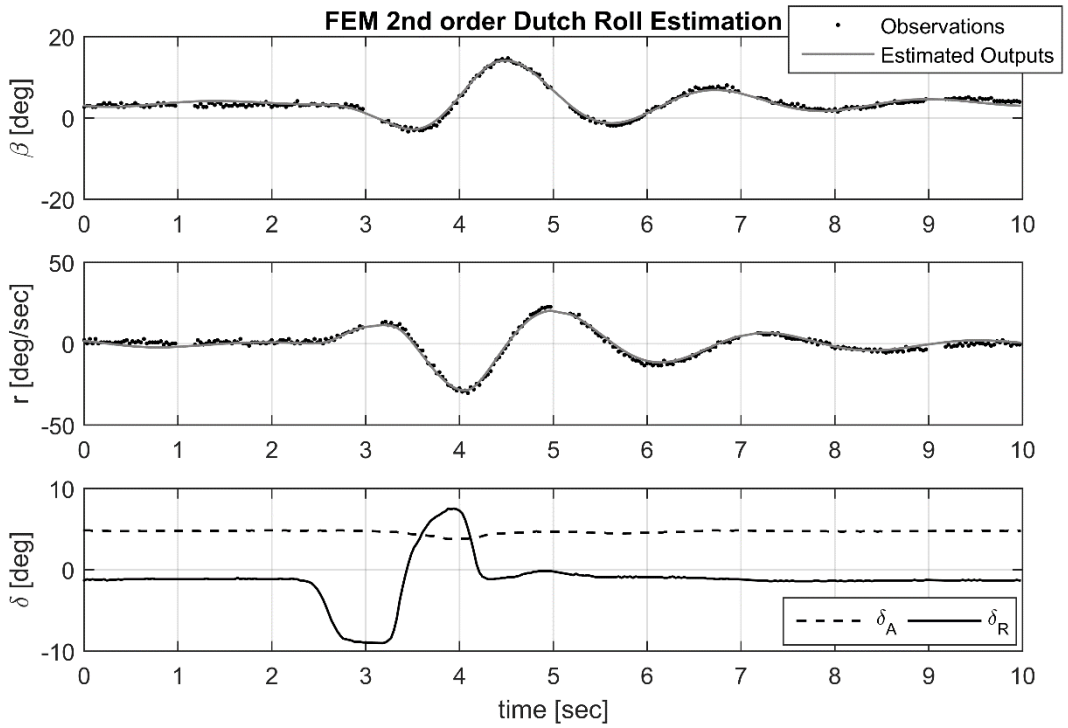

FIGURE 5.45 - Filter Error Method 2nd order model estimation (Sora rudder doublet)

The results for the characterization of the Dutch Roll of this aircraft by using each method are summarized in TAB. 5.12.

TABLE 5.12 - Estimation for each method based on rudder doublet input

	$\omega_{n_{DR}}$ [rad/s]	ζ_{DR}
TPR	2.599	0.171
NLS	2.7767	0.1816
OEM 2nd	2.7960	0.1700
OEM 4th	2.7926	0.1567
FEM 2nd	2.8147	0.1793
FEM 4th	2.8244	0.1811

To observe the quality of the simpler methods a second dataset was used, however, in this comparison process, the data was not filtered. For the TPR and NLS method, the estimated parameters for the natural frequency and the damping coefficient were maintained, while the new values for the gain (K), phase (φ) and equilibrium (β_{eq}) were obtained by the minimization of the least squares function, which is a methodology that intends to benefit such methods for comparison. Both these methods were confronted with the OEM for the 4th and 2nd order models. It this analysis, the parameters of matrices [$\boldsymbol{A}$] and [$\boldsymbol{B}$] are maintained, while new values for the equilibrium and bias parameters are estimated. Then, the RMS error between the sideslip measurements and the obtained curves for each method are calculated in the same time interval, as shown in FIG. 5.46.

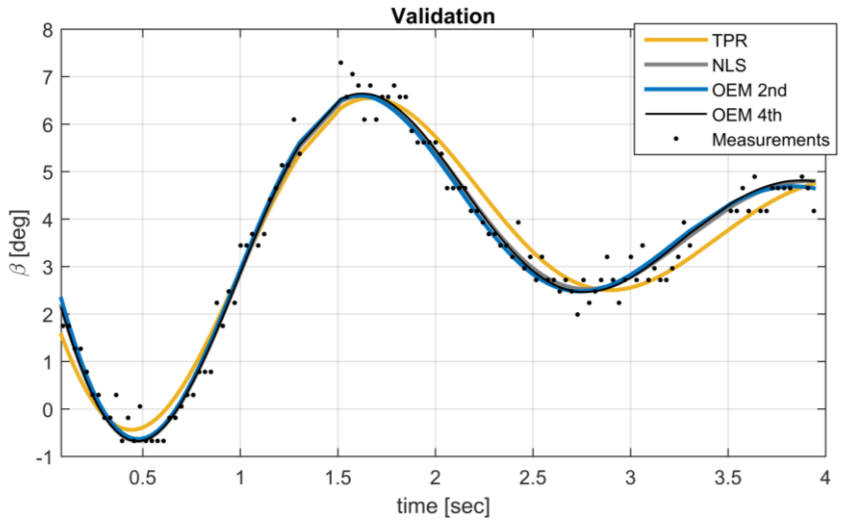

FIGURE 5.46 - Validation of the methods in a rudder doublet (Sora)

The obtained results for the RMS error are shown in TAB. 5.13. We note that from the methods, the TPR is the one which presents the highs values for the error. It is an expected result, since such technique is dependent of graphical interpretation and engineering judgment, bringing more uncertainties for the analysis.

TABLE 5.13 - RMS error obtained in validation process (Sora - Dutch Roll motion)

	RMS error [deg]
TPR	0.4325
NLS	0.3208
OEM 2nd	0.3278
OEM 4th	0.3218

Despite of the differences observed in the error of the NLS and the OEM methods, the OEM has several properties that makes it a more reliable method, however, the results shows that the NLS estimative is quite reliable in this case. Indeed, when we compare the FEM and NLS results, we observe a better proximity for the damping coefficient than for the OEM results. However, it is a hard task to affirm which are the most reliable results. Even knowing the higher level of robustness of the FEM, it is possible to observe that the free simulation of the 4th order presents some slightly differences from measurements. Thus, for more reliable conclusions, these values will be compared with the obtained result for the full dataset (bank-to-bank and rudder doublet) in the end of this section.

For Sora, the bank-to-bank maneuver was not capable to excite the Dutch Roll mode, as shown in the estimation dataset in FIG. 5.47.

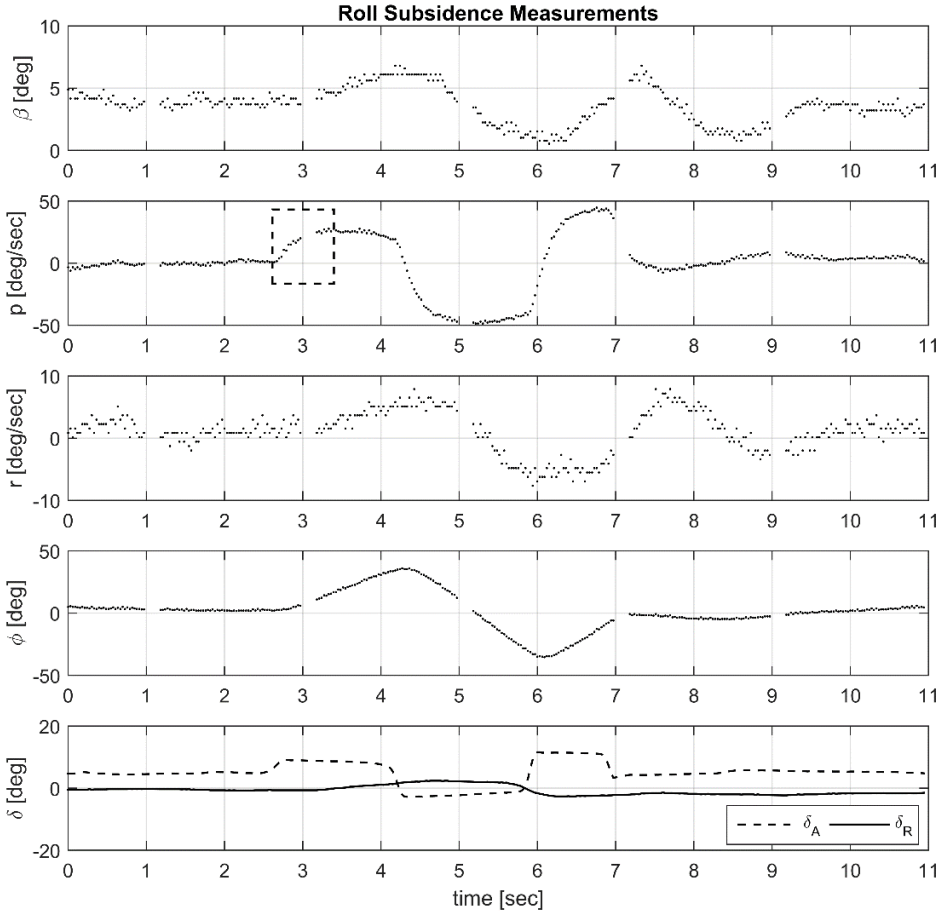

FIGURE 5.47 - Lateral-directional measurements for a bank-to-bank input (Sora)

In this maneuver, the pilot makes the aircraft goes to a bank of $+35°$ to $-35°$ and return it to the equilibrium in approximately 4.5 seconds. Due to its configuration, this aircraft has a faster roll rate than the VFW 614. In this dataset, the pilot holds the stick for one side that is long enough to observe that the roll rate has reached it steady condition. Thus, we expect that the estimation by using the NLS will be more reliable than that of the VFW. The rectangle in FIG. 5.47 shows the region of analysis and the obtained results for the Nonlinear Least Squares, assuming a first order response is shown in FIG. 5.48.

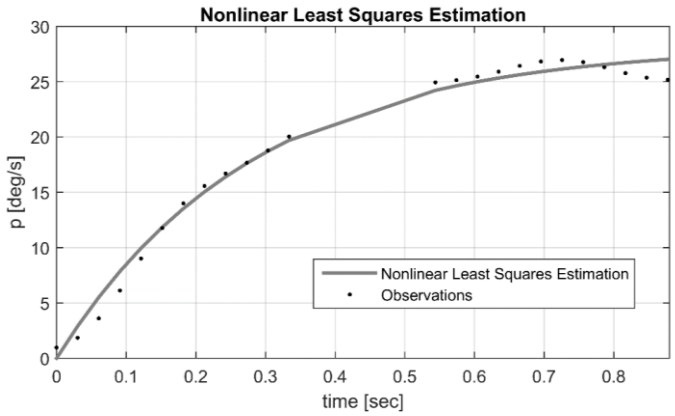

FIGURE 5.48 - NLS 1st order model estimation in a bank-to-bank (Sora)

The estimation process was done by using the OEM and the FEM with a 4th order model. The estimated responses are shown in FIG. 5.49 and in FIG. 5.50.

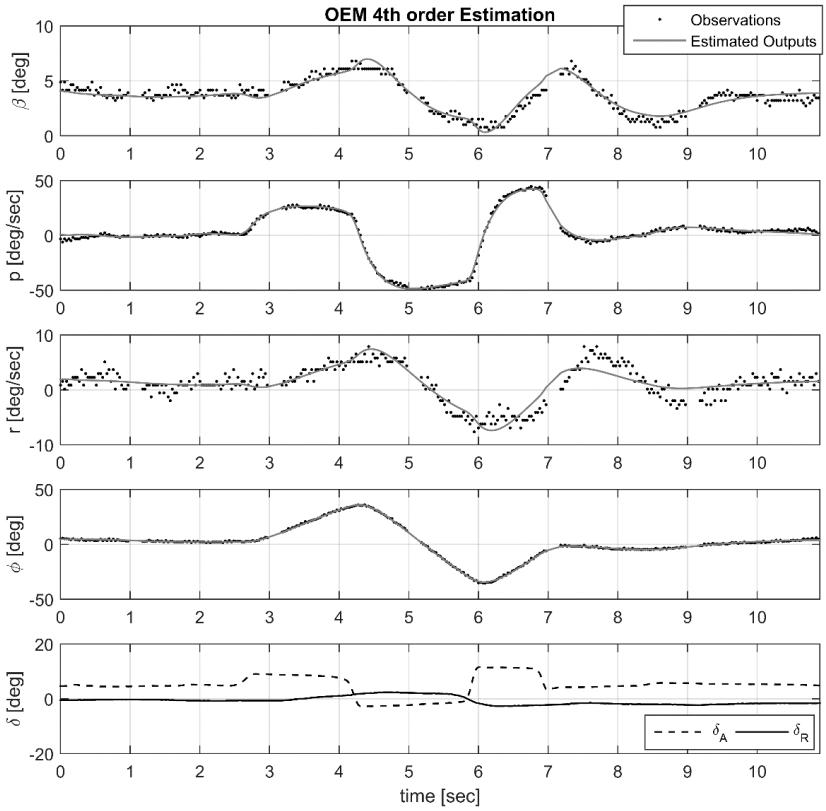

FIGURE 5.49 - OEM 4th order model estimation in a bank-to-bank (Sora)

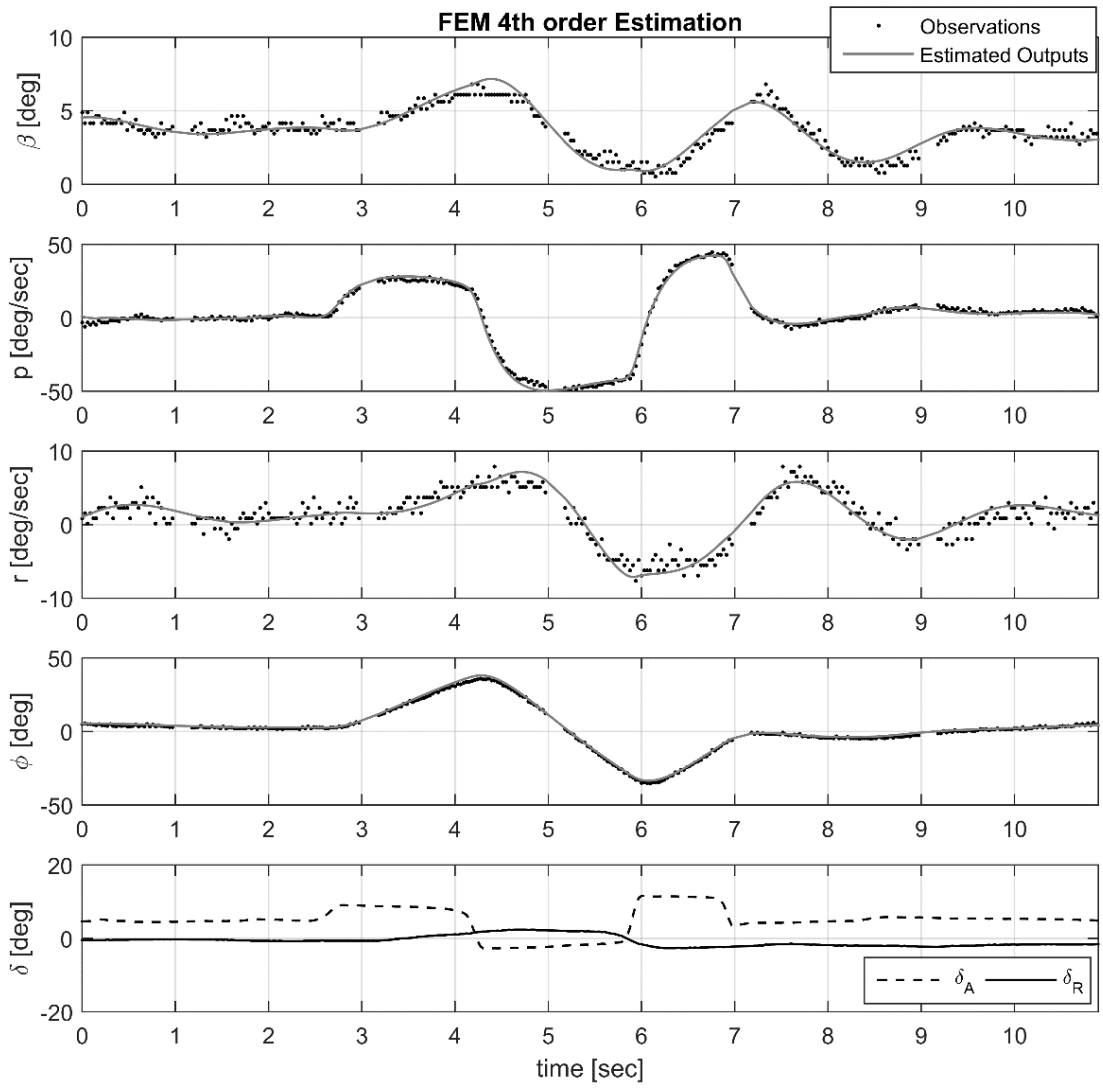

FIGURE 5.50 - FEM 4th order model estimation in a bank-to-bank (Sora)

The time constants obtained by each of the system identification methods and by the NLS are shown in TAB. 5.14.

TABLE 5.14 - Estimation of Roll and Spiral based on bank-to-bank input (Sora)

	τ_R [s]	τ_S [s]
NLS	0.2791	-
OEM 4th	0.4283	4.5966
FEM 4th	0.3045	210.87

We observe that both OEM and FEM have a satisfactory agreement with the measurements. To assess the quality of the NLS method the same comparative process used for the Dutch Roll validation was used for the Roll subsidence. Here we compare the NLS with the OEM results in a second dataset, as can be observed in FIG. 5.51. The calculated RMS error is presented in TAB. 5.15.

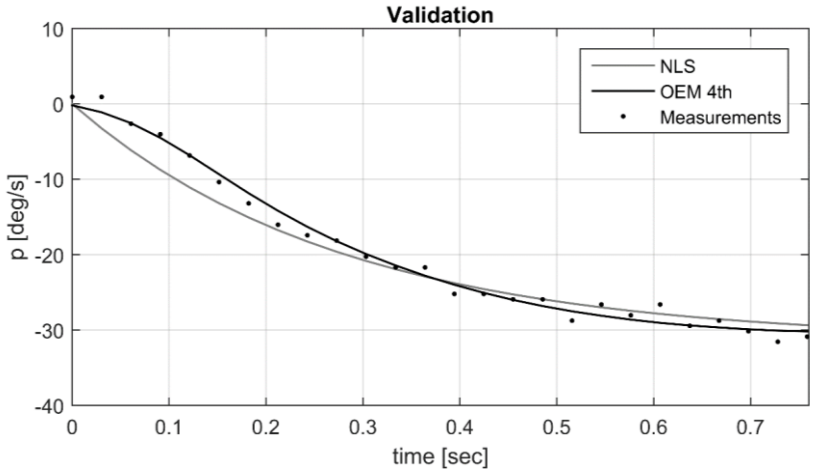

FIGURE 5.51 - Validation of the methods used for Roll estimation (Sora)

TABLE 5.15 - *RMS* error obtained in validation process (Roll motion)

	RMS error [deg/s]
NLS	2.0469
OEM 4th	1.0827

This validation process is used here to evaluate the NLS method when compared with a more robust technique. We observe that the RMS error for the OEM is almost the half of the NLS's. However, observing the FIG. 5.48 we can note that the NLS is still a good method to estimate the roll behavior. It can generate a fast initial guess of the aircraft's behavior for a simple analysis in-site during the flight test campaign.

One last analysis was performed for the lateral-directional behavior of Sora by joining the dataset of the two different maneuvers. As in the VFW 614 data analysis, the maneuvers are concatenated so that the end of the first maneuver bears quite similarity to the beginning of the second. The 4th order model is used for the analysis with the OEM and the FEM techniques. The obtained results in FIG. 5.52 and FIG. 5.53 for each method, and TAB. 5.16 shows the obtained characteristics for each lateral-directional mode.

This last analysis is assumed as the most reliable one, since it involves the observation of the lateral-directional behavior due to the aileron and rudder controls. In addition, it is used the most complete model proposed in this work (4th order) with the two most robust system identification techniques shown here. We observe that after the perturbation, the Spiral mode is excited and it has a very slow response. Observing FIG. 5.39, we can note that it is an unstable motion and that it has high value for its time constant. The better technique to estimate this time constant in this work is by applying the bank-to-bank, generating a quite high excitation in the bank angle (ϕ). The FEM is the method which generates the most concise results for the Spiral, it can be explained due to the properties of this technique, making possible to identify unstable

modes in system. Another method that can be used to evaluate the Spiral is by applying a pulse in the aileron, and observing how does the bank angle transitory response will behave.

TABLE 5.16 - Lateral-Directional estimation for both maneuvers

	$\omega_{n_{DR}}$ [rad/s]	ζ_{DR}	τ_R [s]	τ_S [s]
OEM 4th	2.8247	0.1662	0.3025	53.538
FEM 4th	2.7618	0.1696	0.2951	207.948

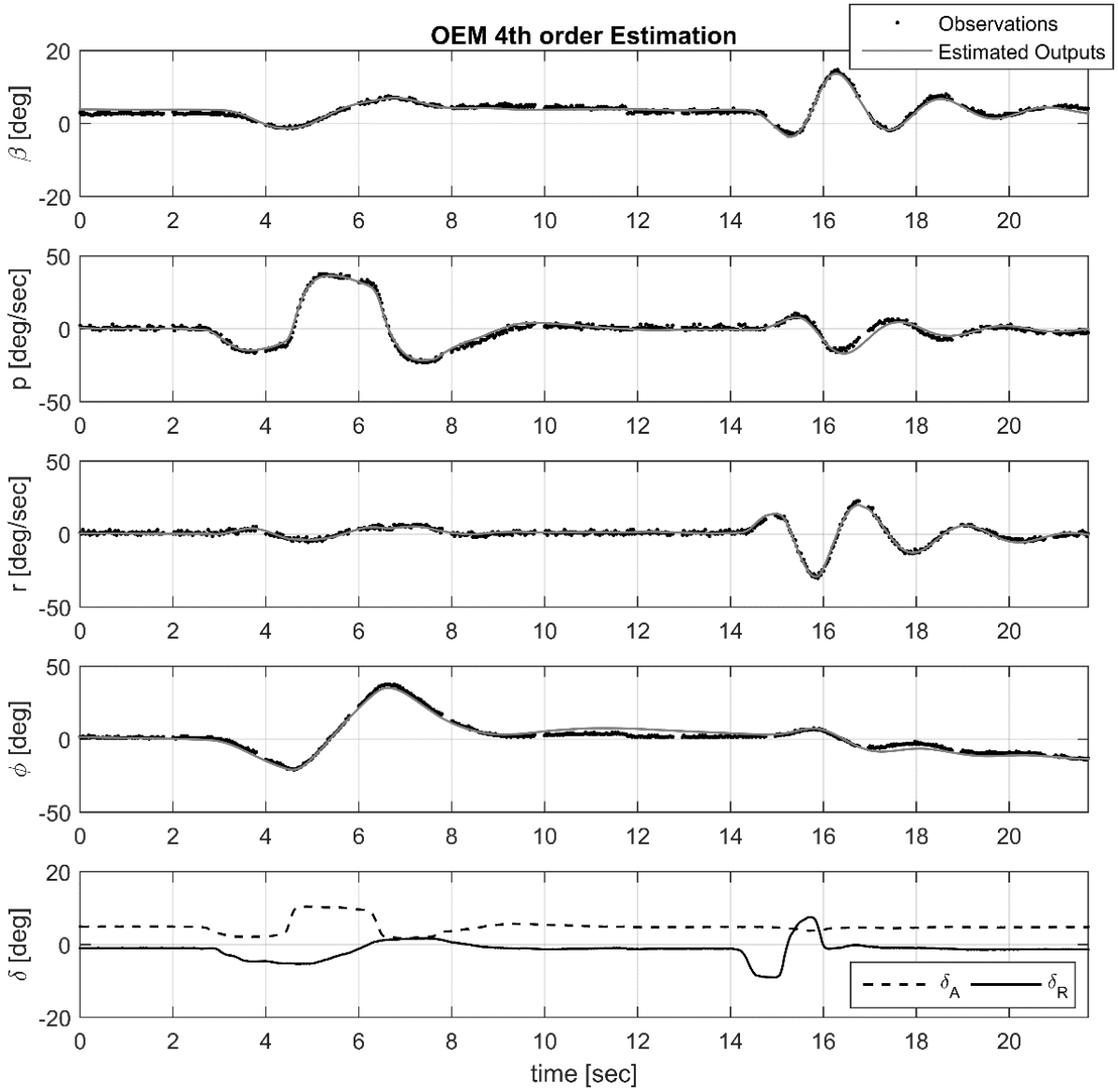

FIGURE 5.52 - OEM 4th order model estimation (Sora both maneuvers)

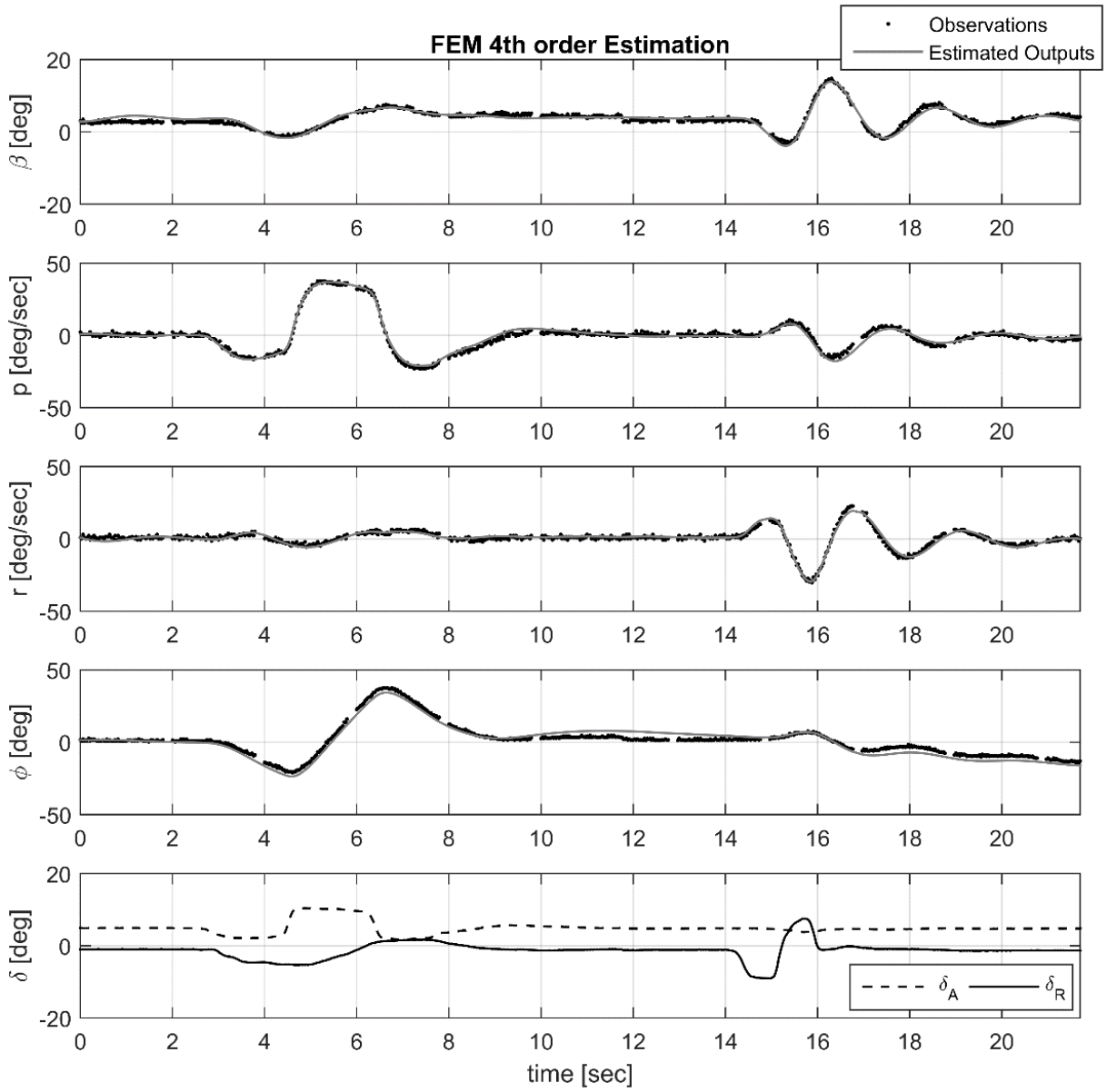

FIGURE 5.53 - FEM 4th order model estimation (Sora both maneuvers)

5.2.2 Longitudinal motion analysis

In the longitudinal motion analysis of Sora both the Short-Period and the Phugoid mode has been excited in flight. The longitudinal motion of the aircraft only depends on one control surface, which simplifies its analysis. A first observation of the Short-Period was realized with a “3-2-1-1” maneuver, as shown in FIG. 5.54.

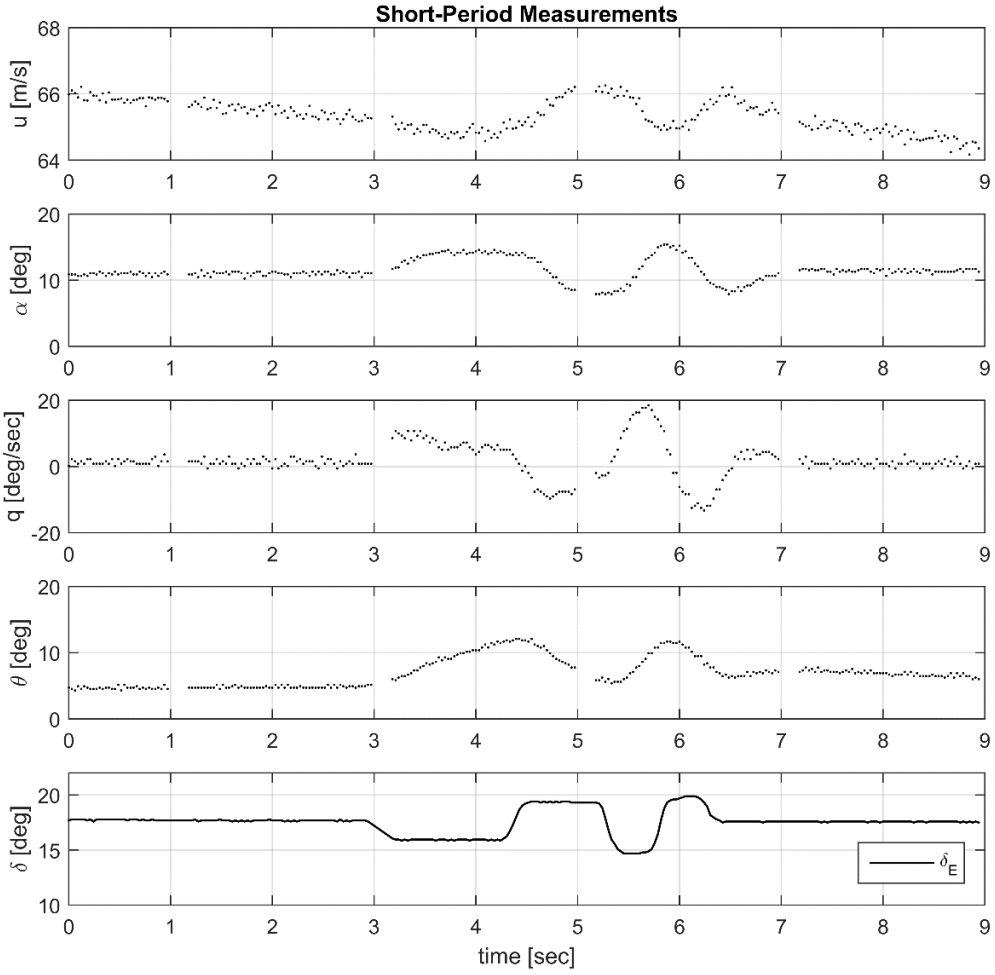

FIGURE 5.54 - Longitudinal measurements for a 3-2-1-1 input (Sora)

The time step used in the 3-2-1-1 maneuver was of 0.5 seconds. We observe that the Short-Period is a fast response, with a relatively high damping. This transient motion was analyzed by two graphical methods, the first was the Maximum Slope method, as shown in FIG. 5.55.

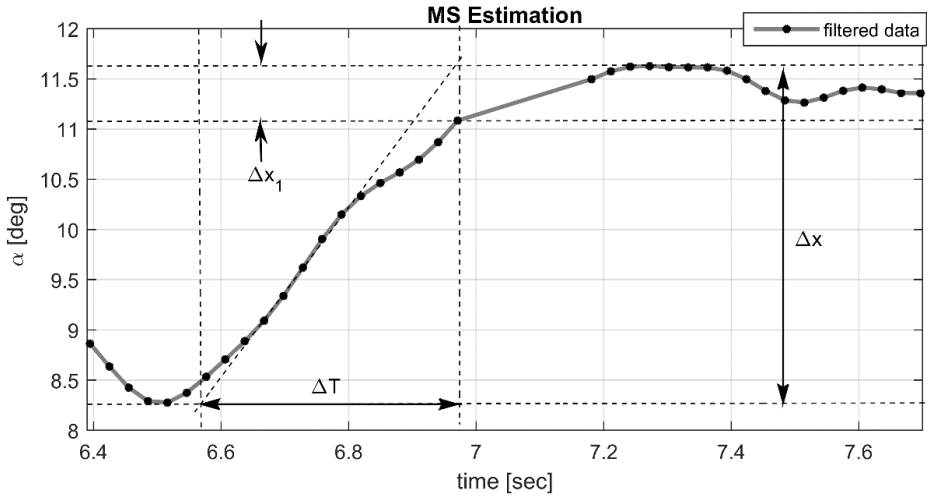

FIGURE 5.55 - MS estimation for a 3-2-1-1 input (Sora)

The maximum response value is measured and also the maximum amplitude. From these values, we use the chart in FIG. 4.4 to obtain both the damping and the natural frequency, which values are $\omega_{n,SP} = 6.49\ \mathrm{rad/s}$ and $\zeta_{SP} = 0.82$. Here we used a low-pass filter for the analysis, due to the relatively high level of noise. This method is very dependent on the engineer interpretation, and noise in the data is one more uncertainty source that must be reduced as much as possible.

We also analyzed the Short-Period motion by using the TR method, as shown in FIG.5.56. From these measurements the ratio are calculated, and then the damping and the natural frequency are obtained from FIG. 4.6. The estimated values for each ratio are $\zeta_1 = 1.32$ and $\omega_{n1} = 7.391\ \mathrm{rad/s}$, for the first ratio; $\zeta_2 = 0.62$ and $\omega_{n2} = 5.780\ \mathrm{rad/s}$, for the second; and $\zeta_3 = 0.83$ and $\omega_{n3} = 6.197\ \mathrm{rad/s}$, for the third. We note that the first value obtained is almost twice the others. Therefore, we took the mean of the last two estimates as the results for this analysis, i.e., $\zeta_{SP} = 0.73$ and $\omega_{n,SP} = 5.988\ \mathrm{rad/s}$.

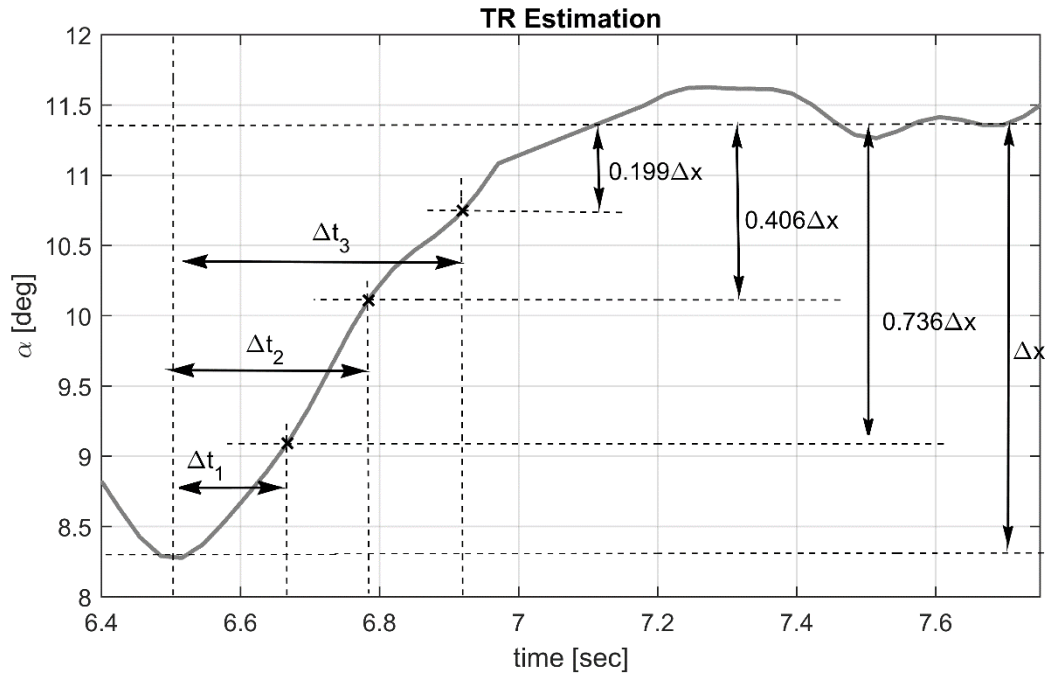

FIGURE 5.56 - TR estimation for a 3-2-1-1 input (Sora)

Assuming that the short-period is a second order response, represented by a damped sinusoid (Eq. (4.33)), we can estimate its properties by using the Nonlinear Least Squares method, where the obtained results are $\zeta_{SP} = 0.6388$ and $\omega_{n,SP} = 5.3569\ \mathrm{rad/s}$. The curve that minimizes the least squares function is shown in FIG. 5.57.

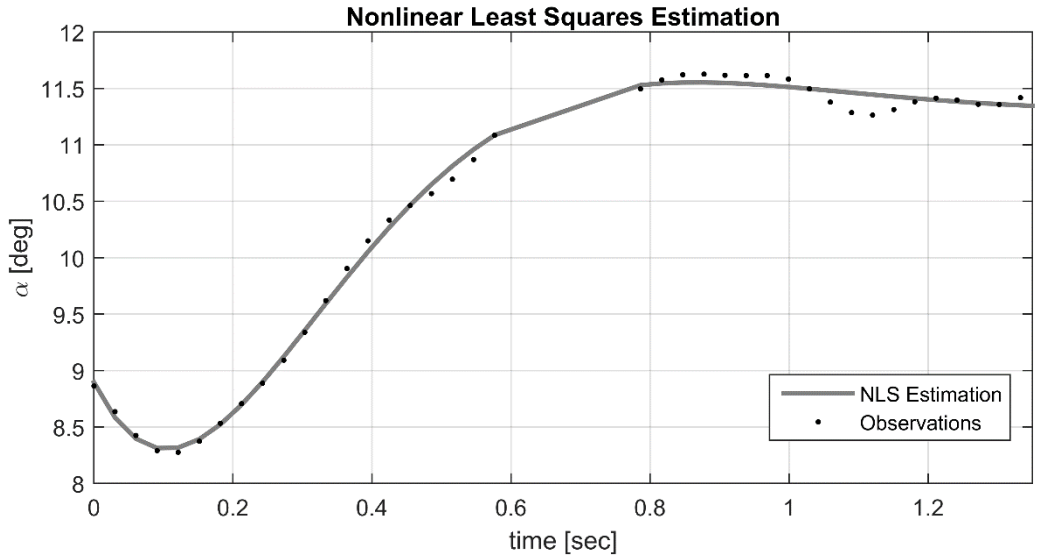

FIGURE 5.57 - NLS estimation for a 3-2-1-1 input (Sora)

The process used in the lateral-directional motion is used here, where we used the Output Error Method and the Filter Error Method for the Estimation by using the 2nd and the 4th order models. The obtained results are shown from FIG. 5.58 to FIG. 5.61, and the estimated parameters for each method is summarized in TAB. 5.17.

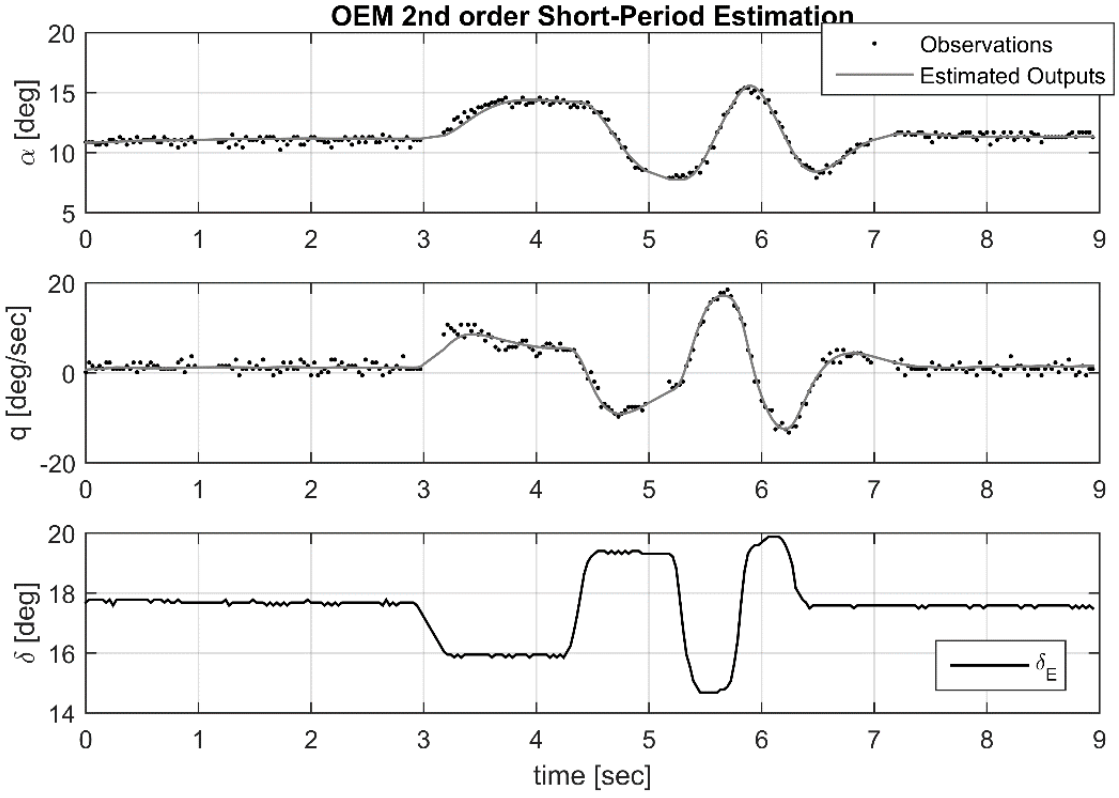

FIGURE 5.58 - OEM 2nd order model estimation for a 3-2-1-1 input (Sora)

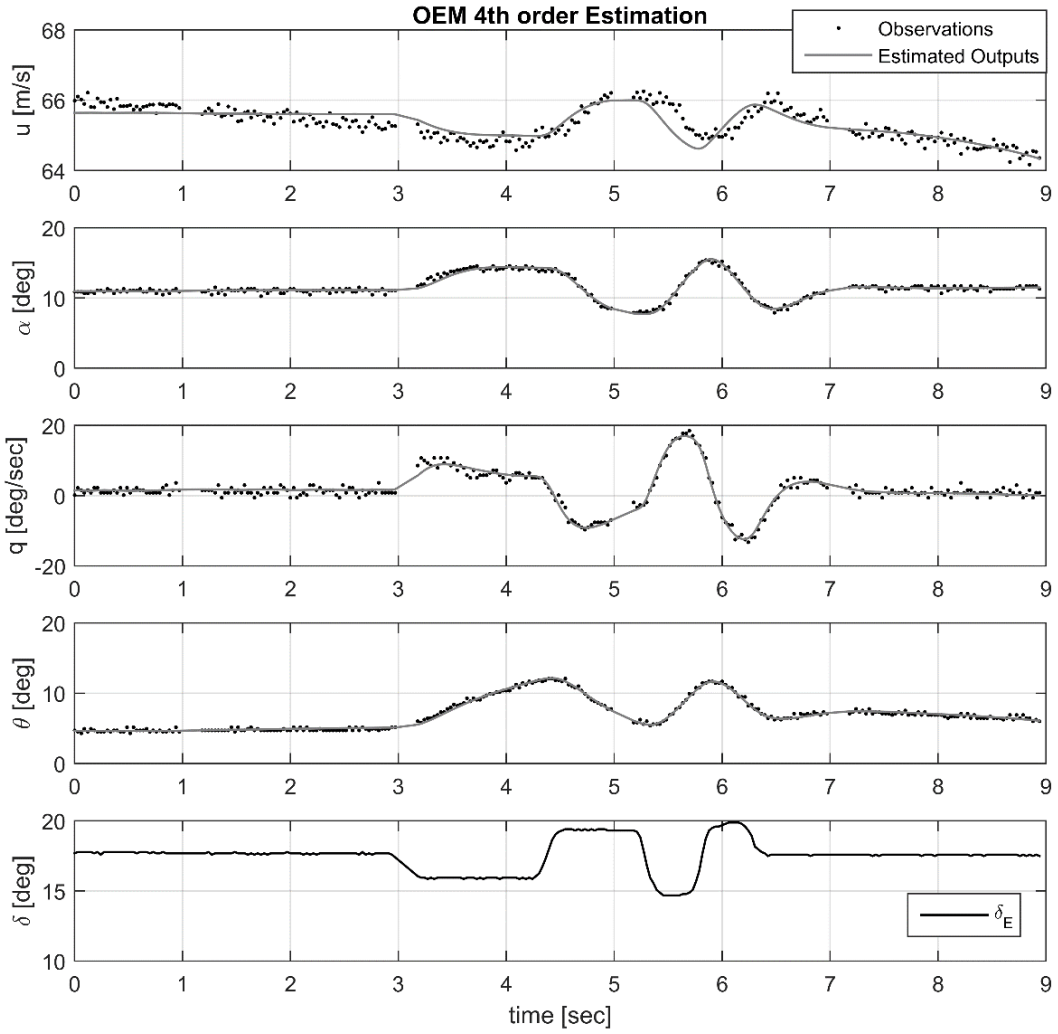

FIGURE 5.59 - OEM 4th order model estimation for a 3-2-1-1 input (Sora)

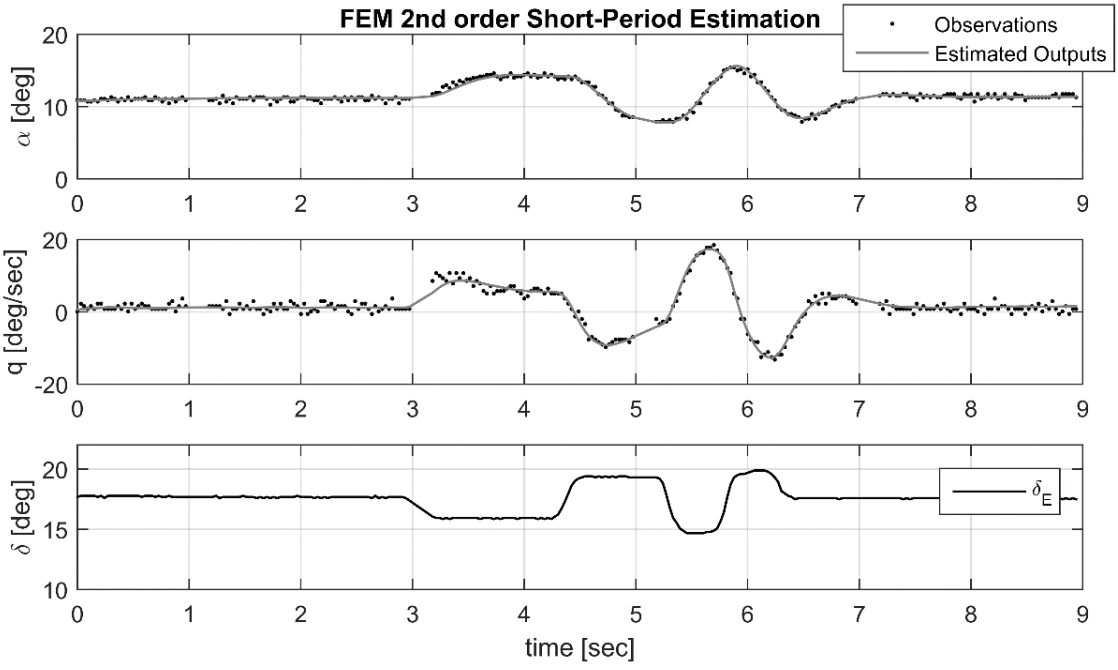

FIGURE 5.60 - FEM 2nd order model estimation for a 3-2-1-1 input (Sora)

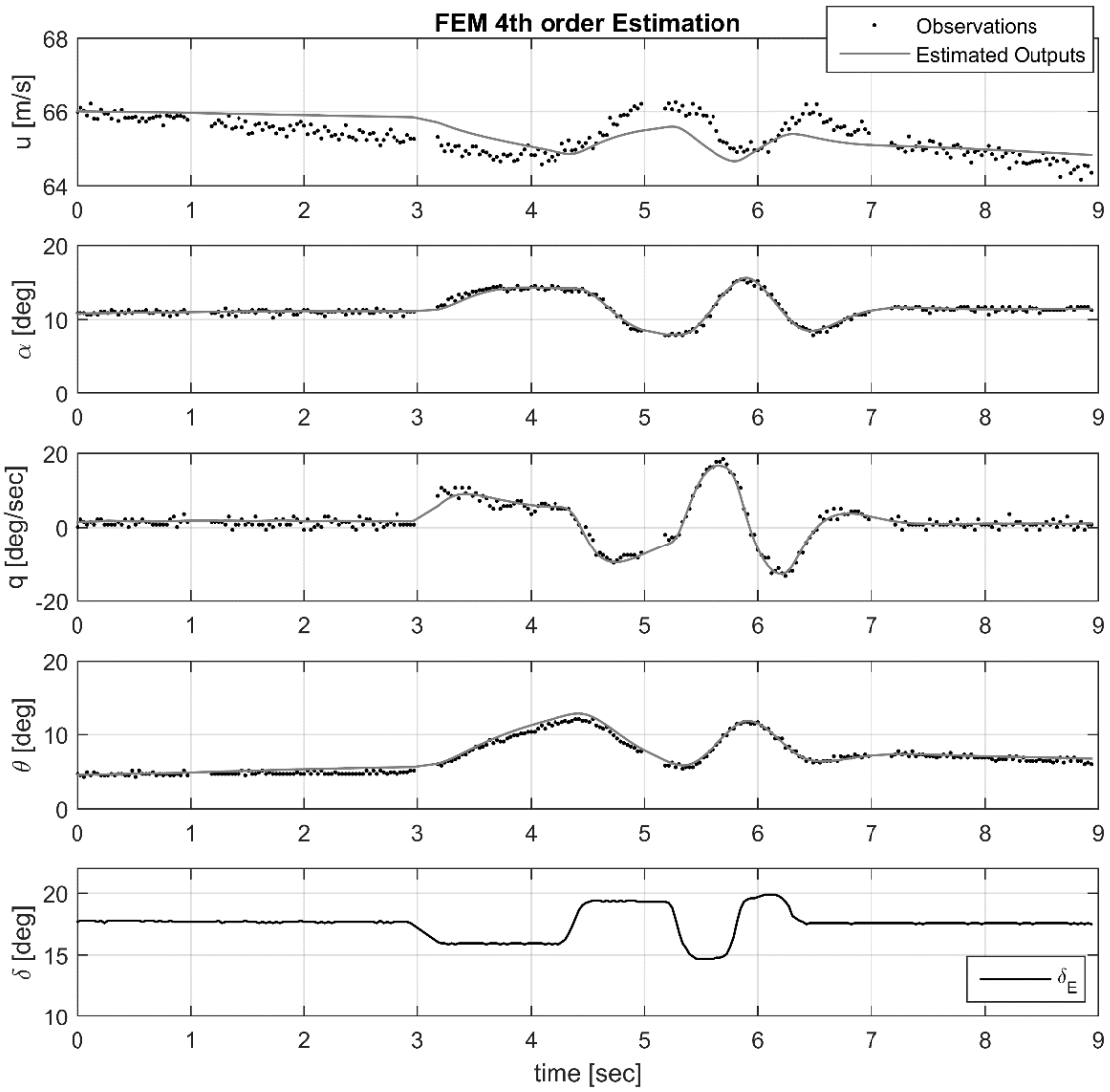

FIGURE 5.61 - FEM 4th order model estimation for a 3-2-1-1 input (Sora)

TABLE 5.17 - Estimation for each method based on 3-2-1-1 input

	$\omega_{n_{SP}}$ [rad/s]	ζ_{SP}
MS	6.49	0.82
TR	5.988	0.73
NLS	5.3569	0.6388
OEM 2nd	4.7160	0.6020
OEM 4th	4.7670	0.6323
FEM 2nd	4.7657	0.5978
FEM 4th	4.9406	0.6268

To check the quality of MS, TR and NLS we compare them with the OEM results, which is a more robust method. For such purpose, we maintain the value of natural frequency and damping estimated with the first dataset, then we use a second dataset to minimize the least squares function in the same way as for the lateral-directional motion. FIG. 5.62 shows the obtained results, and TAB. 5.18 contains the value for the RMS error of each method.

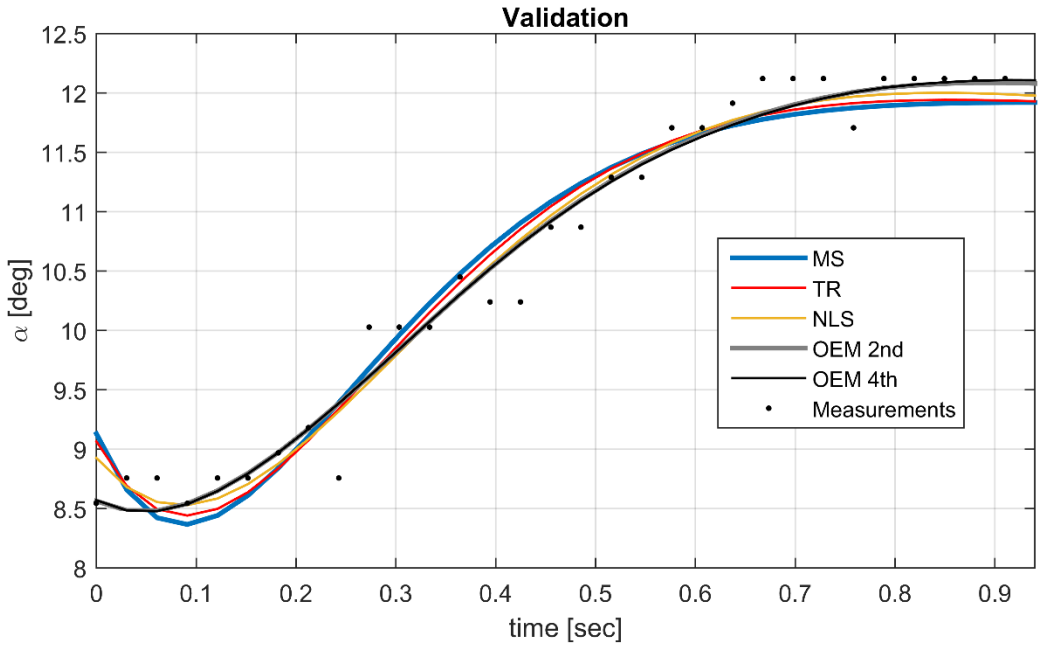

FIGURE 5.62 - Validation of the methods in a 3-2-1-1 (Sora)

TABLE 5.18 - RMS error obtained in validation process (Short-Period motion)

	RMS error [deg]
MS	0.299
TR	0.274
NLS	0.2440
OEM 2nd	0.2405
OEM 4th	0.243

The MS and TR methods show satisfactory results for the estimation process, with a relatively low value for the RMS error when compared with the OEM results, even knowing the difficulties for the measurement interpretations required. The NLS presets a low value for the error, and is observed as an important method analyzed here, since it does not require any engineering judgment during its estimation, but only a careful choose for the initial guess of the parameters.

An elevator doublet has also been used during the flight test campaign to excite the Short-Period mode. We can see that this maneuver has generated a good excitement of the mode. To check the aircraft response after an elevator doublet input, we analyzed the measurements by using the TR, NLS and the OEM with a 2nd order model. The obtained results are shown from FIG. 5.63 to FIG. 5.65, and the mode parameters are described in TAB. 5.19.

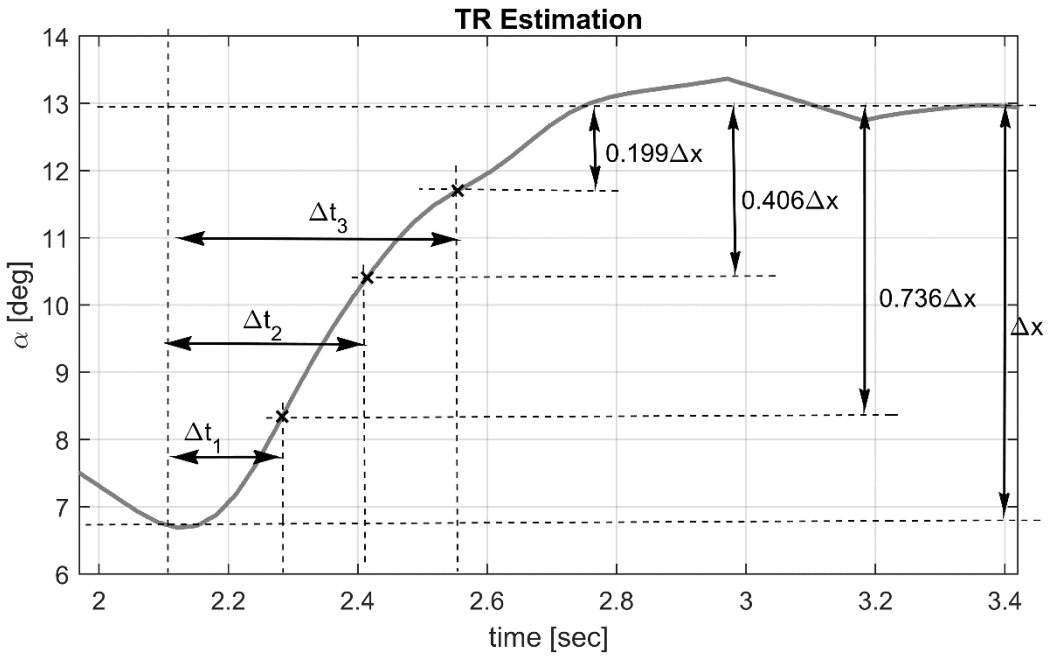

FIGURE 5.63 - TR estimation for a doublet input (Sora)

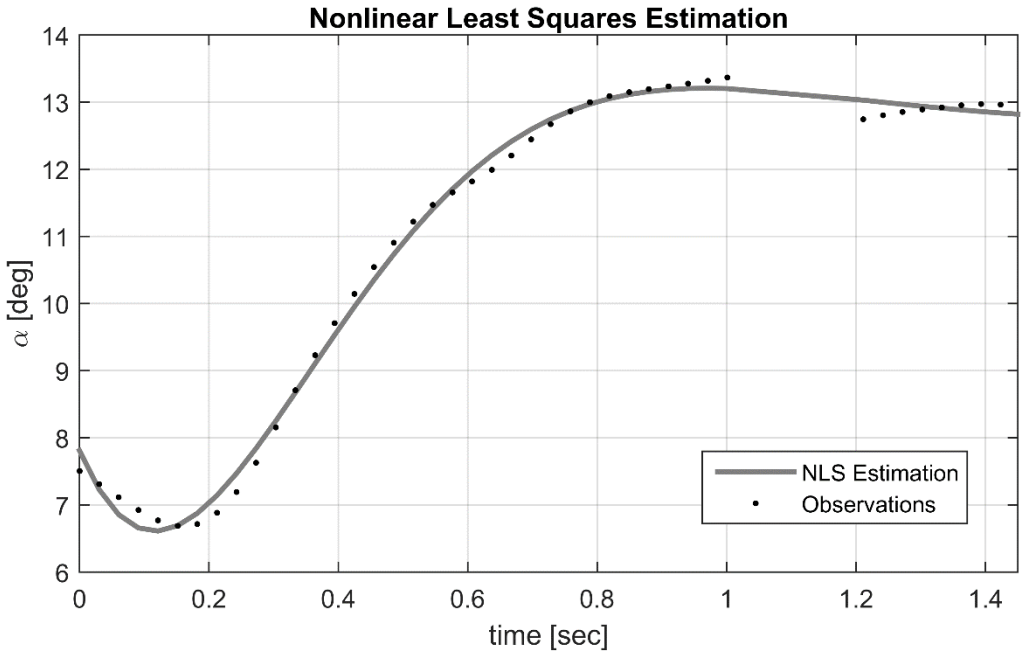

FIGURE 5.64 - NLS estimation for a doublet input (Sora)

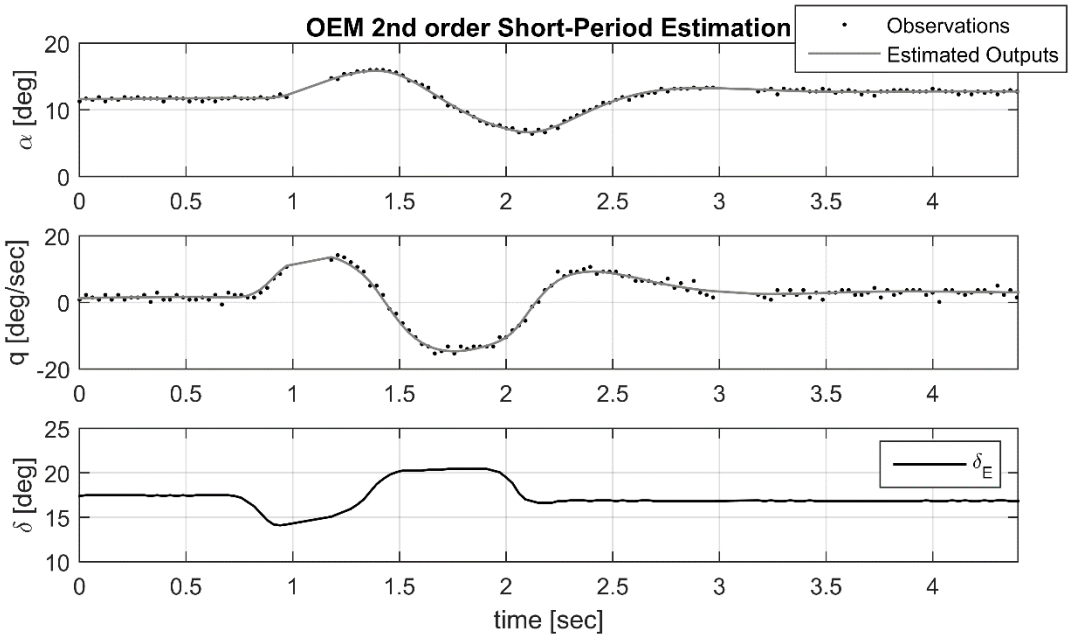

FIGURE 5.65 - OEM 2nd order model estimation for a doublet input (Sora)

TABLE 5.19 - Estimation for each method based on doublet input

	$\omega_{n_{SP}}$ [rad/s]	ζ_{SP}
TR	5.878	0.76
NLS	4.7965	0.6400
OEM 2nd	4.8942	0.6105

The estimated parameters are very close to that obtained with the "3-2-1-1" maneuver. Thus, we note that it is another important maneuver for the Short-Period excitation, mainly for a test where the pilot is having problems to use the "3-2-1-1".

The other important mode of the longitudinal motion is the Long Period motion, or Phugoid. It has a very low response and damping when compared with the Short-Period mode, and its behavior is mainly observed through the linear speed (u) along the longitudinal axis of the airplane body. Here, it was excited by a relatively fast pulse in the elevator. The graphical method used for its analysis is the Transient Peak Ratio. The obtained peak are shown on FIG.5.66. From the measurement of the period T, we used the chart in FIG. 4.2 to determine its natural frequency and damping coefficient: $\zeta_{Ph} = 0.146$ and $\omega_{n,Ph} = 0.176$ rad/s.

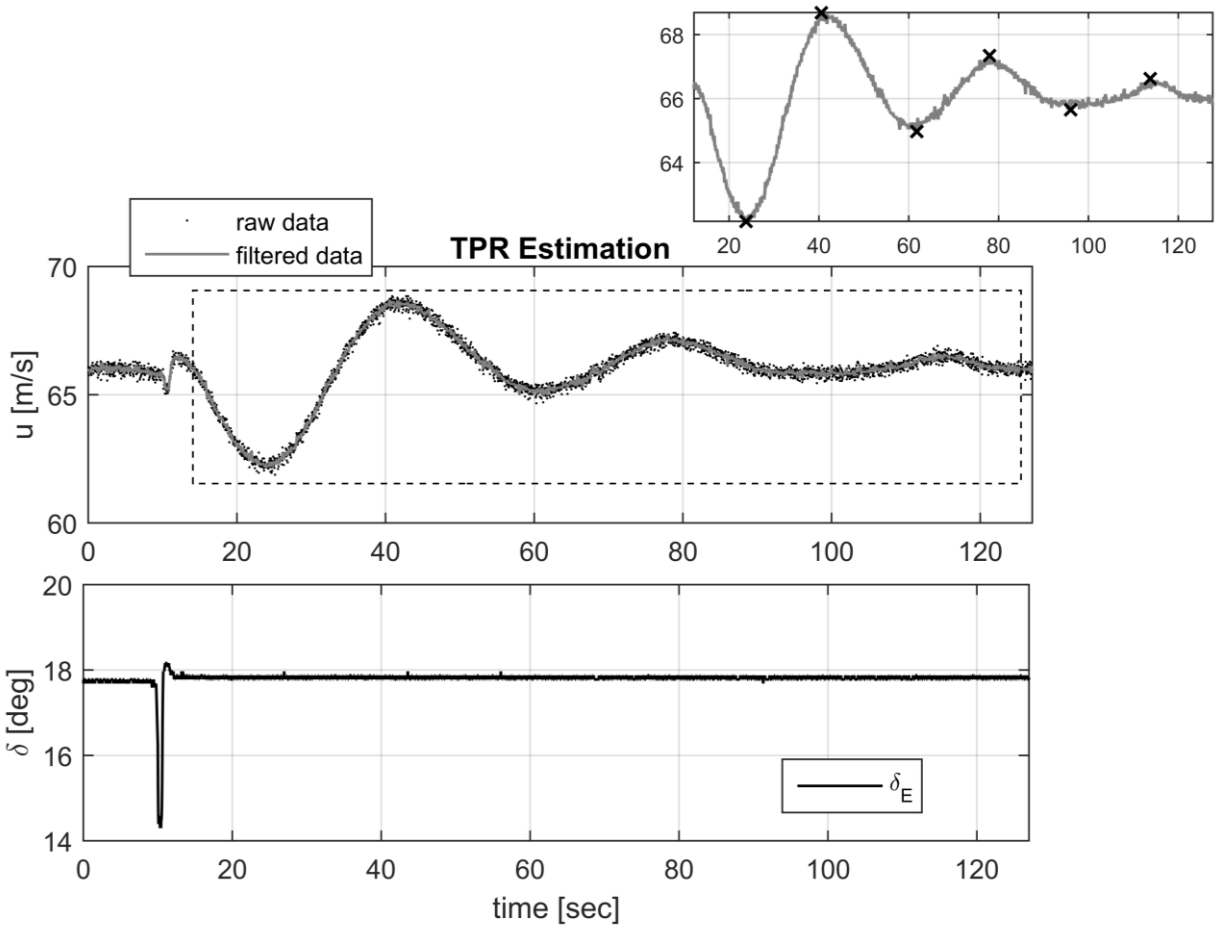

FIGURE 5.66 - TPR estimation for Phugoid mode (Sora)

Despite of a slower response, its behavior is very similar to the Dutch Roll. Therefore, its characteristics where also estimated by using the NLS and the OEM with a 4th order model for a more detailed analysis, as shown in FIG. 5.67 and FIG. 5.68.

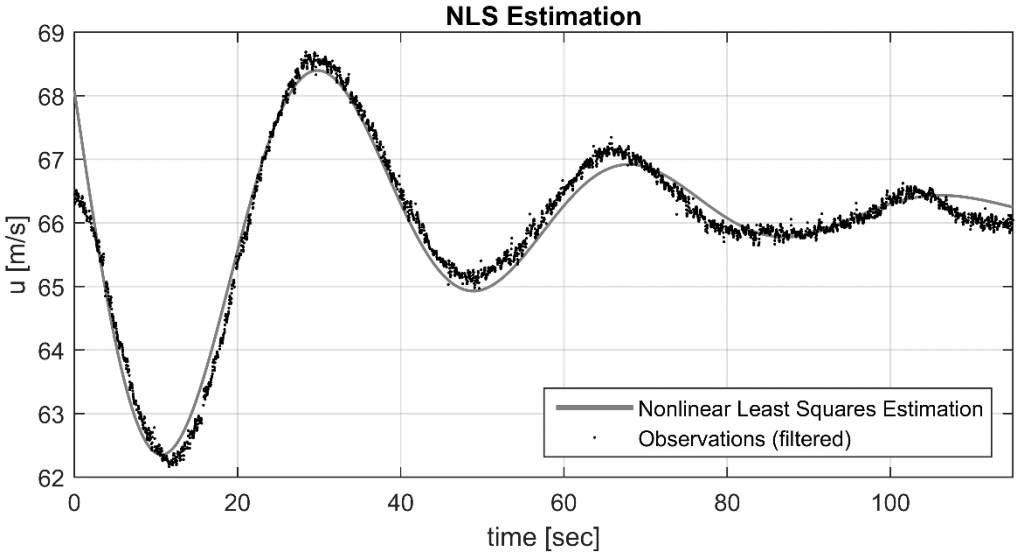

FIGURE 5.67 - NLS estimation for Phugoid mode (Sora)

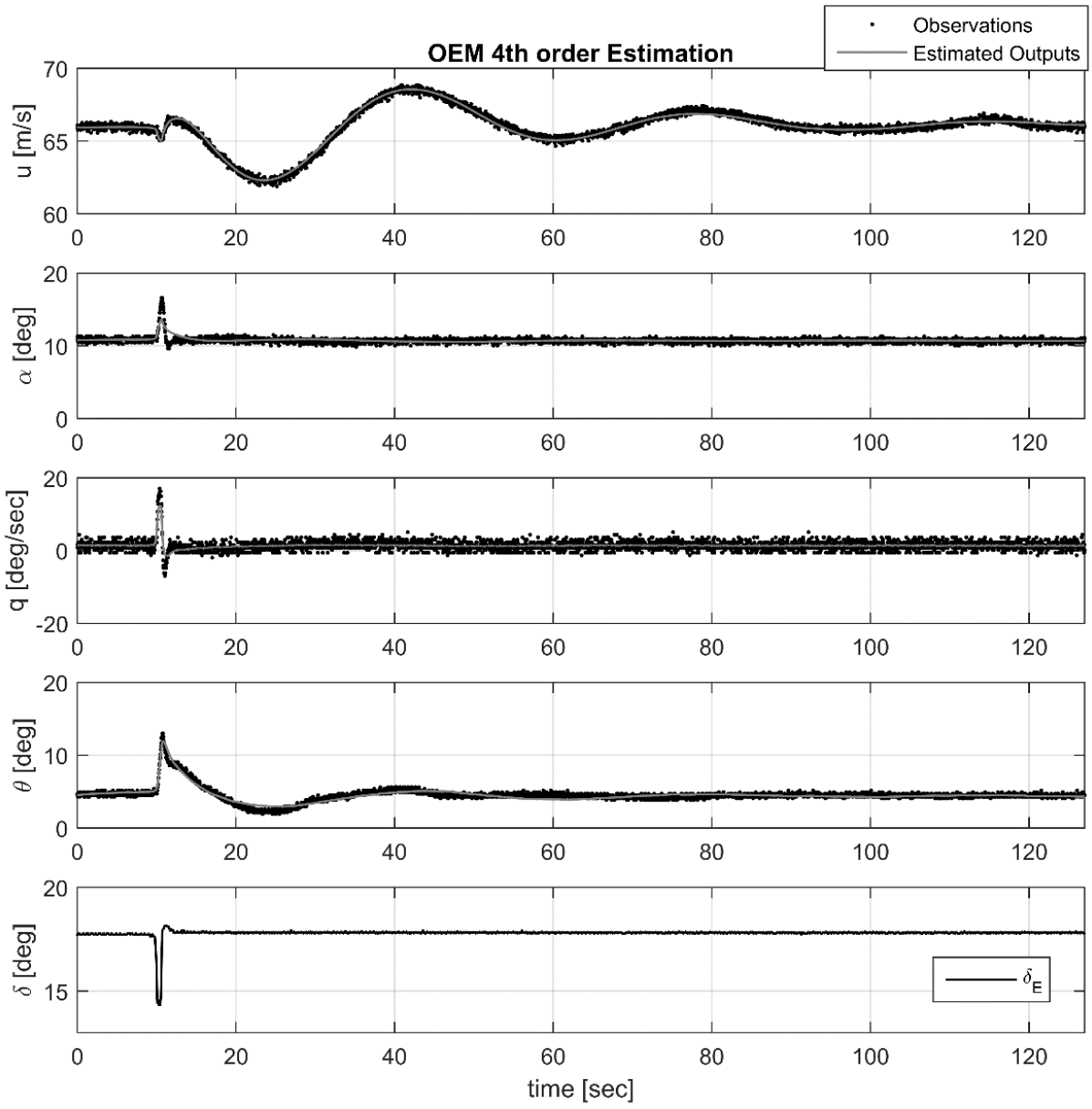

FIGURE 5.68 - OEM 4th order model estimation for Phugoid mode (Sora)

TAB. 5.20 summarized the obtained characteristics for the Phugoid mode for each method used.

TABLE 5.20 - Estimation for Phugoid parameters using for different methods

	$\omega_{n_{PH}}$ [rad/s]	ζ_{SP}
TPR	5.878	0.76
NLS	4.7965	0.6400
OEM 4th	4.8942	0.6105

Due to its similarity with the Dutch-Roll motion, it is not necessary a comparison to evaluate the quality of the methods. The longitudinal motion of the aircraft is much simpler to observe, since it only depends on the elevator controls. During the Phugoid response, the pilot

must use the ailerons controls trying to keep the wings leveled, because high values of bank angle can generate poor results in its analysis.

For both aircrafts under analysis, the Equation Error Method has shown unreliable results. As mentioned, the finite differences technique employed in this work can be one of the reasons for such results. In Sora data analysis, there are two more reasons for these results: first, the available data contain a higher level of noise; second, the data intervals observed can generate even higher errors in the determination of the derivatives by the finite differences method used. One alternative to improve the results of this method, would be applying a more robust method in the determination of the derivatives.

It can be observed that in most of the data the initial measurements are not at exactly zero. For the variables α, u, θ, β, ϕ, this difference is due to the equilibrium values; For the variables p, q, r it is due to the bias in the measurements; And for the control inputs δ, it is due to the trim conditions. This effect is taken into account during the estimation where these bias and equilibrium parameters are obtained in the process.

VFW 614 is bigger aircraft and has a slower response when compared with Sora. Therefore, we expect an aircraft that is easier to be excited in each mode, since the pilot can be more precise in the inputs, which will require a slower time steps. However, it is harder to be instrumented, due to its dimensions it requires longer cables to connects the sensors, which can be a noise source, and takes much more time for the installation. The VFW is a twin engine aircraft, and its thrust must be carefully observed during the tests, mainly during the lateral-directional, where high variations in the differential values can results in the Spiral mode excitation. An advantage of this aircraft is that it has a system augmentation stability that can be turned on to put the airplane in the steady state condition, and be turned off before the inputs. For some aircrafts, such a task may be more difficult to perform than the excitation maneuver. Another complication for the Sora tests, is the fact that the propeller induce vibration in the aircraft structure, which interfere in the acquired data. However, this smaller airplane is much easier for the FDAS installation and for operation, since it is a much simpler system.

6 CONCLUSIONS

This work presented a methodology for the analysis of the dynamic modes of an aircraft based on flight tests, by evaluating two different aircrafts: VFW 614 and ACS-100 Sora. Observing the data and the analysis of each aircraft we note that the time steps must be as much closer as possible from the ideal (Section 3.3), however small variations in the inputs do not generate significant differences for the mode excitation. Also we observe that it is hard for the pilot to return and hold the stick exactly at the equilibrium position. This can be an error source for the graphical methods and for the NLS. On the other hand, the system identification techniques can handle with this fluctuations in the input, which is one of its advantages during the data reduction. Here, most of the analysis were based on stick-fixed condition, however, all the methods applied can also be used with the stick-free. The most recommended maneuvers for the excitation of each mode are: rudder doublet for the Dutch Roll; bank-to-bank for Roll Subsidence; aileron pulse for Spiral; elevator "3-2-1-1" for Short-period; and elevator pulse for Phugoid.

The Transient Peak ratio, used for slower responses, is the less sensitive to the choice of the data points, because there is larger time interval between those measurements. The Maximum Slope and the Time Ratio, on the other hand, depend on data observed over a short period, making its application a harder task. The Time Ratio has the advantage that it gives three estimations for the characteristics of the motion, thus, the engineer can use its judgment to decide how many of these values are reliable. The requirement of the engineer interpretation of the data is a limiter for these methods, and make its automation a harder task. Nevertheless, the graphical methods presented here show coherent values for its estimations and can be used as an initial guess of the characteristics for the aircraft dynamic modes.

The Nonlinear Least Squares method shows to be an important alternative for the graphical methods. This method uses all the data points of the observed variable in the time interval over analysis, while the graphical methods require only specific points. In addition, it does not depend on the engineer interpretation of the data, and its code is readily implanted on several usual programming languages, such as C++, Python, Matlab, and others. However, the graphical methods and the NLS use only the measurements of one variable in their analysis, which is an error source in the estimations.

The Equation Error Method did not presented satisfactory results for any evaluated case. Such divergences in the method are due to the simple finite differences method used in the estimation of the derivatives of the states, which is very sensitive to the noise in the

measurements. In the analysis of the Sora's data, the time intervals also generate problems for such differentiation technique. A most robust method to obtain the derivatives of the states could be used for an improvement in the EEM estimation process.

The Output Error Method and the Filter Error Method are the most recommended methods for the analysis. Both have several statistical properties for a reliable parameter estimation, and use all the data in the maneuver, including the inputs, in the estimation process. Thus, the obtained results takes into account all the aircraft motion, before, during and after the mode excitation. In addition, they can deal with noise in the measurements or even in the process (for the FEM). Since the flight tests are generally performed when there is a low atmospheric turbulence level, we assume that the OEM generate parameters as reliable as the FEM's. Despite the higher reliability of the system identification techniques, their implementation is not always a simple task; it involves several challenges where the engineer must decide which simplifications will be used in programming. The determination of the initial parameters for the OEM and FEM is a task that depends on the engineer experience. For several situation, the initial guess obtained with the EEM will not be precise enough for the estimation process. However, the analysis with such techniques generates more reliable results, and the parameters of the matrices [$\boldsymbol{A}$] and [$\boldsymbol{B}$] can be used to obtain the estimation of aerodynamic and propulsive coefficients of the aircraft. The FEM must be used when the flight test data is acquired over a medium to high level of turbulence, since it predict such effects. It also must be used for the analysis of unstable modes, as the Spiral in several aircrafts.

For the lateral-directional motion we recommend to use a dataset of a maneuver applied with the aileron and rudder. Is allows a better estimation by the system identification techniques, given a higher reliability for the obtained parameters. It is necessary a relatively high input with the aileron to generate variations in the bank angle for the observation of the Spiral mode. For an unstable Spiral response, the FEM method must be used in the identification process, because this technique is the only system identification method shown that can deal with unstable responses.

As a general overview, the most recommended methodology is to use several repetitions of the same maneuvers, intending to reduce the uncertainties of the estimated parameters. In addition, although we observe a higher robustness of some methods, we can note that all of them generate reliable results, and its choice is only dependent on the level of precision required during the analysis.

6.1 Future Work

Some of the most relevant studies to be considered in the next steps of this work are:

- To obtain the aerodynamic, inertial and propulsive data by semi-empirical formulations or by wind tunnel test, and compare with the obtained parameters for each aircraft.
- To develop the analysis using a nonlinear model for the aircraft dynamics and compare with the linearized analyses.
- To develop a computational tool for a faster and easier analysis, allowing a pre-check of the data on site, reducing costs for the flight tests.
- To do a sensitivity analysis with the parameters of the dynamic modes, in order to observe how much the errors between the methods will interfere in the evaluation of the aircraft.

6.2 Produced Papers

- REIS, J. L. C.; DUTRA, D. A.; PINTO, R. L. U. F. **Longitudinal Aircraft Response Analysis Based on System Identification Techniques**. Congresso Brasileiro de Automática. Vitória - ES. 2016. p. 6.
- REIS, J. L. C.; DUTRA, D. A.; PINTO, R. L. U. F. **Data Reduction Methods for Dutch-Roll Analysis**. AIAA SciTech. Grapevine - TX. 2017 (To be published).
- REIS, J. L. C.; DUTRA, D. A.; PINTO, R. L. U. F. **Analysis of the Characteristics of Short-Period and Dutch Roll Modes from Flight Test Data of ACS-100 Sora Aircraft.** Journal of Aerospace Science and Technology. 2016 (Submited).

REFERENCES

ACS AVIATION. ACS - Advanced Composites Solutions. **ACS-100 Sora**, 2006. Disponivel em: <http://www.acs-solutions.com.br/backup/principal_java.htm>. Acesso em: 7 July 2016.

AVIATION FAN CLUB. **VFW-Fokker 614**, 2014. Disponivel em: <http://www.aviation-fan-club.com/vfw_614.htm>. Acesso em: 1 Nov 2016.

BORGES, J. F. A. **Desenvolvimento de um Medidor de Ângulo de Ataque para Aeronaves de Pequeno Porte**. Federal University of Minas Gerais. Belo Horizonte, p. 181. 2008.

BRYAN, G. H. **Stability in Aviation**. London: Macmillan and Co., 1911.

CHALK, C. R. et al. **Background Information and User Guide for MIL-F-8785B(ASG), Military Specification-Flying Qualitites of Piloted Airplanes**. Air Force Flight Dynamics Laboratory. Ohio. 1969.

DUTRA, D. A. **Identificação de Sistema para uma Aeronave Leve - Projeto de fim de curso: Eng. de Controle e Automação**. Federal University of Minas Gerais (UFMG). Belo Horizonte, p. 104. 2010.

FEDERAL AVIATION ADMINISTRATION. **Advisory Circular 23-8C Flight Test Guide for Certification of Part23 Airplanes**. [S.l.]. 2011.

FEDERAL AVIATION ADMINISTRATION. **Advisory Circular 25-7C Flight Test Guide for Certification of Part25 Airplanes**. [S.l.]. 2012.

FEDERAL AVIATION ADMINISTRATION. **United States Code of Federal Regulations, Title 14, Part 23**. [S.l.].

FEDERAL AVIATION ADMINISTRATION. **United States Code of Federal Regulations, Title 14, Part 25**. [S.l.].

FUJINO, M. et al. **Initial Flight Testing of the HondaJet**. 24th International Congress of the Aeronautical Sciences. Yokohama: [s.n.]. 2004.

ILIFF, K. W.; MAINE, R. E. **Identification of Dynamic Systems**. Advisory Group For Aerospace Research & Development. [S.l.], p. 129. 1985. (AD-A153 321).

ILIFF, K. W.; MAINE, R. E. **Identification of Dynamic Systems - Application to Aircraft - Part 1: The Output Error Approach**. Advisory Group For Aerospace Research & Development. [S.l.], p. 167. 1986. (AD-A178 766).

ISCOLD, P. Low-cost Flight Test System for Light Aircrafts. **Aircraft Engineering and Aerospace Technology**, v. 80, n. 3, p. 243-252, 2008.

JATEGAONKAR, R. **Flight Vehicle System Identification:** A Time Domain Methodology. 2nd. ed. Reston: Amerinca Institute of Aeronautics and Astronautics, 2015.

JATEGAONKAR, R.; FISCHENBERG, D.; GRUENHAGEN, W. V. Aerodynamics Modeling and System Identification from Flight Data - Recent Applications at DLR. **Journal of Aircraft**, v. 41, n. 4, p. 681 - 691, July - August 2004.

JORDAN, P. VFW 614. **General History of the VFW 614**, 2000. Disponivel em: <http://www.vfw614.de/die_vfw_614_e.html>. Acesso em: 19 Nov 2015.

KIMBERLIN, R. D. **Flight Testing of Fixed-Wing Aircraft**. Reston: American Institute of Aeronautics & Astronautics, 2003.

KLEIN, V.; MORELLI, E. **Aircraft System Identification:** Theory and Practice. Reston: American Institute of Aeronautics and Astronautics, 2006.

LANCHESTER, F. W. **Aerodonetics**. London: Constable and Co. Ltd., 1908.

MAINE, R.; ILIFF, K. **Aplication of Parameter Estimation to Aircraft Stability and Control**. National Aeronautics and Space Administration. Washington. 1986.

MALAQUIAS, I. M.; FILHO, A. R. S.; OLIVEIRA, P. H. I. A. D. **Design and Development of a Wireless Pitot Tube for Utilization in Flight Test**. ABCM Symposium Series in Mechatronics - Vol.5. Natal: [s.n.]. 2012. p. 1278-1287.

NAPOLITANO, M. R. **Aircraft Dynamics:** From Modeling to Simulation. Hoboken: John Wiley, 2012.

NATIONAL CENTER FOR ATMOSPHERIC RESEARCH. Earth Observing Laboratory. **Bulletin No. 21 - Pressure Measurement From NCAR Aircraft**, 2000. Disponivel em: <https://www.eol.ucar.edu/raf/Bulletins/bulletin21.html>. Acesso em: 15 Feb 2016.

NICOLOSI, A. D.; MARCO, F.; VECCHIA, P. D. **Stability, Flying Qualities and Parameter Estimation of a Twin-Engine CS-23/FAR 23 Certified Light Aircraft**. AIAA Guidence, Navigation and Control Conference. Toronto: [s.n.]. 2001.

NISE, N. S. **Control Systems Engineering**. 6th. ed. [S.l.]: John Wiley & Sons, Inc., 2011.

PAMADI, B. N. **Performance, Stability, Dynamics, and Control of Airplanes**. 2nd. ed. Reston: American Institute of Aeronautics, 2004.

PERKINS, C. D. **Airplane Performance Stability and Control**. [S.l.]: John Wiley & Sons, 1949.

RAOL, J. R.; GIRIJA, G.; SINGH, J. **Modelling and Parameter Estimation of Dynamic Systems**. London: The Intituition of Engineering and Technology, 2004.

REIS, J. L. C.; DUTRA, D. A.; PINTO, R. L. U. F. **Longitudinal Aircraft Response Analysis Based on System Identification Techniques**. Congresso Brasileiro de Automática. Vitória: [s.n.]. 2016. p. 6.

ROSKAM, J. **Airplane Flight Dynamics and Automatic Flight Controls - Part 1**. Lawrence: Design, Analysis and Research Corp., 2001.

SCHMIDT, L. V. **Introduction to Aircraft Flight Dynamics**. Reston: American Institute of Aeronautics and Astronautics, 1998.

SHAMES, I. H. **Dinâmica - Mecânica para Engenharia**. 4ª. ed. São Paulo: Prentice Hall, v. 2, 2003.

STRUTZ, T. **Data Fitting and Uncertainty**. [S.l.]: Vieweg/Teubner, 2011.

UNITED STATES AIR FORCE. **Military Specification MIL-F-8785C, Flying Qualities of Piloted Airplanes**. [S.l.]. 1980.

WARD, D. T.; STRGANAC, T. W. **Introduction to Flight Test Engineering**. 2nd. ed. Dubuque: Kendal/Dubuque, 1998.

WIKIWAND. VFW 614, 2001. Disponivel em: <http://www.wikiwand.com/de/VFW_614>. Acesso em: 7 July 2016.

YECHOUT, T. R. et al. **Introduction to Aircraft Flight Mechanics:** Performance, Static Stability, Dynamic Stability, and Classical Feedback Control. Reston: American Institute of Aeronautics and Astronautics, 2003.